

An embedded genus-one helicoid

By MATTHIAS WEBER, DAVID HOFFMAN and MICHAEL WOLF*

Abstract

There exists a properly embedded minimal surface of genus one with one end. The end is asymptotic to the end of the helicoid. This genus one helicoid is constructed as the limit of a continuous one-parameter family of screw-motion invariant minimal surfaces—also asymptotic to the helicoid—that have genus equal to one in the quotient.

Contents

1. Introduction
 - 1.1. An embedded genus-one helicoid
 - 1.2. The main theorem
 - 1.2.1. The place of an embedded $\mathcal{H}e_1$ in the global theory of minimal surfaces
 - 1.3. $\mathcal{H}e_1$ as the limit of a family of screw-motion-invariant, embedded minimal surfaces
 - 1.4. The ideas behind the proof of Theorem 3
 - 1.5. An outline of the paper
 - 1.6. Acknowledgements
2. Minimal surfaces, cone metrics and the geometry of \mathcal{H}_k
 - 2.1. General background
 - 2.2. The helicoid
 - 2.3. Flat cone metrics
 - 2.3.1. Existence and uniqueness of cone metrics
 - 2.4. The exponential cone as the limit of S_k as $k \rightarrow \infty$
 - 2.5. Preliminaries on extremal length
 - 2.6. The helicoid in terms of cone metrics
 - 2.7. Symmetries of the \mathcal{H}_k
3. The singly periodic genus one helicoid
 - 3.1. The Weierstrass data: derivation from geometric assumptions
 - 3.1.1. The Gauss map and the placement of the ends
 - 3.1.2. The one-form dh

*Weber was partially supported by NSF grant DMS-0139476. Hoffman was partially supported by research grant DE-FG03-95ER25250/A007 of the Applied Mathematical Science subprogram of the Office of Energy Research, U.S. Department of Energy, and National Science Foundation, Division of Mathematical Sciences research grant DMS-0139410. Wolf was partially supported by NSF grants DMS-9971563 and DMS-0139887.

- 3.2. The period problem
 - 3.2.1. Existence of \mathcal{H}_1
 - 3.2.2. The rhombic torus \mathcal{T}_1 and the uniqueness of \mathcal{H}_1
- 3.3. The cone metric construction of \mathcal{H}_1
 - 3.3.1. The cone-metric construction of \mathcal{T}_1 and Weierstrass data for \mathcal{H}_1
 - 3.3.2. The definition of $\frac{1}{g}dh$ and the solution of the horizontal period problem
 - 3.3.3. The Weierstrass data $\{g, dh\}$ and the symmetries of dh
- 3.4. Solving the vertical period problem geometrically
- 4. The construction of screw-motion-invariant \mathcal{H}_k
 - 4.1. The rhombic $|dz|$ model
 - 4.1.1. The period conditions
 - 4.2. The $|gdh|$ model and the solution of the horizontal period problem
 - 4.2.1. The $|\frac{1}{g}dh|$ model and the horizontal period condition
 - 4.2.2. Symmetries inherent in the $|gdh|$ and $|\frac{1}{g}dh|$ models
 - 4.2.3. The placement of the ends and vertical points
 - 4.3. The $|dh|$ model and the global formulation of the vertical period problem
 - 4.4. The (k, d) rectangle \mathcal{P}
 - 4.4.1. The definition of \mathcal{P}
- 5. Continuity and boundary estimates for the height function
 - 5.1. The proof of Proposition 15
 - 5.1.1. Continuity in the interior of \mathcal{P}
 - 5.1.2. Continuity on the top edge away from the right-hand corner.
 - 5.1.3. Uniform estimates near the right-hand edge away from the bottom vertex
 - 5.1.4. Continuity along the right-hand edge away from the bottom vertex
 - 5.1.5. Continuity on the bottom edge
 - 5.2. Estimates for the height function on the top and bottom of the rectangle \mathcal{P} and the solution of the period problem for \mathcal{H}_k .
- 6. The proof of Theorem 3
 - A. Appendix: The Weierstrass data for \mathcal{H}_k in terms of theta functions
 - B. Appendix: Existence and uniqueness of flat cone metrics

1. Introduction

1.1. *An embedded genus-one helicoid.* We prove the existence of a properly embedded minimal surface in \mathbf{R}^3 with finite topology and infinite total curvature.¹ It is the first such surface to be found since 1776, when Meusnier showed that the helicoid was a minimal surface [30]. Our surface has genus one and is asymptotic to the helicoid.

We exhibit this minimal surface as a geometric limit of periodic embedded minimal surfaces. The periodic surfaces, \mathcal{H}_k , indexed by $k \geq 1$, are invariant under a cyclic group of screw motions generated by σ_k . Here σ_k is the rotation by $2\pi k$ about the vertical axis followed by a vertical translation by $2\pi k$. Thus, for fixed k , the quotient surface has two topological ends and genus one. The

¹A surface is said to have *finite topology* if it is homeomorphic to a compact surface with a finite number of points removed.

limit is taken as $k \rightarrow \infty$; a compact set in the limit surface $\mathcal{H}e_1$ is increasingly well-approximated (as $k \rightarrow \infty$) by corresponding pieces of fundamental domains of \mathcal{H}_k/σ_k .

The requirement to prove embeddedness was the main motivation of our work. We prove that embeddedness is inherited from the embeddedness of the approximating simpler (periodic) surfaces, using that in this particular minimal surface setting, the condition of being embedded is both open and closed on families. This method of proving embeddedness for surfaces defined using the Weierstrass representation contrasts with previous methods: here the characteristic of being embedded follows naturally from the property holding for simpler surfaces, while previously one proved embeddedness by *ad hoc* methods, for instance by cutting the surface into disjoint graphs (see, for example [21], [22]).

Recent work of Traizet-Weber [37] suggests that, ultimately, the embeddedness of this genus-one helicoid derives from the embeddedness of the helicoid itself. In particular, families of complete embedded minimal surfaces of finite genus degenerate to the singular union of catenoids and planes. Traizet and Weber realized that for families of symmetric screw-motion-invariant embedded minimal surfaces with helicoidal ends, there is a similar phenomenon: the families degenerate to a formal union of helicoids identified at their ends (three helicoids in the case under consideration in this paper). Traizet and Weber then prove that regeneration is possible; i.e. there is a family of periodic surfaces \mathcal{H}_k for $k > \frac{1}{2}$ (but near $k = 1/2$) that desingularizes triples of embedded helicoids identified at their ends, with the embeddedness of the surfaces in the family inherited from the embeddedness of the original helicoids.

A second important feature is that we approximate a surface of finite topology (and finite symmetry group) by surfaces of infinite topology (and infinite symmetry group). We believe this is the first example of such a construction resulting in the existence of a new surface.

The third feature is that we construct the Weierstrass data of these approximating minimal surfaces in terms of flat singular structures on the tori corresponding to the quotients. The salient feature to note is that the defining flat structures have singularities corresponding to the two ends² with cone angles of $\pm 2\pi k$. Thus, as the size of the twist tends to infinity, the cone angles also tend to infinity, with the limit surface—our genus-one helicoid—represented in terms of flat cone metrics with an infinite cone angle. This corresponds to the Weierstrass data for a helicoid, whose Gauss map has an essential singularity at the end. This required the development of a theory of singular flat structures that admits infinite cone angles.

²There is an additional cone point (with cone angle 6π) in these structures at a vertical point.

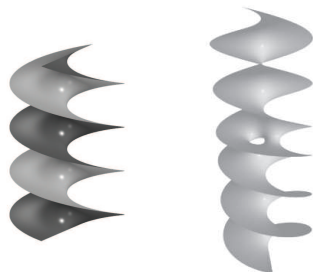


Figure 1: The helicoid and the $\mathcal{H}e_1$ of [18]

Recently, Meeks and Rosenberg [29] have shown that the helicoid is the unique simply connected, properly embedded (nonplanar) minimal surface in \mathbf{R}^3 with one end. The method of proof uses in an essential manner the work of Colding and Minicozzi [7], [8], [9], [10] concerning curvature estimates for embedded minimal disks and geometric limits of those disks. (Colding and Minicozzi have recently shown [6] that a complete and embedded minimal surface with finite topology in \mathbf{R}^3 must be proper.) These results together with the present work and numerical work of Traizet [36] and Bobenko [3] (see Section 1.3) suggest that there may be a substantial theory of complete embedded minimal surfaces with one end, infinite total curvature and finite topology. For complete embedded surfaces of finite total curvature, the theory is surveyed in [16].

1.2. *The main theorem.* In 1993 Hoffman, Karcher, and Wei [18] constructed a surface, $\mathcal{H}e_1 \subset \mathbf{R}^3$, which they called the genus-one helicoid.

It has the following properties:

- (1) (i) $\mathcal{H}e_1$ is a properly immersed minimal surface;
(ii) $\mathcal{H}e_1$ has genus one and one end asymptotic to the helicoid;
(iii) $\mathcal{H}e_1$ contains a single vertical line (*the axis*) and a single horizontal line.

We will take the liberty of referring to *any* surface with the properties (1) as a genus-one helicoid, and of denoting such a surface by $\mathcal{H}e_1$. We emphasize at this point that we do not include embeddedness in the list of properties required by (1).

The $\mathcal{H}e_1$ in [18] was constructed by solving the period problem for a Weierstrass Representation (see (5)–(8)) chosen to force the surface to satisfy conditions (1).

Computer-generated images of this $\mathcal{H}e_1$, and computational estimates produced by first solving the period problem numerically and then triangulating the approximate surface, showed beyond reasonable doubt that this $\mathcal{H}e_1$ was embedded; nevertheless, a noncomputational proof has been elusive. (It is known that any $\mathcal{H}e_1$ must be embedded outside of a compact set. See Proposition 1.)

We prove

THEOREM 1. *There exists an embedded $\mathcal{H}e_1$.*

We believe that the surface we have found is the same one constructed by Hoffman, Karcher and Wei. In fact, we believe

CONJECTURE 1. *There is a unique embedded $\mathcal{H}e_1$.*

Note that Conjecture 1 does not assert that there is a unique $\mathcal{H}e_1$ and that it is an embedded surface. This does not appear to be true, as Bobenko [4] has given strong computational evidence for the existence of an $\mathcal{H}e_1$ that is immersed but *not* embedded.

Condition (1.ii) implies that any $\mathcal{H}e_1$ has finite topology and infinite total curvature. The helicoid—a surface swept out by a horizontal line rotating at a constant rate as it moves up a vertical axis at a constant rate—is clearly properly embedded and has finite topology (in fact it is simply connected). Since it is singly periodic and evidently not flat, it has infinite total curvature.

1.2.1. *The place of an embedded $\mathcal{H}e_1$ in the global theory of minimal surfaces.* That complete minimal surfaces in \mathbf{R}^3 with *finite total curvature* must have finite topology is a consequence of Osserman's theorem³ ([33], [16]). Finite topology does not imply finite total curvature for complete minimal surfaces in R^3 —as the example of the helicoid shows—but Collin's solution of the generalized Nitsche Conjecture [11] implies that a properly embedded minimal surface in \mathbf{R}^3 of finite topology with *more than one end* must have finite total curvature. One is naturally led to the following questions.

Let S be a properly embedded minimal surface of finite topology with infinite total curvature and *one end*:

- (2.i) In addition to the helicoid, what are the other examples?
- (2.ii) Is the end of every S asymptotic to the end of the helicoid?
- (2.iii) Is the helicoid the unique simply connected S ?

In [20], one of the authors (DH) and John McCuan considered properly immersed minimal ends that are conformally equivalent to a punctured disk, upon which the Weierstrass data dg/g and dh both have a double pole. (This condition is satisfied by the helicoid.) They also assume that dh has no residue at the puncture. (This condition must hold if the end appears on a properly immersed minimal surface of finite topology with one end such as an $\mathcal{H}e_1$, because dh is holomorphic away from the puncture.) They show that if the

³Osserman's theorem states that a complete minimal surface with finite total curvature in R^3 is *conformally* diffeomorphic to a compact Riemann surface from which a finite number of points have been removed. Moreover, the Gauss map and coordinate one-forms of such a surface extend meromorphically to the punctures.

end contains a vertical and a horizontal ray, then the end is embedded, and it is asymptotic to the helicoid. Specifically,

PROPOSITION 1 ([20]). *Let E be a complete minimal annular end that is conformally a punctured disk, upon which both dg/g and dh have a double pole and dh has no residue. If E contains a vertical ray and a horizontal ray then that end is asymptotic to a helicoid. In particular, a subend is embedded.*

This proposition allows us to construct Weierstrass data for an $\mathcal{H}e_1$ that meets the conditions of the Proposition and then be assured that the resulting surface, if it exists (i.e. if the period conditions for the Weierstrass data are satisfied), must have an embedded helicoidal end.

In terms of the context for question (2.i)–(2.iii), the techniques of [20] were used and extended by Hauswirth, Perez and Romon [15] to study embedded minimal surfaces of *finite type*,⁴ a strengthening of the condition of finite topology. They prove that questions (1.3ii) and (1.3iii) have affirmative answers if one makes the additional assumption that the minimal surface S has finite type. Meeks and Rosenberg [28] showed that the answer to (2.iii) is “yes” under the assumption that S is also singly periodic. They assume neither bounded curvature nor finite total curvature of the quotient surface. As mentioned in Section 1.1, Meeks and Rosenberg [29] recently resolved (2.iii) in the affirmative.

Concerning (2.i), there is evidence that there are higher genus examples. Traizet [36] (unpublished) devised a computer program to generalize the Weierstrass representation in [18] to higher genus and compute and solve the period problem numerically. This yielded convincing numerical evidence of a genus-two helicoid, analogous to the surface described in Theorem 3. For genus three and genus four, Bobenko also has produced examples computationally. See also Figures 2 and 3 below.

1.3. $\mathcal{H}e_1$ as the limit of a family of screw-motion-invariant, embedded minimal surfaces. The starting point of our investigation is the singly periodic genus-one helicoid.

THEOREM 2 ([17], [19]). *There exists a properly immersed, singly periodic minimal surface \mathcal{H}_1 , whose quotient by vertical translations:*

- (3.i) *has genus one and two ends;*
- (3.ii) *is asymptotic to a full 2π -turn of a helicoid;*
- (3.iii) *contains a vertical axis and two horizontal parallel lines.*

Furthermore, any surface satisfying conditions (i)–(iii) is embedded.

⁴A minimal surface has *finite type*, if it is conformally a compact Riemann surface with a finite number of points removed, and the Weierstrass data dg/g and dh extend meromorphically to the punctures.

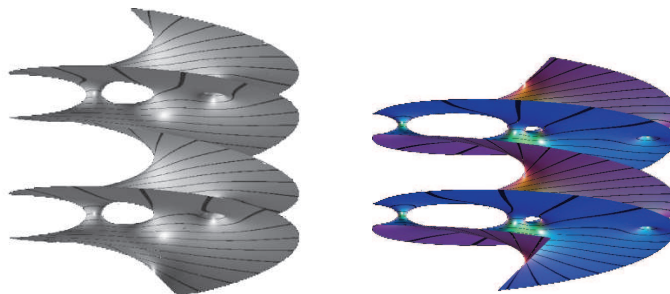


Figure 2: Images of higher genus examples of translation-invariant surfaces with genus two (left) and three (right) in the quotient. They satisfy the other geometric conditions of (4). These images were computed by Martin Traizet. There is at the time of writing no proof that these surfaces exist. See however, the recent work of Traizet and Weber [37].

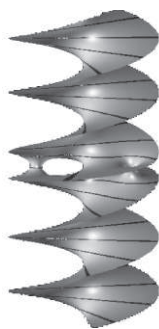


Figure 3: A computed image of a conjectured genus-two analog of $\mathcal{H}e_1$. It satisfies all the other conditions of Theorem 1, also computed by Traizet.

See Figure 4 and the left column of Figure 5 for images of \mathcal{H}_1 . The fundamental domain of the surface can be imagined as a modification of one full turn of the helicoid, a region bounded by two parallel horizontal lines that are identified in the quotient. The modification consists of sewing in a handle at mid-level. In fact,

PROPOSITION 2. *\mathcal{H}_1 is the unique singly periodic minimal surface satisfying the conditions (3.i)–(3.iii) of Theorem 2.*

It was observed by Karcher that the proposition follows from the proof of the existence of \mathcal{H}_1 in [19], together with a fundamental result of Weber about rhombic tori [41]. This is discussed in Section 3. (See Proposition 8.)

In 1993, Hoffman, Karcher and Wei, realized that \mathcal{H}_1 could be conceived as the limit of a one-parameter family of deformations of Karcher's genus-one modification of Scherk's doubly periodic minimal surface. (See [18], [17] for details.) Soon after, Hoffman and Wei imagined that \mathcal{H}_1 could also be deformed

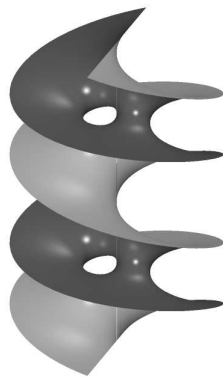


Figure 4: Singly periodic genus-one helicoid, \mathcal{H}_1 .

in a manner suggested by the symmetries of the helicoid. The helicoid is not only invariant under a vertical translation by 2π , it is also invariant under *vertical screw motions* σ_k : for any real number k , the isometry σ_k is defined to be rotation by $2\pi k$ around the vertical axis followed by a vertical translation by $2\pi k$. For $k \geq 1$, imagine a periodic minimal surface, \mathcal{H}_k , invariant under a vertical screw motion σ_k and satisfying the following conditions.

- (4) The quotient of \mathcal{H}_k by σ_k :
- (i) has genus one and two ends;
 - (ii) is asymptotic to a portion of the helicoid that has twisted through an angle of $2\pi k$;
 - (iii) contains a vertical axis and two parallel horizontal lines.

See Figure 5.

Hoffman and Wei defined a Weierstrass representation that was amenable to numerical solution of the period problem. The twist angle $2\pi k$ was not specified in advance and was a calculated function of parameters that specified the conformal type of the rhombus and the location of geometrically specified points. After normalization to make the Gauss curvature equal to -1 at the intersection of the axis and the middle horizontal line, they observed (see Figure 5) that the handle rapidly stabilizes and the surface quickly approaches a helicoid away from the handle [23]. This reinforced the hope that $\mathcal{H}e_1$ could be produced as the limit of the \mathcal{H}_k and that embeddedness could be proved in this manner. However, the form of the Weierstrass representation was not well-suited for proving either existence of the \mathcal{H}_k , or continuous dependence on k .

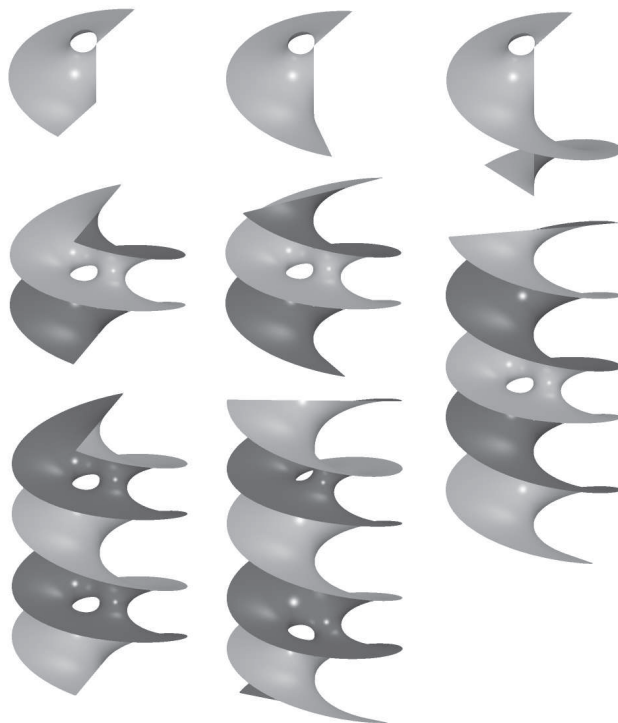


Figure 5: Left column. The surface \mathcal{H}_1 ; on top, one quarter of the fundamental domain of \mathcal{H}_1 modulo σ_1 ; in the middle, one full fundamental domain containing four copies of the region above; on the bottom, two fundamental domains. Middle column: The surface \mathcal{H}_k for $k \sim 1.25$, with images that correspond to those in the first column. Right column: The surface \mathcal{H}_k for $k \sim 2.5$, with images corresponding to the top and middle images of the other two columns.

The limit of these surfaces as $k \rightarrow \infty$, if it existed in a geometric sense, should be an $\mathcal{H}e_1$. More important, if it could be shown that the family depended continuously on k , then the embeddedness of \mathcal{H}_1 would be inherited by the \mathcal{H}_k . It was hoped that, under controlled circumstances, embeddedness could be shown to pass to the limit $\mathcal{H}e_1$.

We show that this can be done.

THEOREM 3. *For every $k > 1$, there exists a complete, σ_k -invariant, properly embedded minimal surface, \mathcal{H}_k , whose quotient by σ_k satisfies conditions (4). As $k \rightarrow \infty$, a limit surface exists and is an embedded $\mathcal{H}e_1$, i.e. a properly embedded minimal surface satisfying conditions (1).*

1.4. *The ideas behind the proof of Theorem 3.* Let ω be a meromorphic one-form on a Riemann surface \mathcal{R} . The developing map $\text{dev} : \mathcal{R} \rightarrow D \subset \mathbf{C}$ given by $p \rightarrow \int_{p_0}^p \omega$ maps \mathcal{R} onto a domain in the complex plane. If z is the variable in \mathbf{C} , then $\omega = \text{dev}^*(dz)$ and the periods of ω can be measured by

subtraction in \mathbf{C} . For example, the statement that a period of ω is real on a cycle $\gamma \subset \mathcal{R}$ is equivalent to the statement that the endpoints of $\text{dev}(\gamma)$ lie on the same horizontal line in $D \subset \mathbf{C}$. If (g, dh) are Weierstrass data on \mathcal{R} for a minimal surface M , we can use the developing map dev for the one-forms gdh , $\frac{1}{g}dh$ and dh to produce domains in $D \subset \mathbf{C}$ that together with the metric $|dz|$ are called *singular flat structures*. These metrics correspond to the metrics $|gdh|$, *etc.* on \mathcal{R} which are flat with isolated cone points at the zeros and poles of the one-form in question.

We will reverse this process. By specifying a domain $D \subset \mathbf{C}$ we will declare that (D, dz) is the image under the developing map of one of the geometrically relevant one-forms on all or part of the underlying Riemann surface of a minimal surface M (e.g., $gdh := \text{dev}^*(dz)$ on $\text{dev}^{-1}(D)$). We can do this in such a way that gdh , $\frac{1}{g}dh$ and dh solve the period problems for the Weierstrass data and force desired symmetries. What remains is to show that this can be done in such a way that the underlying conformal structures coincide. Thus we transform a problem of killing periods into a problem of matching conformal structures.

Weber realized that the Weierstrass data $\{g, dh\}$ for \mathcal{H}_1 of Theorem 2 defined one-forms gdh and $(1/g)dh$ that differed by a scale factor and a translation. He used this to show that the *horizontal-period problem* (12) completely specifies the conformal structure of the quotient of \mathcal{H}_1 modulo translations [39]. Moreover, he noticed that the $|gdh|$ flat structure of the underlying torus had a particularly simple and elegant representation as a planar domain with identifications. (See Figure 12, Sec. 3.3.) This allowed for a relatively simple reconstruction of the singly periodic example \mathcal{H}_1 .

Singular flat structures can be joined together along straight lines to produce new flat structures. This modifies not only the underlying conformal structure but also the associated one-forms. By sewing in a cone of angle $2\pi(k-1)$ (see Example 2 in Sec. 2) into the singular flat structure used to define gdh for \mathcal{H}_1 we produce candidate flat structures for \mathcal{H}_k (See Figure 24, Sec. 4.1.) The position of the vertex of the cone gives a real parameter $d > 0$. (For $k=1$ we do not sew in a cone, but the choice of d determines the placement of the ends.) We know from Theorem 2 and Proposition 8 that, for $k=1$, there is a unique solution to the vertical period problem and it is the embedded example \mathcal{H}_1 . For each $(k, d) \in [1, \infty) \times (0, \infty)$, the construction gives a candidate structure on each of which dh is determined up to a scale factor and the horizontal period problem is solved. These structures depend smoothly on (k, d) .

For each fixed k , we have a single free parameter d . This free parameter is used to satisfy the vertical period condition as follows: First, we realize that the flat structure $|dh|$ of dh can be understood qualitatively as a planar domain (see Figure 16 right, Sec. 3.4). Second, for the parameter values at

their limits, we are able to determine $|dh|$ explicitly which allows us to apply the intermediate value theorem (see the images on the far right of Figures 17 and 19, Sec. 3.4). This solves the vertical period problem for each fixed k .

Of course we need more than simply a single solution for each k : we need a *continuous* family \mathcal{C} of solutions that begins at the point $(1, d_1)$ corresponding to \mathcal{H}_1 , and crosses each $k = \text{const.}$ line segment in the (k, d) rectangle. Each point, (k, d) , on this curve will then define a properly immersed minimal surface satisfying the conditions (4).

To do this, we note that a period of dh for each (k, d) -structure defines a real analytic function, $h = h(k, d) = \text{Re} \int_{\Gamma} dh$ (for an appropriate Γ) whose zeros are what we seek: if $h = 0$ for some (k, d) , then the corresponding (k, d) -flat geometric structure defines a properly immersed minimal surface \mathcal{H}_k satisfying conditions (4). Then, to find this curve \mathcal{C} , we first compactify the “moduli space” of (k, d) -structures, adding in degenerate structures for the loci $k = \infty, d = 0$ and $d = \infty$ in a manner compatible with the topology of $[1, \infty] \times [0, \infty]$. We then show that the height function h is *continuous* on the full compact rectangle $[1, \infty] \times [0, \infty]$ (i.e., h extends continuously to the loci defined by $d = 0, \infty$ and $k = \infty$). This has the advantage that the signs of h on the degenerate surfaces $(k, 0)$ and (k, ∞) are evident and opposite, and so the intermediate value theorem provides for a solution $(k_0, d) \in \mathcal{C}$ for each choice of $k_0 \in (1, \infty)$. More precisely, there must be a curve \mathcal{C} on which $h = 0$ because this curve separates the neighborhoods of the boundary components $\{d = 0\}$ and $\{d = \infty\}$ on which h has opposite signs. Finally, a maximum-principle argument then shows that the embeddedness of \mathcal{H}_1 implies that all the $\mathcal{H}_k, k > 1$, on this curve \mathcal{C} are embedded.

The (k, d) -structures are defined for $k = \infty$ by sewing in an infinite cone. Thus, any structure (∞, d) corresponds to a potential $\mathcal{H}e_1$, which will exist provided $h(\infty, d) = 0$; the endpoint of \mathcal{C} on the locus $\{k = \infty\}$ is then such a point. Thus we obtain a limit flat structure that defines an $\mathcal{H}e_1$ and we argue that, as a limit of a family $\{\mathcal{H}_k\}$ of embedded surfaces, the surface $\mathcal{H}e_1$ is also embedded.

1.5. *An outline of the paper.* In Section 2 we review the Weierstrass representation and the associated period problem for minimal surfaces invariant under a screw motion. We introduce cone metrics and establish existence and uniqueness results for them necessary for our work. A short review of extremal length is presented. The helicoid is presented from both the point of view of the Weierstrass representation and of singular flat structures (cone metrics).

Section 3 is devoted to the singly periodic genus-one helicoid, \mathcal{H}_1 , of Theorem 2. In Section 3.1, we give a derivation of the Weierstrass data for this surface under the geometric assumptions of Theorem 2. In Section 3.2, we state the results of [19] about the existence of \mathcal{H}_1 , i.e. the solution of the period problem. The rest of Section 3 is devoted to an alternate construction of

candidate data and solution of the period problem for \mathcal{H}_1 using singular flat structures.

Section 4 generalizes the cone metric construction of Weierstrass data for \mathcal{H}_1 . We produce analogous Weierstrass data for the surfaces \mathcal{H}_k of Theorem 3. This involves three singular flat structures corresponding to the one-forms gdh , $\frac{1}{g}dh$ and dh . These structures are naturally indexed in a rectangle \mathcal{P} by two real variables which control the twist angle and the conformal type of the underlying punctured tori. These structures are generalized to the boundary of \mathcal{P} by introduction of cone metrics that are natural limits of the candidate cone metrics in the interior. One of the limits involves letting the cone angle tend to infinity; this is what we expect for the genus-one helicoid $\mathcal{H}e_1$.

Section 5 is devoted to the proof that the structures behave continuously on the extended rectangle \mathcal{P} . In particular, the vertical period—a well-defined real number for each structure in the interior—actually extends to a continuous function on the closed extended rectangle. We refer to this function as *the height function*. The surfaces \mathcal{H}_k correspond to the zero locus of this function on the interior of the rectangle.

In Section 6, we prove the first part of Theorem 2 by showing that there is a continuous family of surfaces \mathcal{H}_k which begins with \mathcal{H}_1 and is defined for all $k \geq 1$. We do this by an intermediate-value-theorem argument using the height function on \mathcal{P} . We then show that the limit structure as $k \rightarrow \infty$ produces an $\mathcal{H}e_1$. Embeddedness of this $\mathcal{H}e_1$ is then established by using the fact (Section 3.2) that \mathcal{H}_1 is embedded and an argument that embeddedness propagates along the curve of \mathcal{H}_k structures.

In the appendices, we give an alternate Weierstrass representation of the surfaces \mathcal{H}_k using theta functions, and we present a proof of the existence and uniqueness results for the cone metrics that come up in Section 2.

1.6. Acknowledgements. The authors wish to thank Hermann Karcher for contributing to this paper in many ways. As a collaborator, colleague, advisor and friend, his critical intelligence and spirit have been fundamentally important to our work.

We also wish to acknowledge useful conversations with Harold Rosenberg, Bill Meeks and Fusheng Wei over the past years. Wei's ingenious ideas about how to represent the family \mathcal{H}_k in a computationally tractable manner was key to establishing the belief that the family not only existed but also converged to a genus-one helicoid. The idea that embeddedness was inherited from \mathcal{H}_1 by the family \mathcal{H}_k came from discussions that one of us had with Meeks about the same phenomena for finite-total-curvature surfaces. Rosenberg's pivotal idea to sew a helicoid into a genus-one surface to create a genus-one helicoid (conveyed to Karcher in a conversation reported in [18]) led to the discovery of $\mathcal{H}e_1$. However, the construction of $\mathcal{H}e_1$ in [19] was not that direct. In

this paper, we are able to do this in a concrete manner, realizing directly Rosenberg's idea, but in a way he did not imagine. (See Section 4.)

2. Minimal surfaces, cone metrics and the geometry of \mathcal{H}_κ

2.1. *General background.* We begin with the Weierstrass representation of a minimal surface in \mathbf{R}^3 . Details can be found in [16] or [33].

Let S be an oriented minimal surface in \mathbf{R}^3 . The metric on S induced by the immersion is analytic and allows us to consider S as a Riemann surface. We write M for this Riemann surface. The immersion $X : M \rightarrow \mathbf{R}^3$ is by definition conformal. Minimality of S is equivalent to the anticonformality of the Gauss map $N : M \rightarrow S^2$, which in turn is equivalent to the conformality of $g := \sigma \circ N$ where σ is stereographic projection to the extended complex plane.

Minimality is also equivalent to the harmonicity of the conformal immersion X . In particular, if \hat{f} is a linear function on \mathbf{R}^3 (a coordinate function for example) then \hat{f} is harmonic on M . Let \hat{f}^* be the (locally well-defined) harmonic conjugate of \hat{f} . Then $f := \hat{f} + i\hat{f}^*$ is a locally defined holomorphic function and df is a globally well-defined one-form on M . In particular, we define the one-form dh to be the exterior derivative of the $h = x_3 + ix_3^*$, where $X = (x_1, x_2, x_3)$. We will refer to dh as the "height differential".

The Weierstrass representation allows one to write the conformal parametrization X in terms of g and dh :

$$(5) \quad X(p) = \operatorname{Re} \int_{p_0}^p \Phi, \text{ where } \Phi = \left(\frac{1}{2}(g^{-1} - g), \frac{i}{2}(g + g^{-1}), 1 \right) dh.$$

The immersion will be regular provided the induced metric

$$(6) \quad ds = \frac{1}{2} \left(|g dh| + \left| \frac{1}{g} dh \right| \right)$$

is nowhere zero. This requires the zeros of dh to coincide with (and have the same order as) the zeros and poles of g (points where the Gauss map is vertical).

The integral formula (5) can be used to construct minimal surfaces. Given a Riemann surface M , a meromorphic function g , and a holomorphic one-form η , on M , the integral (5) – with η substituted for dh – defines a conformal and harmonic mapping of M into \mathbf{R}^3 whose image is a minimal surface. The mapping will be regular, provided $|g\eta| + \left| \frac{1}{g}\eta \right| \neq 0$. The stereographic projection of the Gauss map of this surface will be g and the one-form η will be equal to the holomorphic one-form dh that is constructed above from $h = x_3$. When constructing minimal surfaces by specifying "Weierstrass data," that is, when specifying M , g and η , we will use the notation dh for η .

The Weierstrass representation is, in general, multivalued. In order for (5) to be single-valued on M , it is necessary and sufficient that

$$\operatorname{Re} \int_{\alpha} \Phi = 0$$

for all closed cycles α on M . Using (5), this can be rewritten as

$$(7) \quad \overline{\int_{\alpha} g dh} - \int_{\alpha} (1/g) dh = 0 \quad (\text{Horizontal Period Condition})$$

$$(8) \quad \operatorname{Re} \int_{\alpha} dh = 0 \quad (\text{Vertical Period Condition}).$$

In dealing with *periodic* minimal surfaces N , it is often useful—and sometimes necessary—to work with g and dh on the Riemann surface of the quotient of N by translations or screw motions. We will be dealing with singly periodic surfaces invariant under screw motions; without loss of generality, we may assume that the translational part of the screw motion is vertical, and that the axis of the screw motion is the x_3 -axis. Let M denote the Riemann surface of the quotient surface under the screw motion σ_k . The Weierstrass representation (5) defines an immersion of \tilde{M} , the universal cover of M , into \mathbf{R}^3 . Screw-motion invariance means that there is a basis $[\alpha_i]$ for the homology of M such that if $A_{[\alpha_i]}$ is the deck transformation associated to $[\alpha_i]$, then $X \circ A_{[\alpha_i]} = X$ or $X \circ A_{[\alpha_i]} = \sigma_k X$.

2.2. The helicoid. The helicoid, \mathcal{H} , is a singly periodic minimal surface swept out by horizontal lines moving at a constant speed up the x_3 -axis while rotating at constant speed. (See Figure 1.) It is invariant under any vertical screw motion around the x_3 -axis, in particular vertical translation by 2π . In the quotient of \mathcal{H} by σ_k , the screw motion with twist angle $2\pi k$, the Weierstrass data on $M = \mathbf{C} - \{0\}$ can be chosen to be

$$(9) \quad g = iz^k \text{ and } dh = \frac{kidz}{z}.$$

When k is not an integer, the Gauss map on the quotient is multivalued, and so is g . From the Weierstrass representation (5) we have

$$2(x_1 + ix_2) = \overline{\int \frac{1}{g} dh} - \int g dh = z^k - \bar{z}^{-k},$$

$$x_3 = -k \cdot \arg(z).$$

The only relevant cycle is represented by a circle α around the origin. Hence $X \circ A_{[\alpha]} = \sigma_k X$, when α is oriented in a clockwise direction. The Riemann surface upon which dh is well-defined is the Riemann surface of $w = \ln(z)$, i.e. \mathbf{C} . The globally defined function $z = e^w$ on \mathbf{C} allows the

expression of the Weierstrass data for the helicoid in a univalent manner: $g = ie^w, dh = -idw$. This gives a global representation on \mathbf{C} of \mathcal{H} . Note that in the representation on the quotient surface, $\mathbf{C} - \{0\}$, there are two ends (one at 0, the other at ∞) at which g has a simple zero and a simple pole, respectively, while dh has a simple pole at both ends. In the global representation, there is a single end at infinity where g has an essential singularity and dh has a double pole.

Since we will be using the helicoid as a model, we restate the well-known facts above in terms of cone metrics.

2.3. *Flat cone metrics.* Consider, for $k > 0$, the cone A_k , described as an identification space

$$A_k = \{(r, \theta) | 0 \leq r < 1, |\theta| \leq \pi k\} / \sim,$$

where \sim identifies the top and bottom edges and collapses the left-hand edge: $(r, -\pi k) = (r, \pi k)$ and $(0, \theta) = (0, 0)$. Via the identification $(r, \theta) \rightarrow z = re^{i\theta}$, we may regard A_k as a possibly multisheeted “sector” with vertex at the origin $0 \in \mathbf{C}$ and edges identified. Away from the origin, the sector A_k inherits the flat metric $|dz|$ on the plane. This metric is the metric of a flat cone with vertex at the origin. We observe that a neighborhood of the vertex is isometric to a neighborhood of the vertex of another identification space $A_{k'}$ if and only if $k = k'$: this is because the circumference of a circle of radius ε linking the distinguished point of A_k has length $2\pi k\varepsilon$.

We extend this definition of A_k to $k = 0$ by taking A_0 to be the identification space of $\{z \in \mathbf{C} | |\operatorname{Im} z| \leq 1, \operatorname{Re} z \leq 0\}$, where we identify the boundary rays by a vertical translation and consider the distinguished point (the vertex) to be a point that compactifies the left end of the cylinder.

A neighborhood of the vertex of A_k is topologically (and conformally) a disk. Consider the map $w : \mathbf{D} \rightarrow A_k$ from the disk \mathbf{D} to a neighborhood of the distinguished point given by $z = w^k$ for $k \neq 0$, and $z = \log w$, when $k = 0$. We can pull back the metric on A_k to \mathbf{D} :

$$|dz| = |kw^{k-1}dw|.$$

	$z = 0$	$z = \infty$
dh	∞	∞
g	0^k	∞^k
gdh	0^{k-1}	∞^{k+1}
$\frac{1}{g}dh$	∞^{k+1}	0^{k-1}

Figure 6: The divisors of g, dh, gdh and $\frac{1}{g}dh$ for the helicoid modulo σ_k , a vertical screw motion with twist angle $2\pi k$.

In particular, we see that a metric $ds = |w^\alpha dw|$ on the disk \mathbf{D} defines a metric isometric (up to a scale factor, which is unimportant in the present discussion) to one in a neighborhood of the distinguished point on A_k , with $k = \alpha + 1$. In particular, we may define for $k = 0$ the metric $|\frac{dw}{w}|$ on the unit disk, and consider it to be a flat cone with cone angle zero at the vertex.

We now extend the range of definitions of these local neighborhoods to all $k \in \mathbf{R}$ by working with these flat singular metrics defined on the disk \mathbf{D} .

Definition 1. Cones and cone points with cone angle $2\pi k$, $k \in \mathbf{R}$. The cone C_k is defined to be the disk D with the metric given up to scaling by $|w^{k-1}dw|$ on $\{w : |w| < 1\}$. The origin is the cone point of the cone C_k .

Note that when $k = 1$, this formula is the standard regular metric $|dw|$ on the w -disk. We will adopt the convention of not referring to the origin in C_1 as a cone point but as a regular point. Also note that the metric $|w^{k-1}dw|$ on the (compactified) exterior of \mathbf{D} defines a metric with vertex at infinity that is isometric to C_{-k} . This follows immediately from pulling the exterior domain back to \mathbf{D} by $w \rightarrow \frac{1}{w}$ and pulling back the metric to the disk.

We will need to consider infinite cones of a specific type.

Definition 2. An exponential cone of simple type. The cone C_e is the disk D with the metric $|e^{\frac{1}{w}} \frac{dw}{w^2}|$. The origin is the cone point of C_e .

Note that the metric in the definition of C_e is the pullback of the metric $|e^w dw|$ on the (compactified) exterior of the unit disk. Therefore we may (equivalently) consider C_e to be the (compactification of the) exterior of the unit disk with metric $|e^w dw|$ and cone point at ∞ .

The following definition is nearly standard (see [38]): our extension allows the presence of cone points with negative cone angles and exponential cone points of simple type.

Definition 3. Flat cone metric. Let M be an oriented surface and let $\{p_1, \dots, p_n\}$ be a discrete set of points of M . A flat cone metric on M is a metric on M so that every point on M has a neighborhood as follows:

(1) *Regular points.* If $q \notin \{p_1, \dots, p_n\}$, then q has a neighborhood that is isometric to a neighborhood in the Euclidean plane.

(2) *Cone points.* Every point p_i in the distinguished set has a neighborhood that is isometric to a neighborhood of the vertex in either C_k or C_e . In the first case, the point p_i is a cone point with finite cone angle and in the second case, it is a cone point with cone angle of simple exponential type.

The definition naturally requires transition maps between neighborhoods to be Euclidean isometries. This defines a conformal, hence complex, structure on $M - \{p_1, \dots, p_n\}$. Further, deleted neighborhoods of the cone points are

clearly conformally punctured disks, so that the Riemann surface structure on $M - \{p_1, \dots, p_n\}$ then extends naturally to a Riemann surface structure on M .

The simplest example of a cone metric is the extended complex plane with metric $|dz|$. There is a single cone point at infinity with cone angle -2π . More generally, consider a compact Riemann surface M and ω a meromorphic one form on M . Define the metric $ds = |\omega|$. Since $\log|\omega|$ is harmonic, the Gauss curvature of the metric is zero: $K = \frac{-\Delta \log|\omega|}{2|\omega|^2} = 0$, valid away from the poles and zeros of ω . A zero (resp. pole) of order k of ω represents a cone point with cone angle $2\pi(k+1)$ (resp. $2\pi(-k+1)$) of the metric $|\omega|$. This is evident by looking at local expansions but it is useful to show this by use of the developing map F given by

$$F(p) = \int_a^p \omega : M - \{p_1, \dots, p_n\} \rightarrow \mathbf{C},$$

where $\{p_1, \dots, p_n\}$ are the zeros and poles of ω . Values of F at a point p differ by periods of ω so we can pull back the flat metric on \mathbf{C} to a well-defined flat metric on $M - \{p_1, \dots, p_n\}$. (This gives another way to show that the metric is flat away from the poles and zeros of ω .) Near p_i , the surface M has a local chart in which ω takes the form $\omega = z^{k_i} dz$. If $k_i \neq -1$, then we can explicitly integrate to obtain that

$$F(z) = \frac{z^{k_i+1}}{k_i+1}$$

near p . Thus, p_i is a cone point with cone angle $2\pi(k_i+1)$.

In the previous paragraph, a cone metric was defined via metric expressions. As we shall see in Examples 2 and 3 below, they can also be pieced together from pieces of flat cones like C_k or C_e . The two methods of construction are related via the developing map. It is important to our approach to be able to pass freely between the two descriptions.

There is a natural version of the Gauss-Bonnet formula for cone metrics on a surface M with finite cone angles. Let γ_i be a small circle around p_i , $i = 1, \dots, n$. Then $\bigcup_{i=1}^n \gamma_i$ bounds a connected flat surface, M' , whose Euler characteristic is $2 - 2g - n$, where $g = \text{genus}(M)$. Each γ_i has total geodesic curvature on M' equal to $-2\pi k_i$. The Gauss-Bonnet formula for M' gives

$$(10) \quad \sum_{i=1}^n k_i = n + 2(g-1).$$

We will see in Proposition 3 below that there is an extension of this necessary condition to the case of cone metrics with exponential cone points of simple type.

Example 1. The cone metrics S_k . First let $k > 0$, and let M be the extended complex plane and $\omega = z^{k-1} dz$. The cone points of M with cone

metric $|\omega|$ are 0 and ∞ with cone angles $2\pi k$ and $-2\pi k$, respectively. From a constructive point of view, for $k \in (0, 1)$, let S_k be the infinite sector of angle $2\pi k$, with edges identified. When $k = 1$, let S_1 be the extended complex plane, equipped with the metric $|dz|$. This surface has a single cone point of cone angle -2π at ∞ . When $k > 1$, consider that sector to be a multiple covering of $\mathbf{C} - \{0\}$, with metric $|dz|$. If z is the variable in that plane, then for $w = \frac{1}{k}z^k$, we have $\omega = dw$. Note that S_k and S_{-k} are isometric with $z \rightarrow 1/z$ producing the isometry. Finally, for $k = 0$, we set the metric $\omega = \frac{dz}{z}$, and S_0 is an infinite cylinder.

Given two flat cone metrics, we can perform surgery to produce a third one. Let M_1 and M_2 be cone metrics and let $L_i \subset M_i, i = 1, 2$, be geodesics (straight lines) of the same length that do not pass through (but may terminate at) cone points. Join M_1 to M_2 along the L_i by identifying opposite edges of $M_1 - L_1$ to $M_2 - L_2$ in a manner that produces a surface with orientation consistent with the orientations of M_1 and M_2 .

The end points of the lines on the joined surface will, in general, be cone points with cone angles equal to the sums of the angles at the corresponding cone points of the M_i .

Example 2. Sewing an S_k into a cone metric, $k > 0$. Let M be a cone metric and L a straight line in M of infinite length, beginning at a point p of positive cone angle $2\pi k_p$ and terminating at a cone point, q , of nonpositive cone angle $2\pi k_q$. Sew in S_k to M along L by matching the positive real axis in S_k — joining 0 to ∞ — to L with 0 matched to p . The resulting cone metric will have cone points at p and q of cone angles $2\pi(k_p + k)$ and $2\pi(k_q - k)$, respectively (in addition to any other cone points of M).

This is an example of the process of grafting of projective structures (see e.g. [26] and [14].) See Figure 24, where S_{k-1} is grafted onto a flat torus. In that example, $k_p = 1$ and $k_q = -1$.

Example 3. Removing an S_k from a cone metric. Let M be a cone metric, $p \in M$ a point with cone angle $2\pi k_p$ with $k_p \geq k > 0$, and L_1 and L'_1 two rays of infinite length in M that satisfy the following properties: L_1 makes an angle of $2\pi k$ with L'_1 at p ; the lines L_1 and L'_1 terminate at the same point $q \in M$; the union $L_1 \cup L'_1$ bounds a simply connected region. Remove that region from M , with L_1 identifying L'_1 . The region removed is an S_k (a fact that can be seen easily or deduced from Proposition 4 below). The resulting cone metric has cone points at p and q of cone angles $2\pi(k_p - k)$ and $2\pi(k_q + k)$ respectively.

2.3.1. *Existence and uniqueness of cone metrics.* The next two propositions show that cone metrics are essentially determined by their cone points,

and that the Gauss-Bonnet condition (10) and its natural extension (11) are the only obstructions to existence. Here we aim to extend work of Troyanov [38] on cone metrics with positive and finite cone angles to the cases where the cone angles may be negative or of simple exponential type.

PROPOSITION 3. *Let M be a compact Riemann surface, $\{p_1 \dots p_r \dots, p_{r+\ell}\}$ a collection of distinct points, $r > 0$, $\ell \geq 0$. Suppose $\{a_1 \dots a_r\}$ is a collection of real numbers satisfying (11)*

$$(11) \quad \sum_{j=1}^r a_j = -(2 - 2\text{genus}(M)) + r + 2\ell.$$

Then there exists a cone metric on M with finite cone points p_j with cone angles a_j , $j = 1 \dots r$, and exponential cone points p_k , $0 \leq k \leq \ell$ of simple type.

In order to state the uniqueness theorem for cone metrics we must introduce the following definition.

Definition 4. Two exponential cone points of simple type with local representations $|e^{\frac{1}{w}} \frac{dw}{w^2}|$ and $|e^{\frac{1}{z}} \frac{dz}{z^2}|$ are asymptotically isometric provided $\frac{dw}{dz}(0) = 1$

PROPOSITION 4. *A cone metric on a compact Riemann surface with cone points with finite cone angles is determined up to scaling by the location of the cone points and their cone angles. The same result is true if one or more of the cone points is an exponential cone point of simple type, provided that the corresponding cone points are asymptotically isometric.*

The proofs of these propositions are given in Appendix B.

The hypothesis of “asymptotically isometric” cone points in Proposition 4 is necessary as the following example shows.

Example 4. *Cone metrics* with the same cone points and cone angles are not necessarily scalar multiples of one another. Consider on $S^2 = \mathbf{C} \cup \{\infty\}$ the family of cone metrics given by

$$\mu_\beta = \left| \frac{z+1}{z-1} \cdot \frac{z+2}{z-2} e^{\beta z} dz \right|,$$

$\beta > 0$. All of the cone metrics μ_β have cone points at ± 1 , ± 2 , and ∞ with cone angles -4π at $z = 1$ and $z = 2$, cone angles $+4\pi$ at $z = -1$ and $z = -2$, and an exponential cone point of simple type at ∞ . From the definition of μ_β it is evident that the cone point at ∞ of μ_{β_1} is asymptotically isometric to the cone point at ∞ of μ_{β_2} if and only if $\beta_1 = \beta_2$. For any choice of β , since $\mu_\beta|_z = \mu_\beta|\bar{z}$, any segment of the real axis is a geodesic. (In fact, the real axis is a length-minimizing geodesic between the cone points ∞ and -2 (and between -2 and -1) but we will not need to use this observation.) Even though the

cone points and angles are the same for all $\beta > 0$, we will show that these metrics are not all scalar multiples one of the other. Define

$$f(\beta) = \int_{-\infty}^{-2} \mu_\beta \quad \text{and} \quad g(\beta) = \int_{-2}^{-1} \mu_\beta.$$

It is straightforward to show that

$$0 < g(\beta) \leq \frac{e^{-\beta} - e^{-2\beta}}{\beta},$$

which implies that $\lim_{\beta \rightarrow 0} g(\beta) \leq 1$. Since $\lim_{t \rightarrow -\infty} \frac{t+1}{t-1} \frac{t+2}{t-2} = 1$ and $e^{\beta t} > \frac{1}{2}$ for $t > \frac{-\log 2}{\beta}$, it follows that $\lim_{\beta \rightarrow 0} f(\beta) = \infty$. Now suppose that the conclusion of Proposition 4 is true for the metrics μ_β . Then

$$\mu_\beta = c(\beta)\mu_1$$

for some positive, real-valued function $c(\beta)$. Moreover, since $f(\beta)$ is the length of $(-\infty, -2)$ in the μ_β metric and $g(\beta)$ is the length of $(-2, -1)$ in the μ_β metric, we would have

$$\frac{f(\beta)}{f(1)} = c_\beta = \frac{g(\beta)}{g(1)}.$$

But we have shown that $f(\beta)$ diverges as $\beta \rightarrow 0$, and that $g(\beta)$ is bounded as $\beta \rightarrow 0$. Hence, it is not possible that all the μ_β metrics agree up to a scalar stretch factor.

2.4. The exponential cone as the limit of S_k as $k \rightarrow \infty$. In our construction of the surfaces \mathcal{H}_k in Section 4, we will sew the cone metrics S_k into a torus and let $k \rightarrow \infty$, with the expectation that the limit corresponds to the creation of an exponential cone point of simple type. We will show here that the limit of S_k as $k \rightarrow \infty$ (in an appropriate sense of limit) is a cone metric on the sphere with one exponential cone point of simple type.

Let z be the variable on S_k (considered as a multisheeted sector with $|\theta| \leq k\pi$ in the $z = re^{i\theta}$ -plane), and let $z = z(w) = (1 + \frac{w}{k})^k$. The metric $|dz|$ on S_k with cone points at 0 and ∞ is isometric to the cone metric $|(1 + \frac{w}{k})^{k-1} dw|$ on $\mathbf{C} - \{-k\}$, whose cone points at $w = -k$ and $w = \infty$ have cone angles $2\pi k$ and $-2\pi k$, respectively. As $k \rightarrow \infty$, these metrics on $\mathbf{C} - \{-k\}$ tend to $|e^w dw|$ uniformly on compact subsets.

We understand convergence of metric spaces here as relative to a fixed base point; in this case, we take the origin as the fixed point for each S_k . Note that this point corresponds to $z = 1$. The point $w = 1$ corresponds to a point in S_k that is converging in the $|dz|$ metric to e . Then the uniform convergence of the metrics on compacta, and the choice of the origin as fixed for all k , means that we may regard the point $w = 1 \in \mathbf{C}$ as the limit of a bounded sequence of points p_k in S_k .

Consider the annulus in \mathbf{C} that is centered at the origin and has inner radius $1 + \frac{1}{2}$ and outer radius $k - \frac{1}{2}$. This annulus separates the pair of points $\{0, 1\}$ from the pair of points $\{-k, \infty\}$. The modulus of this annulus (see Definition 6) is equal to $\frac{1}{2\pi} \log \frac{2}{3}(k - \frac{1}{2})$, which goes to infinity with k . From this it follows from Proposition 5 in Section 2.5 that the extremal length of the class of curves that separate these pairs of points goes to zero as $k \rightarrow \infty$. This shows that the points $-k$ and ∞ “coalesce” as $k \rightarrow \infty$. What we mean by this is explained in the next subsection in Remark 2. We consider two types of limits of the spaces $\{S_k\}$: the conformal limit of the punctured Riemann surfaces $\mathbf{C} - \{-k, \infty\}$ and the (metric) limit of the metric spaces S_k . The analysis above shows that the conformal limit is $\mathbf{C} \cup \{\infty\}$ with a distinguished point at ∞ , and the metric limit is $|e^w dw|$ uniformly on compacta. This implies that, metrically, the spaces S_k limit on the sphere $\mathbf{C} \cup \{\infty\}$ with a single cone point of simple exponential type at ∞ .

Remark 1. (i) Pulling back the metric on S_k to the strip $|Im\zeta| < k$ by the map $z = \log \zeta$, one can consider the metric $|e^\zeta d\zeta|$ on the strip to be a representation of S_k with cone points at $Re\zeta = -\infty$ and $Re\zeta = +\infty$ corresponding to the cone points 0 and ∞ in the “ z model” of S_k . As $k \rightarrow \infty$, the metric converges to $|e^\zeta d\zeta|$ on the entire complex plane. The argument using extremal length can be repeated here to show that the strips converge to a cone metric with one cone point at infinity.

(ii) We note here that there is a difference between the exponential cone points and the cone points with finite cone angle. In any cone metric, cone points with finite *positive* cone angles have neighborhoods where the metric is precisely equivalent to the metric on a Euclidean cone, so that every curve from a regular point to such a cone point has finite length. However, every curve that goes from a regular point to a cone point with a finite, *nonpositive* cone angle has infinite length. In particular, a cone metric with all cone angles finite defines a complete metric space on the underlying Riemann surface with the nonpositive cone points removed; each such point corresponds to an end and the metric-space topology is identical to the topology of the underlying punctured Riemann surface.

The situation is not the same in the presence of cone points of simple exponential type. Consider the extended complex plane with metric $|e^\zeta d\zeta|$, a cone metric with one cone point of simple exponential type at ∞ . Horizontal curves of the form $\{t + iy_0 | t < t_0\}$ have finite length while those of the form $\{t + iy_0 | t > t_0\}$ have infinite length. If the point at infinity is removed, the metric is not complete. If it is left on the surface, then the metric is complete but defines a topology that is not the same as the topology of the Riemann sphere: for example, the sequence of positive integers eventually leaves any neighborhood of ∞ .

2.5. *Preliminaries on extremal length.* We will make use of arguments using extremal lengths, and so we record the basics of this subject in this subsection.

Extremal length assigns a conformal invariant $\text{Ext}_{\mathcal{R}}(\Gamma)$ to a set of curves Γ on a Riemann surface \mathcal{R} . A flexible tool for distinguishing conformal structures, extremal length is especially useful when the set of curves Γ is the free homotopy class of a simple closed curve. For such a class of curves, there are two equivalent definitions of the extremal length $\text{Ext}(\Gamma)$, with one definition naturally suggesting lower bounds and the other definition naturally suggesting upper bounds. We can often use this principle to obtain good estimates (see e.g. [32]) for the asymptotics of $\text{Ext}_{\mathcal{R}}(\Gamma)$ in many situations under which \mathcal{R} degenerates, sending $\text{Ext}_{\mathcal{R}}(\Gamma)$ to zero or infinity.

We begin with the general definition.

Definition 5 (Analytic). Let Γ be a set of curves on a Riemann surface \mathcal{R} . Then

$$\text{Ext}_{\mathcal{R}}(\Gamma) = \sup_{\rho} \frac{\inf_{\gamma \in \Gamma} [\ell_{\rho}(\gamma)]^2}{\text{Area}(\rho)},$$

where the supremum is taken over measurable conformal metrics $\rho|dz|^2$ on \mathcal{R} , the notation $\ell_{\rho}(\gamma) = \int_{\gamma} \sqrt{\rho}$ refers to the ρ -length of a curve $\gamma \in \Gamma$ on \mathcal{R} , and $\text{Area}(\rho) = \iint_{\mathcal{R}} \rho$ is the ρ -area of \mathcal{R} .

Example 5. Let \mathcal{R} be the annulus $A(r_1, r_2) = \{r_1 < |z| < r_2\}$ in the plane, and let Γ consist of all curves freely homotopic to the core curve $\{|z| = \frac{r_1+r_2}{2}\} \subset A(r_1, r_2)$. Then a simple length-area argument [1] shows that $\text{Ext}_{\mathcal{R}}(\Gamma) = \frac{2\pi}{\log(r_2/r_1)}$.

Definition 6. The number $\frac{1}{2\pi} \log(r_2/r_1)$ is known as *the modulus mod $A(r_1, r_2)$ of the annulus $A(r_1, r_2)$* .

This leads to the second definition of extremal length in the case that Γ is a free homotopy class of curves, all of whose members are freely homotopic to a simple closed curve on \mathcal{R} .

Definition 7 (Geometric). The extremal length $\text{Ext}_{\mathcal{R}}(\Gamma)$ of a curve system $\Gamma \subset \mathcal{R}$ is defined to be

$$\text{Ext}_{\mathcal{R}}(\Gamma) = \inf_{A \subset \mathcal{R} \text{ mod } A} \frac{1}{\text{mod } A}$$

where the infimum is taken over all conformal embeddings of annuli A into \mathcal{R} which take the core curve of A into some $\gamma \in \Gamma$.

It is an important result (see [35]) that

PROPOSITION 5. *The geometric and analytic definitions of extremal length coincide.*

Naturally, if we are interested in lower bounds for extremal length, we compute $\inf_{\gamma \in \Gamma} [\ell_\rho(\gamma)]^2 / \text{Area}(\rho)$ for a specific conformal metric ρ on \mathcal{R} , and obtain a lower bound on $\text{Ext}_{\mathcal{R}}(\Gamma)$. On the other hand, if we are interested in upper bounds, we compute the modulus of some specific annulus embedded in \mathcal{R} with core curve homotopic to Γ , and obtain an upper bound on $\text{Ext}_{\mathcal{R}}(\Gamma)$.

Remark 2. In many of our applications, we will wish to show that a sequence of pairs of points, say $\{p_n, p'_n\}$, “coalesce” to a single point p_∞ . Conformally, this means that the set Γ , of curves which encircle p_n and p'_n , have arbitrarily small extremal length, i.e. the neck linking a neighborhood of p_n and p'_n is pinching off as $n \rightarrow \infty$. In this case, by the geometric definition of extremal length, it is then enough to show that there is a sequence of annuli A_n with $\text{mod } A_n \rightarrow \infty$ so that A_n can be conformally mapped into \mathcal{R} in a way that disconnects a disk containing p_n and p'_n from the rest of \mathcal{R} .

2.6. *The helicoid in terms of cone metrics.* We conclude the background discussion by presenting the helicoid from the point of view of cone metrics. From (9), we have for the helicoid, \mathcal{H} , modulo the screw motion σ_k :

$$gdh = kz^{k-1}dz, \quad \frac{1}{g}dh = \frac{-k dz}{z^{k+1}}$$

on $\mathbf{C} - \{0\}$ with ends at 0 and ∞ . We may consider these forms to be defined on the cone metrics S_k and S_{-k} respectively. They are related by the inversion $z \rightarrow \frac{1}{z}$, so we may consider them both to be defined on the same domain. This is precisely the local expression of the form that produces the metrics on S_k and S_{-k} defined in Example 1 in Section 2.3.

We may run this discussion backwards to construct \mathcal{H}/σ_k from cone metrics. Both S_k and S_{-k} are defined on the extended plane. We may develop (isometrically) both of these metrics onto the Euclidean plane. If we pull back the naturally defined one-form, say dw , from that Euclidean plane to the original extended plane, we obtain two one-forms we may use to define gdh and $\frac{1}{g}dh$, respectively. Straightforward integration of (5) gives, as in Section 2.2, $x_1 + ix_2 = \frac{1}{2}(z^k - \bar{z}^{-k})$. Moreover,

$$dh^2 = gdh \cdot \frac{1}{g}dh = -\frac{k^2 dz^2}{z^2},$$

so that $dh = \frac{\pm ik dz}{z}$; thus we may recover the third component of \mathcal{H}/σ_k from these data. Also

$$g^2 = gdh / (\frac{1}{g}dh) = -z^{2k},$$

so the Gauss map $g = \pm iz^k$ may also be recovered from this data.

We showed in the previous section that S_k converges, as $k \rightarrow \infty$, to a cone metric with a single exponential cone point of simple type. Following the



Figure 7: A fundamental domain of \mathcal{H}_1 can be imagined qualitatively as a region of the helicoid bounded by two horizontal lines between which the helicoid turns by an angle of 2π and in the middle of which there is a handle. Illustrated here is one-half of the fundamental domain; this half is on the side of the vertical plane that contains the vertical axis and the two horizontal lines. The other half of the fundamental domain is produced by reflection through the vertical axis. The boundary lines, top and bottom, are identified in the quotient as a single line. The only other line, besides the vertical axis, that survives the surgery necessary to insert the handle is a horizontal line in the middle, at the level of the handle. The normal symmetry line L is not illustrated here but can be easily visualized as the horizontal line perpendicular to the vertical and horizontal line through the center point. (See [23].)

procedure there gives a global representation of the limit of the cone metric representation for \mathcal{H}_k/σ_k , yielding a representation of the defining Weierstrass data of the helicoid by $gdh = e^z dz$ and $\frac{1}{g}dh = -e^{-z} dz$.

2.7. *Symmetries of the \mathcal{H}_k .* We conclude this section with a derivation of the symmetry properties and the conformal structure of the surfaces \mathcal{H}_k modulo σ_k . We assume properties (i)–(iii) of (4), which are the defining properties of the \mathcal{H}_k , whose existence is asserted by Theorem 3. The results of this subsection are collected in the lemma at the end of the discussion.

From the assumptions (4), we know that the periodic surface is invariant under a vertical screw motion, σ_k , of angle $2\pi k$, and that it contains a vertical axis. By the Schwarz Reflection Principle, which states that if a minimal surface contains a straight line then it is invariant under 180° -degree rotation about that line, the surface is invariant under 180° -degree rotation about the vertical axis. In each fundamental domain (a region of the surface that generates the whole surface by the action of σ_k), there are by assumption, two parallel horizontal lines. It is easy to see that—under the assumption that the surface is singly periodic but not doubly or triply periodic—the horizontal lines meet the vertical axis. To see this, recall that successive reflection in two distinct lines in R^3 results in a Euclidean motion with the following properties: its translational component is in the direction of the segment of shortest

length between the lines; its rotational component has this direction as axis and rotation angle equal to twice the angle between the lines. If either line does not intersect a third, say vertical, axis, then the surface is invariant under a Euclidean motion with a nonzero horizontal translational component. Since we have assumed the existence of a vertical translation T , this contradicts our assumption of single-periodicity. In addition, if there were another nonhorizontal line on the surface, then the surface would be invariant under a screw motion along the line connecting the vertical axis to that fourth line: thus the surface would be invariant under a nonvertical screw motion, which is also a contradiction.

Consider two consecutive horizontal lines, L_0, L_1 , on the surface with L_0 above L_1 . The pair of lines $L_0, \sigma_k L_0$ bounds a domain, say S , and by hypothesis L_1 must be the only horizontal line in the interior of S . Let μ_i denote reflection in the line L_i . If $\mu_1 L_0$ lies strictly below $\sigma_k L_0$, then $\mu_1 L_0 = L_1$ or $L_0 = \mu_1 L_1 = L_1$, a contradiction. If $\mu_1 L_0$ lies strictly above $\sigma_k L_0$, then $\mu_1 L_0$ and $\sigma_k L_1$ lie in the interior of $\sigma_k S$ and therefore must be the same line. We then have $\mu_1 L_0 = \sigma_k L_1$, or $L_0 = \mu_1 \sigma_k L_1$, a contradiction since $\mu_1 \sigma_k L_1$ lies in the interior of $\sigma_k^{-1} S$. Thus $\mu_1 L_0 = \sigma_k L_0$. In particular, L_0 and L_1 are separated by a vertical distance πk . Moreover since $\mu_1 \sigma_k$ is an orientation-reversing symmetry of our surface that fixes L_0 , it follows that $\mu_1 \sigma_k = \mu_0$, that is, $\mu_1 = \mu_0 \pmod{\sigma_k}$.

Successive reflection in the vertical axis and a horizontal line on the surface that meets the axis at a point p , produces a reflection in the horizontal line through p that is normal to the surface at p . Call this line L . Reflection in L is referred to as a *normal symmetry* of the surface. Modulo σ_k , this is the same symmetry no matter which horizontal line is chosen.

Reflection in the vertical axis is an involution of the minimal surface, which leaves height unchanged and fixes pointwise the vertical axis. Its fixed-point set on the quotient surface consists precisely of those points that get mapped to the vertical axis, a connected set. The normal symmetry around L fixes a point on the vertical axis and leaves the vertical axis invariant. In the quotient surface, the normal symmetry fixes *two* points on the vertical axis, the points where the horizontal lines meet the vertical axis: this follows because the normal symmetry acts as an isometry on the segment of the vertical axis in one fundamental domain of the surface. Hence as it inverts this segment about the point where the line L meets the axis, it fixes exactly that intersection point and the (end)point at distance $2\pi k$ along the segment.

By hypothesis, the quotient surface is a torus, and we may model it as the region bounded by a parallelogram in the complex plane, with opposite edges identified. (When we refer to a "parallelogram," we will mean the closed region bounded by a quadrilateral with opposite sides parallel, or, depending on the context, the Riemann surface of genus one produced by identifying the

opposite edges of its boundary.) The normal symmetry fixes two points on the vertical axis. Without loss of generality, we assume that one of those points corresponds to the center of the parallelogram. We label the center \mathcal{O} .

On the torus, there is a holomorphic one-form with no zeros. Up to scaling, this one-form is equal to the one-form that descends to the parallelogram from the one-form dz on the complex plane. We will also refer to this one form as dz . Let ρ be the involution on the quotient surface that is induced by the normal symmetry. Let r be 180°-rotation about the center of the parallelogram, also an involution of the torus. Both $\rho^*(dz)$ and $r^*(dz)$ are zero-free holomorphic one-forms and so must agree up to a scalar multiplicative factor. Since they are involutions that fix the center point, $r^*(dz) = -dz = \rho^*(dz)$ at that point. Hence $r^*(dz) = \rho^*(dz)$ everywhere, which implies that $\rho = r$.

Let μ_v be the (anticonformal) involution of the parallelogram corresponding to the involution of the quotient surface produced by reflection in the vertical axis. We know that the fixed-point set of μ_v is a connected curve that passes through the center of the parallelogram. We look at the action of μ_v near the center point of the parallelogram. If W is the line through the center point of the parallelogram that is tangent to the fixed-point set of μ_v , let r_W be reflection across W in the complex plane. At the center, $\mu_v^*(dz) = \lambda(d\bar{z}) = r_W^*(dz)$, for some complex number λ , $|\lambda| = 1$. As in the previous paragraph, we can conclude $\mu_v^*(dz) = r_W^*(dz)$ and hence that $\mu_v = r_W$ near the center, hence everywhere. In particular, we have shown that reflection in the line W is an involution of the parallelogram. This implies that the parallelogram is either a rhombus with a diagonal on W , or a rectangle with a side parallel to W . But we know that the fixed-point set of μ_v is connected, which implies that the parallelogram is a rhombus.

Rotate the rhombus if necessary so that the diagonal on W is a vertical line segment. We will refer to this diagonal as the vertical diagonal. Reflection in the other diagonal of the rhombus is equal to $\mu_h := \mu_v \circ \rho$, and so must correspond to the reflection in the horizontal lines of the quotient surface. Since this diagonal represents both lines and since the lines diverge, the punctures at the ends must appear on this diagonal. We will denote the end punctures by E_1 and E_2 . Because r leaves $\{E_1, E_2\}$ invariant—in fact, it interchanges E_1 and E_2 —they must be symmetrically placed with respect to \mathcal{O} .

The careful reader will note that we have specified \mathcal{O} to correspond to one of the two points where a horizontal line on the surface meets the vertical axis. The rotation r by 180°-degrees about \mathcal{O} fixes four points; the center, the vertex, and the two half-periods. Since r corresponds to the normal symmetry, and $r \circ \mu_v$ corresponds to reflection in the horizontal lines, the two off-vertical-axis fixed points of r must lie on the same horizontal line. *Without loss of generality, we may assume that it is this horizontal line that crosses the axis at \mathcal{O} .* We collect the above discussion as

LEMMA 1. *The defining properties (4)(i)–(iii) of the surfaces \mathcal{H}_k of Theorem 3 imply that*

- (iv) *The horizontal lines on \mathcal{H}_k meet the vertical axis. Two successive horizontal lines are separated by a vertical distance of πk . Composition of rotation about two successive lines is a vertical screw motion σ_k , which descends to the identity transformation on \mathcal{H}_k/σ_k . Rotation by 180° about one of the horizontal lines is a symmetry of the surface that descends to an involution of quotient surface, and that involution does not depend on the choice of horizontal line.*
- (v) *Rotation by 180° about the vertical axis is a symmetry of \mathcal{H}_k . The composition of this rotation with rotation about a horizontal line on the surface is rotation by 180° around a line orthogonal to the axis and the horizontal line. These order-two symmetries—referred to as a normal symmetries—induce the same involution on the quotient surface of \mathcal{H}_k/σ_k .*
- (vi) *The quotient surface of \mathcal{H}_k/σ_k has the conformal structure of a rhombic torus with two punctures. Without loss of generality, we may assume this rhombus: is conformally modelled by the domain bounded by a rhombus in the plane with opposite edges identified; and is oriented so that the one of the diagonals is vertical, the other horizontal; the vertical diagonal is mapped into the vertical axis; the horizontal diagonal is mapped onto the horizontal lines of \mathcal{H}_1 . In particular, the two punctures—corresponding to ends—occur on the horizontal line, and they are symmetrically placed with respect to the origin. They separate it into segments mapped to the two different horizontal lines.*
- (vii) *On the rhombus, the reflection μ_v in the vertical axis corresponds to 180° -rotation about the axis of \mathcal{H}_k . The reflection μ_h in the horizontal diagonal corresponds to 180° -rotation around a horizontal line of \mathcal{H}_k . The 180° -rotation, $r = \mu_v\mu_h$, about the center, \mathcal{O} , of the rhombus corresponds to the normal symmetry of the quotient surface. Two of the fixed points of r , namely \mathcal{O} and the vertex of this rhombus, correspond to the two points in the quotient of \mathcal{H}_k/σ_k where the horizontal lines cross the vertical axis. The two other fixed points of r lie at the half-period points and correspond to two off-axis fixed points of the normal symmetry. These points lie at the same height as one of the on-axis fixed points: without loss of generality, we may assume that they lie at the same height as the point corresponding to \mathcal{O} .*

3. The singly periodic genus-one helicoid

We give a new proof of the existence of the surface \mathcal{H}_1 of Theorem 2 in Section 1.3. The alternative construction presented here is due to Weber [39],

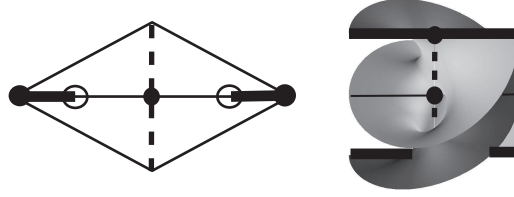


Figure 8: The conformal structure of \mathcal{H}_k/σ_k is a rhombic torus punctured in two points. The vertical diagonal (represented here by a vertical dashed line) corresponds to the vertical axis. The horizontal diagonal corresponds to *two* horizontal lines, represented here by two line segments of different thicknesses. The thinner one crosses the vertical diagonal at the center of the rhombus. The thicker one crosses the vertical diagonal at the vertex. Note that in the computed image of the surface there are two thick horizontal lines, one on top, the other on the bottom. In the quotient, these are the same line. The symmetries of the rhombic torus—reflection in the vertical diagonal and the horizontal diagonal—correspond to Schwarz reflection in the vertical axis and the horizontal lines on \mathcal{H}_k/σ_k , respectively. The thin and thick horizontal line segments in the rhombus meet at two points corresponding to the punctures in the torus. These punctures correspond to the ends of \mathcal{H}_k/σ_k . The two circles that surround the puncture points at the ends correspond to the two helicoidal edges in the computed image.

and is key to the proof of the existence of the \mathcal{H}_k of Theorem 3 in Sections 4 and 5. It is in this section that the transformation of the problem from an analysis of forms and functions on Riemann surfaces to geometric manipulation of singular flat structures is most clearly displayed. The existence and embeddedness of \mathcal{H}_1 was originally proved in [19].

In 3.1, we derive necessary conditions for the Weierstrass data of \mathcal{H}_1 that are sufficient to specify them uniquely. Together with a real parameter that gives us the underlying rhombic torus, this determines not only the Riemann surface structure of the quotient surface but also the Weierstrass data g (up to a unitary multiplicative factor) and dh (up to a positive real multiplicative factor). (Geometrically, the surface is determined up to a rotation about the vertical axis and a scaling in \mathbf{R}^3 . If we make the reasonable assumption that the horizontal lines on the surface are parallel to the x_2 -axis, and that the translational symmetry of the surface is generated by a vertical translation of length 2π , then the Weierstrass data are completely determined.)

In Section 3.2, we formulate the period problem for \mathcal{H}_1 and state the main results of [19], namely that there exists a choice of parameters that solve the period problem. Any such choice produces a minimal surface that has all the required properties of Theorem 2 in Section 1.3, including the property of embeddedness. It is instructive to prove the existence of \mathcal{H}_1 using the methods

here because of the relevance of the methods to the construction of the surfaces \mathcal{H}_k in Section 4.

In Sections 3.3–3.4 we present an alternative proof of the results of Theorem 2 (excluding embeddedness). We begin in Section 3.3 by showing that the properties of the Weierstrass data derived in Section 3.1 uniquely determine the rhombic torus. This means that there is in fact only one parameter in the Weierstrass data: the position of the ends. Next we construct this special torus, which we call \mathcal{T}_1 , by cone-metric methods. This method actually determines not only the torus but also the one-form gdh . For any placement of the ends on \mathcal{T}_1 , we use a symmetry construction to produce a candidate for $(1/g)dh$ for which the horizontal period problem is *automatically solved*. In Section 3.4, we then show that there is a placement of the ends for which the vertical period problem is also solved.

3.1. *The Weierstrass data: derivation from geometric assumptions.* We want a singly periodic, properly immersed, minimal surface with the properties 3(i)–3(iii) of Theorem 2 in Section 1.3. Namely, \mathcal{H}_1 modulo translations has the properties stated in (3):

- (i) \mathcal{H}_1 has genus one and two ends,
- (ii) \mathcal{H}_1 is asymptotic to a full 2π -turn of a helicoid, and
- (iii) \mathcal{H}_1/σ_1 contains a vertical axis and two horizontal parallel lines.

See Figure 4, Section 1, for an image of this surface.

We will now assume that such a surface exists and derive its Weierstrass data.

3.1.1. *The Gauss map and the placement of the ends.* The total curvature of the quotient surface, $M = \mathcal{H}_1/\sigma_1$, is $2\pi(\chi(M) - W(M))$, where $\chi(M)$ is the Euler characteristic of M and $W(M)$ is the total winding number at the punctures [24]. We know that M is a twice-punctured torus so that $\chi(M) = -2$; further, each end is, by assumption, asymptotic to a single full turn of the helicoid, and so $W(M) = 2$. Hence, the total curvature of M is equal to -8π . This implies that the the degree of the Gauss map is equal to two.

The assumption (iii) that each end is asymptotic in the quotient to a single full turn of the helicoid forces us to assume, according to (9), that the Gauss map is vertical at the ends. Let g be the stereographic projection of the Gauss map, defined on the underlying Riemann surface. Since the degree of the Gauss map is two, there must be one other point where $g = 0$ and one other point where $g = \infty$. According to Lemma 1,(vi) and (vii), the underlying Riemann surface may be modelled by a rhombic domain, and reflection in the diagonals of that rhombus correspond to rotation by 180° about the lines on \mathcal{H}_1 . These rotations are orientation-reversing and preserve verticality. Therefore, the reflections in the diagonal preserve verticality and

so must leave the collection of poles and zeros of g invariant. If g has a zero or pole that is not on the diagonals of the rhombus, then it has *at least* two zeros and two poles not on the diagonals, in addition to the two ends that are located on the horizontal diagonal. This implies that the degree of g is at least three, contradicting the fact that the degree of g is two. Hence the other points where $g = 0$ or $g = \infty$ lie on the diagonals. Since the vertical diagonal corresponds to the vertical axis, we require the Gauss map to be horizontal there: $|g| = 1$ on the vertical diagonal. We conclude that the other two vertical points of the Gauss map lie on the horizontal diagonal.

Label the ends E_1 and E_2 and the vertical points V_1 and V_2 . Since reflection in the vertical diagonal corresponds to the orientation-reversing symmetry of rotation about the vertical axis, a symmetry that preserves verticality of the Gauss map, the pair of ends and the pair of vertical points must be symmetrically placed with respect to the center, \mathcal{O} , of the rhombus.

For the remainder of Section 3, we will assume that the length of the horizontal diagonal is two, that \mathcal{O} is placed at the origin of \mathbf{C} , and that E_1 lies to the left of \mathcal{O} . Then we may write

$$\begin{aligned} E_1 &= -b, & E_2 &= b, \\ V_1 &= -a, & V_2 &= a, \end{aligned}$$

for some real numbers, $0 < a, b < 1$, the strict inequality is required in order to have two ends and two vertical points. Also, we require $a \neq b$ to prevent the ends from coinciding with the finite points. Without loss of generality, we may also assume that the surface is oriented so that $g(E_1) = \infty$ (and therefore $g(E_2) = 0$).

Either $g(V_1) = \infty$ and $g(V_2) = 0$ or $g(V_1) = 0$ and $g(V_2) = \infty$. Applying Abel's theorem to g yields $|a - b| = 1$ in the first case and $a + b = 1$ in the second case. The first case is impossible because $0 < a, b < 1$. Therefore $g(V_1) = \infty$ and $g(V_2) = 0$ and

$$a + b = 1.$$

We have now determined the divisor of g . (See Figure 9). The points E_i, V_i are symmetrically placed with respect to the quarter points of the horizontal diagonal. (For *any* degree-two elliptic function, the branch points are symmetrically placed with respect to the zeros and poles of the function.) Also, the branch points must be symmetric with respect to the symmetries of the surface. We conclude from this that the quarter points of the horizontal diagonal are branch points of g and that there are two symmetrically placed branch points of g on the vertical diagonal: in fact they are also the quarter points.

We will assume that the surface is rotated so that its normal vector at \mathcal{O} is $(1, 0, 0)$: that is, $g(\mathcal{O}) = 1$. This rotation makes the horizontal lines parallel to the x_2 -axis.

	E_1	V_1	V_2	E_2
dh	∞	0	0	∞
g	∞	∞	0	0
gdh	∞^2	*	0^2	*
$\frac{1}{g}dh$	*	0^2	*	∞^2

Figure 9: The divisors of g , dh , gdh and $\frac{1}{g}dh$.

Remark 3. At this point, our specification of Weierstrass data depends on the choice of rhombic torus and a choice of b between 0 and 1 to place the ends E_i . We will see in Section 3.1.2 that dh is determined by these choices. We note that we have not specified whether or not $a < b$, i.e. whether or not the vertical points lie on the line that passes through the image of \mathcal{O} . We do not at this point have the freedom to assume one way or the other. It turns out that, in fact, $a < b$, and the V_i lie closer to \mathcal{O} than do the E_i . This is the result of a computation (see Proposition 6, Statement 3) that shows that the period problem *cannot be solved if $b > a$* .

3.1.2. *The one-form dh .* The expression (6), for the induced metric on M show that dh has simple zeros at the vertical points V_i . Because we want the ends to be helicoidal, we require dh to have simple poles at the ends E_i . (See Section 2.2 and Figure 6.) The one-form dh can have no other poles or zeros. Hence we know the divisor of dh . Because we require the horizontal diagonal to be mapped into horizontal lines, dh must be purely imaginary on the horizontal diagonal. This determines dh up to a real scalar factor, which corresponds to scaling the surface in \mathbf{R}^3 .

3.2. *The period problem.* In Section 3.1, we specified a Weierstrass representation for \mathcal{H}_1 which was forced by the geometric conditions 4(i)–(iii) of Theorem 2 in Section 1.3. The underlying torus is rhombic and the ends are placed on one of the diagonals. The divisors of g and dh are determined. The situation is encapsulated in Figure 9. The function g is then completely determined by the condition that $g = 1$ at the center of the rhombus, and the one-form dh is determined up to a real scaling (We could of course determine that factor by the condition imposed by Theorem 2 and (5), that $\text{Re} \int dh = 2\pi$ on the vertical diagonal, but we do not do that at this time.)

We still have to impose the period conditions (7) and (8). In Figure 11, the indicated cycles B and β , together with their reflections in the vertical axis, generate a homology basis for M . The nonzero translational period we require to produce a singly periodic surface will be evident on the cycle β that surrounds an end. By the symmetry we have imposed upon the Weierstrass representation, we need only consider these two cycles. The horizontal and

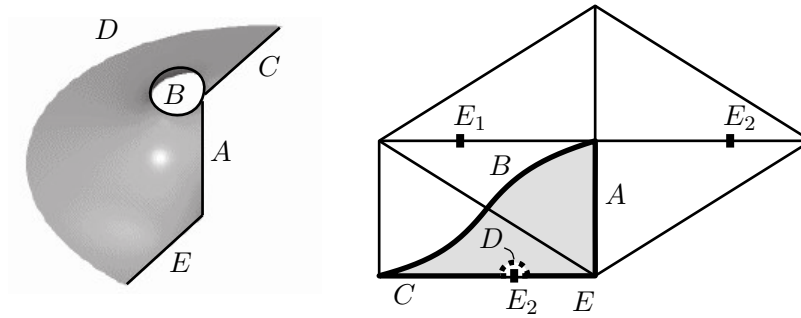


Figure 10: One quarter of a fundamental domain of \mathcal{H}_1 modulo translation is illustrated on the right. It is bounded by a vertical line segment, two horizontal line segments, a portion of a curve that approximates part of a turn of a helix, and a closed loop that is a closed cycle on the quotient torus. On the right the associated region of a rhombic torus is drawn, the desired image of which is the minimal surface on the left. Corresponding curves in the two images are similarly labelled. Note that the curve B is drawn to pass through a fixed point of 180° -rotation about the center of the rhombus. On the minimal surface, this point is a fixed point of the *normal symmetry* described in Lemma 1(vii) of Section 2.7.

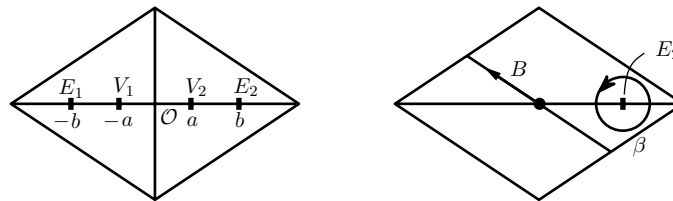


Figure 11: The rhombus model for the underlying Riemann surface of the quotient surface of \mathcal{H}_1 modulo translations is drawn on the left. The vertical points, V_i and the horizontal points, E_i , on the horizontal diagonal are included. The cycles β and B , illustrated on the right, and their reflections in the vertical diagonal, generate a homology basis for the punctured torus.

vertical period conditions for \mathcal{H}_1 can be written as follows:

$$(12) \quad \int_B g dh = \overline{\int_B \frac{1}{g} dh}, \quad \text{and}$$

$$(13) \quad \operatorname{Re} \int_B dh = 0.$$

3.2.1. *Existence of \mathcal{H}_1 .* The following result, translated into the terminology used here, is proved in [19].

PROPOSITION 6 ([19]). *Every regular, complete, periodic minimal surface satisfying the conditions of Theorem 2 (stated in (3)) may be represented by Weierstrass data that satisfies all of the conditions described in the table of Figure 9 in Section 3.1. Conversely,*

1. *For any rhombic torus and any $b \in (0, 1)$, there exist Weierstrass data $\{g, dh\}$ on a rhombic torus with ends and vertical points determined by the choice of b as in Section 3.1.1, whose divisors are specified in the table of Figure 9. The Weierstrass integral (5) produces a multivalued, regular, minimal and complete immersion of this punctured torus into \mathbf{R}^3 with all the required symmetry properties of Lemma 1;*
2. *The immersion described in Statement 1 above will be singly periodic if and only if the Weierstrass data satisfy (12) and (13). The translational period T is determined to be the vertical vector $(0, 0, c)$ where*

$$\pm c = \int_{\beta} dh = 2\pi i \operatorname{Res}_{E_i} dh;$$

3. *The period conditions (12) and (13) cannot be satisfied unless $\frac{1}{2} < b < 1$. In particular, $1 - b = a < b$. Thus it is necessary that the vertical points, V_i , be located (as illustrated in Figure 9) closer to the center, \mathcal{O} , than the end points E_i .*

This proposition is proved in Section 1 of [19]: see page 259. How Theorem 2 is proved from Proposition 6 we outline in the following remark.

Remark 4. One can establish the existence of \mathcal{H}_1 in two steps. These are carried out in Section 2 of [19].

Rhombic tori may be parametrized by a single real variable, say ρ . On such a torus, a choice $b \in (0, 1)$ determines the placement of the ends and the Weierstrass data (g, dh) satisfying the specifications in the table of Figure 9. This is the content of Statement 1 of Proposition 6. In the first step, it is shown that there is an open interval, I , of values of ρ so that, outside of I , no

choice of b will satisfy the vertical period condition (13), and inside of I , there exists a unique choice of $b = b(\rho)$ for which (13) is satisfied. Moreover $b(\rho)$ depends smoothly on ρ .

Equation (12) can be considered to define a smooth function $F(\rho, b) = \int_B gdh - \int_B \frac{1}{g}dh$, whose zeros occur at Weierstrass data that satisfy the horizontal period condition. In the second step it is shown that $f(\rho) = F(\rho, b(\rho))$ changes sign on I , and hence has at least one zero. This gives the existence of an \mathcal{H}_1 in Theorem 2.

Embeddedness of \mathcal{H}_1 is proved by a separate argument (in Section 3 of [19]) as is almost always the case in these matters. See [13] for an alternative argument.

In the next section, it will be shown that the form of the Weierstrass data and the horizontal period condition *determine the conformal structure*. Putting that together with the Remark above will show that the singly periodic genus-one helicoid is unique. See Proposition 8.

3.2.2. *The rhombic torus \mathcal{T}_1 and the uniqueness of \mathcal{H}_1 .* We assume that the Weierstrass data for \mathcal{H}_1 has divisors described in Figure 9 and that the zeros and poles are symmetrically placed along a diagonal of a rhombus. Note that the divisors of gdh and $\frac{1}{g}dh$ each have one double zero and one double pole (with no residue) on a diagonal, and no other zeros or poles. Since the torus is a group, it follows that the divisors of gdh and $\frac{1}{g}dh$ differ by a translation. Hence

$$gdh = ct^* \left(\frac{1}{g}dh \right),$$

for some translation, t , of the torus and nonzero constant c . Then, for any closed curve α on the torus, we have

$$(14) \quad \int_{\alpha} gdh = c \int_{\alpha} t^* \left(\frac{1}{g}dh \right) = c \int_{t^{-1}(\alpha)} \frac{1}{g}dh = c \int_{\alpha} \frac{1}{g}dh,$$

the last equality following because the form $\frac{1}{g}dh$ has no residue. If $\{\alpha_1, \alpha_2\}$ is a basis for the homology of the torus, then

$$r := \frac{\int_{\alpha_1} gdh}{\int_{\alpha_2} gdh} = \frac{\int_{\alpha_1} \frac{1}{g}dh}{\int_{\alpha_2} \frac{1}{g}dh}.$$

The horizontal period condition (7)

$$\int_{\alpha_i} gdh = \overline{\int_{\alpha_i} \frac{1}{g}dh}$$

now implies that $r = \bar{r}$, i.e. r is real. If we modify gdh by multiplication by a constant—if necessary—to make $\int_{\alpha_1} gdh$ real, then $\int_{\alpha_2} gdh$ must also be real.

Weber [41] notes that this simple condition characterizes the underlying rhombic torus.

PROPOSITION 7 ([41]). *There exists a unique rhombic torus carrying a one-form η with the following properties: the form η has a double zero and a double pole (with no residue) on a diagonal, no other poles or zeros, and all periods real.*

Definition 8. We will use the symbol \mathcal{T}_1 to refer to the rhombic torus of Proposition 7.

Proposition 7 can be used to prove (see also the recent article [2] by Alarcon-Ferrer-Martín)

PROPOSITION 8 ([25]). *\mathcal{H}_1 is unique.*

Proof. In Lemma 1, we showed that the geometric conditions of Theorem 2 in Section 1.3 implied that the quotient surface of any \mathcal{H}_1 had to be a rhombic torus upon which the one form gdh satisfied the conditions on η in Proposition 7. Therefore any \mathcal{H}_1 has a quotient whose underlying Riemann surface is the unique rhombic torus of Proposition 7.

In Remark 4, we showed that all possible \mathcal{H}_1 's lie on a smooth curve parametrized by a variable ρ that is in one-to-one correspondence with the underlying rhombic conformal structures. Therefore, there is *at most one* \mathcal{H}_1 . That there is at least one example is the content of Theorem 2 (whose proof is outlined in the same Remark 4). \square

Remark 5. The rhombic torus \mathcal{T}_1 is the torus \mathbf{C} modulo the lattice generated by $\{1, e^{i\theta_1}\}$, where $\theta_1 \approx 1.7205$ [23].

3.3. *The cone metric construction of \mathcal{H}_1 .* In Section 3.1, and in Lemma 1, various conditions for the Weierstrass data of \mathcal{H}_1 were derived using geometric and analytic arguments. In Section 3.2, we stated the period problem for \mathcal{H}_1 . In this section, we give a cone-metric derivation of the Weierstrass data, the most important feature of which is that it solves the horizontal period problem (12) by construction. It does not use Proposition 6 of Section 3.2, which depends on the analysis and estimates of [19].

3.3.1. *The cone-metric construction of \mathcal{T}_1 and Weierstrass data for \mathcal{H}_1 .* We will construct the torus \mathcal{T}_1 in a manner that produces, at the same time, a candidate for the one-form gdh .

A torus may be constructed by identification of opposite edges of a parallelogram. Consider the region bounded by a parallelogram with vertices 0 , 1 , τ and $1 + \tau$ in \mathbf{C} . The one-form dz on \mathbf{C} induces a holomorphic one-form on the torus. For the cycles on this torus that correspond to the edges $\overline{0,1}$ and $\overline{0,\tau}$, the periods of this one-form are clearly visible in the construction; they are the complex numbers 1 and τ .

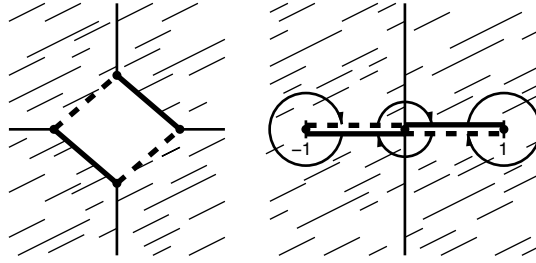


Figure 12: On the left: a rhombus removed from the extended complex plane. Identification of the opposite sides of the remaining set produces a Riemann surface of genus one that is also a rhombic torus. On the right: a degenerate rhombus is removed from the extended plane. Identification of opposite sides produces a nondegenerate rhombic torus. The one-form $d\zeta$ on the extended complex plane has a double pole at infinity. On the torus constructed, the one-form $d\zeta$ descends to define a one-form with a double pole at the point corresponding to ∞ and a double zero at the vertex point of the removed rhombus. The periods of this induced form on the edge cycles of the excised rhombus are given by the complex numbers defined by the edges themselves. In the case of the torus on the right, these periods are real.

Instead of the region bounded by the parallelogram, consider its complement in the extended ζ -plane. Identify opposite boundary edges; again, this is topologically a torus. We have flat charts given by $\int d\zeta$ away from the vertex point. On this torus, with the induced flat metric from the plane, the vertex is a cone point with cone angle 6π . (See Section 2.3 for a discussion of cone points and cone metrics.) Allowing a slight abuse of notation, we will write $d\zeta$ for the induced one-form and $|d\zeta|$ for the associated metric on the torus. In this language then, the form $d\zeta$ must have a double zero at the vertex point and, of course, it has a double pole at infinity. The periods of $d\zeta$ along the cycles corresponding to the edge vectors of the parallelogram are 1 and τ .

Recall that we desire to produce \mathcal{T}_1 , a rhombic torus carrying a one-form with a double pole, a double zero and real periods as in Proposition 7. If we construct the torus from the point-of-view of the previous paragraph, we are forced to choose both the edge vectors of our parallelogram to be real. Even though such a “parallelogram” is degenerate, the construction produces a topological torus with a flat structure given by $|d\zeta|$, which has isolated conical singularities. Therefore it has a regular conformal structure.

Essentially, we are slitting the plane (without loss of generality, along $[-1, 1]$), choosing $c \in [0, 1)$, and connecting the region above (below) $[-1, -c]$ with the region below (above) $[c, 1]$ by identifying these boundary segments. Only for the choice of $c = 0$ will the torus be rhombic; reflection in the imaginary axis provides an involution with a connected fixed point set. The rhombic torus so constructed carries a one-form descended from $d\zeta$, with one double

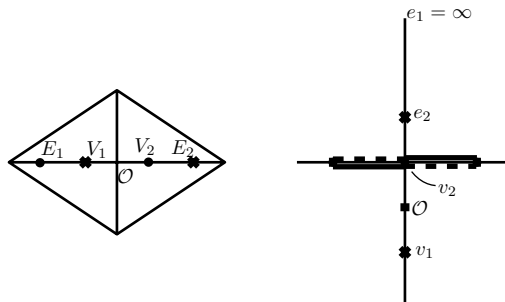


Figure 13: The slit model for the rhombic torus has two distinguished points, e_1 and v_2 . We may identify the slit model with a rhombus so that the imaginary axis is identified with the horizontal diagonal. Labelling the points on the rhombus corresponding to e_1 and v_2 in the same manner, but with upper-case letters, we may translate the rhombus horizontally to place the center, \mathcal{O} , of the rhombus to the right of E_1 and to the left of E_2 . The points V_1 and E_2 are defined to be the points on the horizontal diagonal symmetric (with respect to \mathcal{O}) to V_2 and E_1 , respectively.

pole and one double zero on a diagonal, no other zeros or poles, and all periods of this one-form are real. Because the sum of the residues of any one-form is zero and there is only one pole, this form $d\zeta$ has no residue at its pole. This torus satisfies the requirements of Proposition 7, and therefore must be the unique \mathcal{T}_1 .

We will take $d\zeta$ as a candidate for gdh on \mathcal{T}_1 , and we will refer to this presentation of \mathcal{T}_1 as the *slit model*.

Remark 6. In the construction of tori by removal of the interior of a parallelogram, P , from the plane, it is important to note that the torus constructed is not, in general, conformal to the torus produced by taking the interior of P and identifying opposite sides. This is clear in the limit case of \mathcal{T}_1 , constructed by removal of a slit from the extended plane; the torus \mathcal{T}_1 is a nondegenerate rhombic torus conformal to the one produced by $\mathbf{C}/\{1, e^{i\theta_1}\}$ with, according to Remark 5, $\theta_1 \sim 1.7205$. It is true, however, that removing the square from the extended plane produces the square torus; the torus produced is both rhombic and rectangular and such a torus must be square.

We now relate the slit model of \mathcal{T}_1 to the rhombic model, which we will take, as in Section 3.1, to be the region bounded by a rhombus whose diagonals are parallel to the coordinate axes. (See Figure 13, left.) We will scale the rhombus so that the length of the horizontal diagonal is equal to two. The slit model and the rhombic model are conformally diffeomorphic. We choose a conformal map from the slit model to the rhombus—in terms of Figure 13, a mapping from the domain on the right to the domain on the left—that

takes the imaginary axis of the slit model onto the horizontal diagonal of the rhombus: both of these lines are symmetry lines of the conformal structure. We will do this in such a manner as to have the standard vertical orientation of the imaginary axis in the slit model correspond to the standard left-to-right orientation of the horizontal diagonal. The conformal diffeomorphism between the slit model and the rhombic model is now completely determined up to the action of a translation on the rhombus, which with our normalization must be a horizontal translation. Therefore, the conformal diffeomorphism is determined up to composition on the left by a horizontal translation.

We label by v_2 the vertex point in the slit model and refer to the point at infinity in the slit model as e_1 . We want the pullback of $d\zeta$ from the slit model to correspond to the one-form gdh on the rhombic model. This pullback will have a double pole at the inverse image of the point at infinity and a double zero at the inverse image of the vertex point in the slit model. Since the double pole of gdh occurs at the end where $g = \infty$ (that is at E_1) and the double zero of gdh must occur at V_2 , we see that the inverse image of v_2 is V_2 and the inverse image of e_1 is E_1 . In Section 3.1, we saw that we could assume without loss of generality that E_1 lies to the left of the center of the rhombus. Without loss of generality we restrict ourselves to conformal diffeomorphisms with this property.

As in Section 3.1, we define E_2 and V_1 to be the points on the horizontal diagonal symmetric—with respect to \mathcal{O} —to E_1 and V_2 , respectively. We may again write

$$\begin{aligned} E_1 &= -b, & E_2 &= b, \\ V_1 &= -a, & V_2 &= a \end{aligned}$$

for some real numbers a, b with $0 < a, b < 1$, $a \neq b$. Abel's theorem applied to gdh requires $a + b = 1$. We do not know at this point whether or not we may assume that $a < b$. This does follow from the estimate of [19] discussed in Remark 4 but as we shall see, we can achieve our result without this external reference.

We will adopt the convention that the points on the slit model that are labelled by letters in lower case will have corresponding points on the rhombus labelled by the same letter in upper case.

Remark 7. As discussed in Section 3.1, it does not make geometric sense to allow a or b to take on the values $0, 1/2$ or 1 . There are three possibilities: $a = 0$ and $b = 1$; $a = 1$ and $b = 0$; $a = b = 1/2$. In the first two cases, the ends coincide, while in the third case each end coincides with a vertical point on the surface; in all three cases, the data are incompatible with our geometric assumptions. *However, it does make analytic sense to allow this to happen.* The pullback of dz will define a one-form on the rhombus with one double pole and one double zero. In the cases where $a = 0$ or $a = 1$, the pole occurs at

the center or at the vertex point. In the case where $a = 1/2$, the pole and zero occur at the half-period points on the horizontal diagonal.

3.3.2. *The definition of $\frac{1}{g}dh$ and the solution of the horizontal period problem.* Let \mathbf{t} be the translation of the torus in the rhombic model that is induced by the translation in the plane satisfying $\mathbf{t}(E_1) = E_2$ (and therefore $\mathbf{t}(V_1) = V_2$). In terms of our normalization, \mathbf{t} is the translation on the torus induced by the translation in \mathbf{C} by $2b$, where $E_1 = -b$. (Note that by Abel’s Theorem, this translation $2b$ can be written as $2b = 2(1 - a) = 2 - 2a$, and so an equivalent translation is by $-2a$. We will use this observation in the proof of Proposition 9.) We define

$$\frac{1}{g}dh := \mathbf{t}^*(gdh).$$

The one-forms gdh and $(1/g)dh$ have the divisors as specified in Figure 9, and they automatically satisfy the horizontal period condition (12). To see this, recall that the periods of gdh are real by construction and, by (14),

$$\int_{\alpha_i} \frac{1}{g}dh = \int_{\alpha_i} \mathbf{t}^*(gdh) = \int_{\mathbf{t}^{-1}(\alpha_i)} gdh = \int_{\alpha_i} gdh.$$

It is important to observe that while we have one free parameter to define gdh —essentially the parameter a defined in Section 3.1 that places the point V_2 —the choice of $\frac{1}{g}dh$ is determined by the horizontal period condition (12). We now seek a choice of a for which the vertical period condition (13) is satisfied. This condition requires us to integrate dh over a specified cycle on the rhombus. To find a value of a that satisfies (13) we first need to define dh in terms of gdh and $\frac{1}{g}dh$ and to verify that it has the desired symmetries.

3.3.3. *The Weierstrass data $\{g, dh\}$ and the symmetries of dh .* Since $dh^2 = gdh \cdot \frac{1}{g}dh$ and $g^2 = \frac{gdh}{\frac{1}{g}dh}$, we can use these forms to determine g and dh —up to sign—by taking a square root. The one-form dh defined in this manner will have simple zeros at the V_i and simple poles at the E_i , precisely what is required by the divisor diagram in Figure 9.

To prove the existence of \mathcal{H}_1 , we must find a choice of the value a so that the one-forms gdh and $\frac{1}{g}dh$ determined by this choice yield a candidate $dh = \pm\sqrt{gdh \cdot \frac{1}{g}dh}$ that satisfies the vertical period condition (13). (We discuss below how the sign is determined.) We solve this problem in Section 3.4. First, we establish some expected but important properties of any dh defined in the manner just described.

LEMMA 2. (i) *The one-form dh , considered as a one-form on the rhombus, is imaginary on the horizontal diagonal and real on the vertical diagonal.*

(ii) Let μ_v and μ_h be reflection in the vertical diagonal and the horizontal diagonal, respectively, and let ρ be 180°-rotation about \mathcal{O} , the center of the rhombus. Then

$$-\rho^*dh = -\overline{\mu_h^*dh} = \overline{\mu_v^*dh} = dh.$$

By saying that a one-form is real or imaginary on a curve we mean that evaluation of the one-form on tangent vectors to that curve produces real or imaginary values. Lemma 2 does not depend on our choice of sign of dh . We will make the choice of sign according to the following geometric consideration. *According to the lemma, the form dh is real along the vertical diagonal, where it is never zero. We choose the sign of dh so that dh is positive on upward-pointing vectors tangent to the vertical diagonal.*

It follows immediately from Lemma 2 above and our choice of sign of dh that:

COROLLARY 1. *The involutions μ_v , μ_h , and ρ are isometries of the cone metric $|dh|$. In particular, the fixed point sets of the reflections (the vertical and the horizontal diagonals) develop into straight lines under the developing map*

$$p \rightarrow \int_{\mathcal{O}}^p dh.$$

The developed image of the horizontal diagonal is a vertical line. The developed image of the vertical diagonal is a horizontal line, and the upper half of the vertical diagonal develops to the positive x -axis (i.e., the image of p develops to the right on a horizontal line as one moves up the horizontal diagonal from \mathcal{O}).

Proof of Lemma 2. In the slit domain, the one-form gdh is given by $d\zeta$: here we set $\zeta = \xi + i\eta$. On the rhombus, the one-form gdh is produced by pulling back $d\zeta$ from the slit domain. The imaginary axis in the slit domain corresponds to the horizontal diagonal in the rhombus model: it is the developed image under gdh of the horizontal diagonal. (See Figure 13.) Along the imaginary axis in the slit domain, $d\zeta$ is imaginary: $d\zeta(\frac{\partial}{\partial\eta}) = i$.

If we parametrize the horizontal diagonal from left to right by s , then the point s on the rhombus develops to a point $i\eta = if(s)$ on the imaginary axis in the slit model, for some real-valued function $f(s)$ with $f'(s) > 0$. Then at s :

$$gdh\left(\frac{d}{ds}\Big|_s\right) = f'(s)d\zeta|_{if(s)}\left(\frac{\partial}{\partial\eta}\right) \in i\mathbf{R}.$$

Since on the rhombus $(1/g)dh = \mathbf{t}^*(gdh)$, where \mathbf{t} is a horizontal translation, we can write

$$\begin{aligned} \frac{1}{g}dh \left(\frac{d}{ds} \Big|_s \right) &= \mathbf{t}^*(gdh) \left(\frac{d}{ds} \Big|_s \right) \\ &= (gdh) \left(\mathbf{t}_* \frac{d}{ds} \Big|_s \right) \\ &= (gdh) \left(\frac{d}{ds} \Big|_{\mathbf{t}(s)} \right) \in i\mathbf{R}_+. \end{aligned}$$

But then

$$dh^2 \left(\frac{d}{dt}, \frac{d}{dt} \right) = gdh \left(\frac{d}{dt} \right) (1/g)dh \left(\frac{d}{dt} \right)$$

is negative. Therefore $dh(\frac{d}{ds})$ is imaginary along the horizontal diagonal.

Recall that $dh = \pm\sqrt{gdh \cdot (1/g)d\bar{h}}$ has simple zeros at the points V_1 and V_2 , and simple poles at the points E_1 and E_2 . Also, the pair of points E_1 and E_2 and the pair of points V_1 and V_2 are each interchanged by the reflection μ_v in the vertical diagonal. Therefore, $\overline{\mu_v^*dh}$ is a meromorphic one-form whose poles and zeros match those of dh . Hence, up to a nonzero scale factor, the form $\overline{\mu_v^*dh}$ is equal to dh . To determine the scale factor we evaluate the form at \mathcal{O} , the center point of the rhombus. Since \mathcal{O} is on the horizontal diagonal where dh is imaginary, since \mathcal{O} is fixed by μ_v , and since μ_{v*} changes the sign of horizontal vectors, we have that

$$\overline{\mu_v^*dh \left(\frac{d}{ds} \right)} = \overline{dh \left(-\frac{d}{ds} \right)} = dh \left(\frac{d}{ds} \right)$$

at \mathcal{O} . Hence $\overline{\mu_v^*dh} = dh$ on the torus. On the vertical diagonal, which is fixed by μ_v , vertical vectors are also fixed by μ_{v*} . Hence $\overline{d\bar{h}} = \overline{\mu_v^*dh} = dh$ along the vertical diagonal, which implies that dh is real along the vertical diagonal.

In an analogous manner, observe that ρ^*dh has the same poles and zeros as dh , and that, at \mathcal{O} , we have $\rho^*dh = -dh$. Hence, $\rho^*dh = -dh$ everywhere. Since $\mu_h = \mu_v\rho$, we have $\overline{\mu_h^*dh} = -dh$. This completes the proof of the lemma. \square

3.4. *Solving the vertical period problem geometrically.* In order to try to satisfy the vertical period condition (13) we will vary the conformal diffeomorphisms with which we pull back $d\zeta$ in the slit model to produce gdh on the rhombus. Any such conformal diffeomorphism is determined by the position of the inverse image, V_2 , of the vertex point v_2 of the slit model. We may write $V_2 = a$, $0 < a < 1$, $a \neq 1/2$. Our goal is to find a value of a between 0 and 1/2 for which the vertical period problem (13) is solved by using the intermediate value theorem.

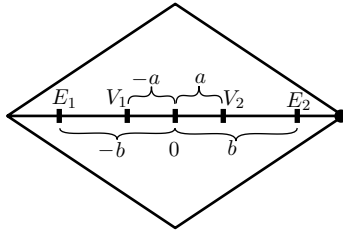


Figure 14: We label the points V_i and E_i according to their signed and scaled distance from \mathcal{O} . From Abel’s Theorem we know that $a + b = 1$.

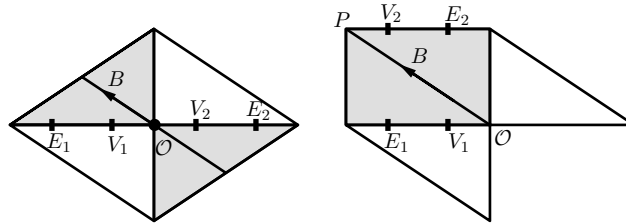


Figure 15: On the left, the path, B , is illustrated on \mathcal{T}_1 . On the right, an equivalent path, also labelled B , is drawn on the shaded rectangle \mathcal{R} .

Remark 8. Because $a + b = 1$, the restriction of a to lie in the interval $(0, \frac{1}{2})$ is equivalent to the requirement that $a < b$. It follows from Proposition 6 that there are no values of $a > 1/2$ that satisfy the horizontal period condition (12).

Even though they do not produce admissible Weierstrass data—see Remark 7—the values $a = 0$, and $a = \frac{1}{2}$ do define conformal diffeomorphisms from the rhombus to the slit model, and hence they produce well-defined one-forms gdh . The extreme value $a = \frac{1}{2}$ represents the case where $E_i = V_i, i = 1, 2$; the extreme value $a = 0$ is the case where $E_1 = E_2$ and $V_1 = V_2$. In each of these cases we may define dh by translating gdh to produce $(1/g)dh$ and then taking the square root of the product of these two forms.

For each $a \in [0, \frac{1}{2}]$, define the map $F_a : \mathcal{T}_1 \rightarrow \mathbf{C}$ by

$$F_a(z) = \int_{\mathcal{O}}^z dh.$$

The vertical period condition (13) is

$$\operatorname{Re} \int_B dh = 0,$$

where B is the curve in the rhombus illustrated in Figure 15.

We may also consider F_a to be a map from \mathcal{R} in Figure 15—a rectangle that comprises half of \mathcal{T}_1 —to the complex plane. According to Lemma 2, we

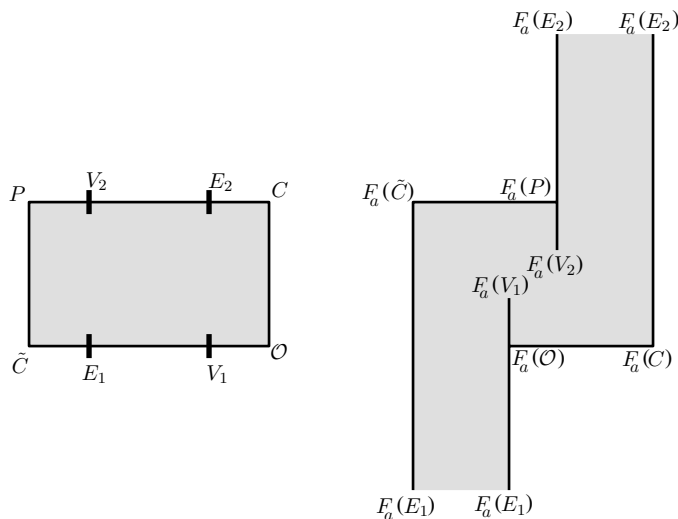


Figure 16: On the left is the rectangle \mathcal{R} . The points V_i and E_i are placed for a generic value of a between 0 and $1/2$. On the right is the image of \mathcal{R} under the mapping F_a .

have $\rho^*dh = -dh$. Therefore, we may reexpress the period condition (13) as

$$(15) \quad \operatorname{Re} \int_B dh = 0,$$

where B is now considered to be the diagonal in \mathcal{R} from \mathcal{O} to P . (See Figures 15 and 16.)

Considering F_a as a map from \mathcal{R} to \mathbf{C} , we define

$$(16) \quad f(a) := \operatorname{Re}\{F_a(P) - F_a(\mathcal{O})\},$$

in terms of which we may restate the vertical period condition (15) as asserting that our choice of a must satisfy

$$(17) \quad f(a) = 0$$

PROPOSITION 9. *There exists a value of a , with $0 < a < \frac{1}{2}$ for which the vertical period condition (15) is satisfied.*

Proof. We will prove the proposition by showing the existence of a value of a satisfying (17). We begin with a discussion of the continuity of F_a and f . Recall that dh is defined as a square root of $(\frac{1}{g})dh \cdot gdh$. The one-form gdh is a pullback to the rhombus of $d\zeta$ in the slit model. We will write η_a for the pullback of $d\zeta$ that corresponds to the choice of gdh with a double zero at $z = a$ and a double pole at $z = -(1 - a)$. In particular, η_0 has a double zero at $z = 0$, (which is the center point \mathcal{O}) and a double pole at the vertex at $z = 1$.

Let \mathbf{t}_a be the conformal diffeomorphism $\mathbf{t}_a(z) = z - a$ of the rhombus induced by horizontal translation by $-a$, with $a \in \mathbf{R}$. Then

$$\eta_a = \mathbf{t}_a^* \eta_0.$$

The one-form η_a has a double zero at a and a double pole at $-b = -(1 - a)$ as required. For $(gdh)_a = \eta_a$, the corresponding one-form $(\frac{1}{g}dh)_a$ is $\mathbf{t}_{-2a}^*gdh = \mathbf{t}_{-2a}^*\mathbf{t}_{+a}^*\eta_0 = \mathbf{t}_{-a}^*\eta_0$. Then,

$$dh_a^2 = \mathbf{t}_{-a}^*\eta_0 \cdot \mathbf{t}_a^*\eta_0 = \eta_{-a} \cdot \eta_a.$$

In particular,

$$(18) \quad dh_0^2 = \eta_0^2,$$

while $dh_{\frac{1}{2}}$, having no poles or zeros, is a constant multiple of dz^2 :

$$(19) \quad dh_{\frac{1}{2}} = cdz.$$

It is clear that dh_a depends continuously on a on the open interval $(0, \frac{1}{2})$.

Claim. (dh_a) depends continuously on a on the closed interval $[0, \frac{1}{2}]$.

The claim has two immediate consequences. According to Corollary 1, for $a \in (0, \frac{1}{2})$, the developed image under dh of the upper half of the vertical diagonal lies on the positive x -axis (assuming \mathcal{O} develops to the origin in the plane). By the claim, the same must be true for dh_0 and $dh_{\frac{1}{2}}$. It follows immediately from (19) that

$$(20) \quad dh_{\frac{1}{2}} = -c_1 idz$$

for some positive real constant c_1 . Turning our attention to dh_0 , it follows from (18) that dh_0 must have a double zero at \mathcal{O} , and the developed image of the horizontal diagonal to the right of \mathcal{O} must lie on the negative imaginary axis. Using the fact that η_0 is the pullback to a rhombus of $d\zeta$ in the slit model by an orientation-preserving diffeomorphism, it follows from (18) that

$$(21) \quad dh_0 = \eta_0.$$

Proof of claim. There is a potential problem at the endpoints where either a zero coalesces with a pole (at $a = 1/2$) or the zeroes coalesce and the poles coalesce (at $a = 0$). We will address this by using sigma functions to represent the one-forms η_a .

We recall from the theory (see [27]) of the sigma function $\sigma(z)$ on a lattice that any meromorphic form $\varphi(z)dz$ on a torus may be expressed as a ratio

$$\varphi(z)dz = C \prod_{k=1}^n \sigma(z - s_k)\sigma(z - t_k)^{-1}dz,$$

where each s_k represents an orbit of zeros and each t_k represents an orbit of poles. In this representation, it is crucial that $\sum_{k=1}^n s_k = \sum_{k=1}^n t_k$, and zeros of multiplicity are considered as separate entries in the list in the customary way.

With this representation, we may write

$$\eta_0 = C \frac{\sigma^2(z)}{\sigma(z-1)\sigma(z+1)} dz$$

for some complex constant C (independent of a). It then follows, using $t_a(z) = z - a$, that

$$(gdh)_a = \eta_a = t_a^* \eta_0 = C \frac{\sigma^2(z-a)}{\sigma(z-a-1)\sigma(z-a+1)} dz$$

and

$$\left(\frac{1}{g} dh\right)_a = t_{-a}^* \eta_0 = C \frac{\sigma^2(z+a)}{\sigma(z+a-1)\sigma(z+a+1)} dz.$$

Therefore

$$\frac{(dh)_a^2}{dz^2} = C^2 \frac{\sigma^2(z-a)\sigma^2(z+a)}{\sigma(z-a-1)\sigma(z-a+1)\sigma(z+a-1)\sigma(z+a+1)}.$$

As $a \rightarrow 1/2$, this function converges to $C^2 \frac{\sigma(z-1/2)\sigma(z+1/2)}{\sigma(z-3/2)\sigma(z+3/2)} = C^2$, since $\sigma(z+2) = \sigma(z+\omega_1+\omega_2)$ differs from $-\sigma(z)$ by a factor of the form $e^{\alpha z + \beta}$ where α and β depend only on the lattice. Also, note that as $a \rightarrow 0$, the function $(dh_a/dz)^2$ converges to η_0^2/dz^2 . This completes the proof of the claim.

In the three-dimensional product $[0, \frac{1}{2}] \times \mathcal{R}$ of the interval $[0, \frac{1}{2}]$ with the rectangle \mathcal{R} , the set

$$\{(a, p) | dh_a \text{ has a pole at } p\}$$

consists of two line segments on the boundary of this (three-dimensional) box. One line segment connects the bottom left corner of $\mathcal{R} \times \{0\}$ to the midpoint of the top of $\mathcal{R} \times \frac{1}{2}$. The other line segment connects the midpoint of the bottom of $\mathcal{R} \times \{0\}$ to the top right corner of $\mathcal{R} \times \frac{1}{2}$. After removing from $[0, \frac{1}{2}] \times \mathcal{R}$ a small tubular neighborhood \mathcal{N} of these line segments, we may assert that $F : [0, \frac{1}{2}] \times \mathcal{R} \setminus \mathcal{N} \rightarrow \mathbf{C} \cup \infty$ defined by

$$F(a, p) = F_a(p) = \int_0^p dh_a$$

is continuous and bounded. Since $[0, \frac{1}{2}] \times B$, where B is the path of integration from \mathcal{O} to P , lies in the domain of F , we may assert that

$$f(a) := \text{Re}\{F_a(P) - F_a(\mathcal{O})\}$$

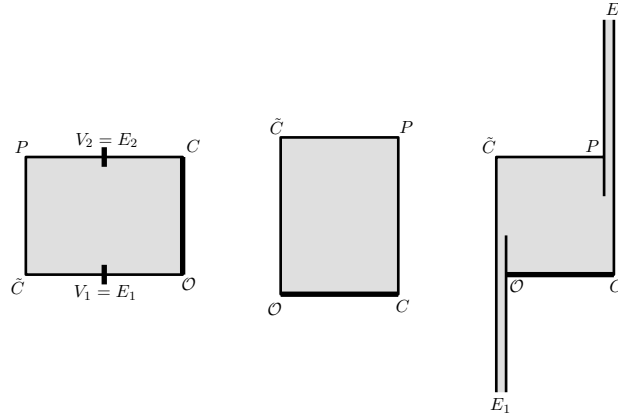


Figure 17: The case $a = \frac{1}{2}$. When $a = \frac{1}{2}$, we have $E_i = V_i$ as is illustrated in the picture of \mathcal{R} on the left. In this case, the one-form dh is regular and the image of \mathcal{R} under $F_{\frac{1}{2}}$ is illustrated in the center image. Up to scaling, $F_{\frac{1}{2}}$ is clockwise rotation by 90° . The image of \mathcal{R} under F_a for a near $\frac{1}{2}$ is illustrated on the right.

is continuous on $[0, \frac{1}{2}]$. (The generic image of F_a , $0 < a < \frac{1}{2}$, is illustrated in Figure 16. In this case, $a \neq b$ and $E_i \neq V_i$, $i = 1, 2$.) According to (20),

$$F_{\frac{1}{2}}(p) = \int_0^p dh_{\frac{1}{2}} = -c_1 i \int_0^p dz = -c_1 ip,$$

where c_1 is a positive constant; i.e. $F_{\frac{1}{2}}$ is clockwise rotation by $-\pi/2$ followed by a scaling. (See Figure 17.) In particular,

$$(22) \quad f\left(\frac{1}{2}\right) = \operatorname{Re}\{F_{\frac{1}{2}}(P) - F_a(\mathcal{O})\} > 0.$$

We now consider the other extreme case: $a = 0$.

Claim.

$$(23) \quad f(0) < 0.$$

Proposition 9 then follows from (22), (23) and the intermediate value theorem.

Proof of Claim (23). According to (21), $dh_0 = \eta_0$. The symmetry lines of $|dh|$ on the rhombus—the horizontal and vertical diagonals according to Corollary 1—correspond to the imaginary and real axes, respectively, in the slit model.

If we remove the symmetry lines from the rhombus—also the symmetry lines of $|dh|$ according to Corollary 1— what is left consists of two rectangles, one of which is \mathcal{R} . If we remove the symmetry lines from the slit model, what is left consists of two conformal rectangles, the ones illustrated in Figure 18.

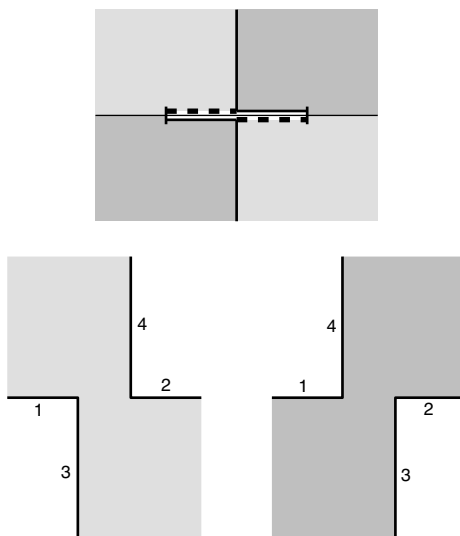


Figure 18: \mathcal{R} in the slit model. The slit model of \mathcal{T}_1 (in Figure 13) can be cut along symmetry lines—the real and imaginary axes—to produce two conformal rectangles. In the illustration, they are the two differently shaded regions. As described in the text, one of them, the one on the right, must be (up to scaling) the image of \mathcal{R} under F_0 .

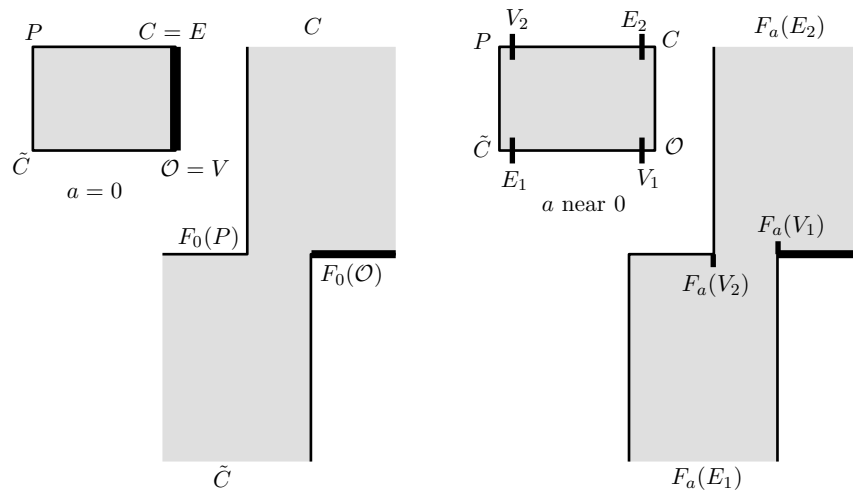


Figure 19: On the extreme left, the rectangle \mathcal{R} is drawn with $V_1 = V_2 = \mathcal{O}$ and $E_1 = E_2$ at C and \tilde{C} . The image of \mathcal{R} under F_0 is drawn just to the right, illustrating that $F_0(\mathcal{O})$ lies to the right of $F_0(P)$ when $a = 0$. On the right-hand-side, \mathcal{R} and $F_a(\mathcal{R})$ are drawn for $a \neq 0$ small.

Each rectangle has two vertices at infinity. Since $dh_0 = \eta_0$ is the pullback of $d\zeta$ on the slit model, the developing map F_0 must send \mathcal{R} onto one of these rectangles. Again, as with all F_a , the map F_0 takes vertical (resp. horizontal) boundary segments to horizontal (resp. vertical) lines. Using Lemma 2, we know that the image under F_a of the right-hand side of \mathcal{R} is a horizontal line going to the right as one ascends from \mathcal{O} . Therefore, the image $F_0(\mathcal{R})$ must be the conformal rectangle on the right of Figure 18 and the left of Figure 19, with $F_0(\mathcal{O})$ equal to the right-hand vertex of this rectangle and $F_0(P)$ equal to the left-hand vertex. Hence $F_0(P)$ lies to the left of $F_0(\mathcal{O})$ which means that

$$f(0) = \operatorname{Re}\{F_0(P) - F_0(\mathcal{O})\} < 0,$$

which is (23). This completes the proof of the claim, which completes the proof of the proposition. \square

4. The construction of screw-motion-invariant \mathcal{H}_k

Our plan is to construct a family of surfaces $\{\mathcal{H}_k\}$ that includes the surface \mathcal{H}_1 ; in this family, there should exist at least one surface of the type \mathcal{H}_k for each $k \geq 1$. We begin by specifying necessary conditions for the Weierstrass data of \mathcal{H}_k/σ_k . A fundamental domain of \mathcal{H}_k is the image of \mathcal{H}_k/σ_k under the Weierstrass mapping. It is a genus-one surface with two ends, possessing a vertical axis and containing two horizontal lines making an angle of πk , one with the other. We have established in Lemma 1 of Section 2 that \mathcal{H}_k/σ_k is a rhombic torus and that it has the same symmetries as \mathcal{H}_1/\mathbf{T} , where $\mathbf{T} := \sigma_1$ is vertical translation by 2π .

Because we want the \mathcal{H}_k family to give a deformation of \mathcal{H}_1 , we are justified in assuming that the placement of vertical points of \mathcal{H}_k conforms qualitatively to what happens on \mathcal{H}_1 . Specifically, the vertical points lie on the same lines in \mathcal{H}_k as they do on \mathcal{H}_1 , and in the same relative position. As we did in Section 3, label the ends E_1, E_2 and the vertical points V_1, V_2 . All four of these points lie on a curve fixed by a symmetry of the underlying Riemann surface \mathcal{T}_1 of \mathcal{H}_k/σ_k . We require that this curve be mapped onto horizontal lines on \mathcal{H}_k . Another curve fixed by a different symmetry of \mathcal{T}_1 will be mapped into the vertical axis of \mathcal{H}_k . This curve must meet the first one orthogonally in two points, which we may assume, without loss of generality, lie between E_1 and E_2 and between V_1 and V_2 respectively. Also, we assume that $g(E_1) = \infty$ and $g(E_2) = 0$. We expect the Gauss map to behave locally—near E_1 and E_2 —like z^k near infinity and the origin, respectively. At one end we expect a pole of order k , and at the other a zero of order k . Since we will consider k to take on all real values greater than $1/2$, we will be considering multivalued Gauss maps and one-forms gdh and $(1/g)dh$. (In particular, when k is not an integer, the screw-motion Euclidean isometry σ_k has a nontrivial rotational component. Hence,

	E_1	V_1	V_2	E_2
g	∞^k	∞	0	0^k
dh	∞	0	0	∞
gdh	∞^{k+1}	$-$	0^2	0^{k-1}
$\frac{1}{g}dh$	0^{k-1}	0^2	$-$	∞^{k+1}
$\frac{dg}{g}$	∞	∞	∞	∞
residue $\frac{dg}{g}$	k	1	-1	$-k$

Figure 20: Divisor and residue requirements for the Weierstrass data of \mathcal{H}_k .

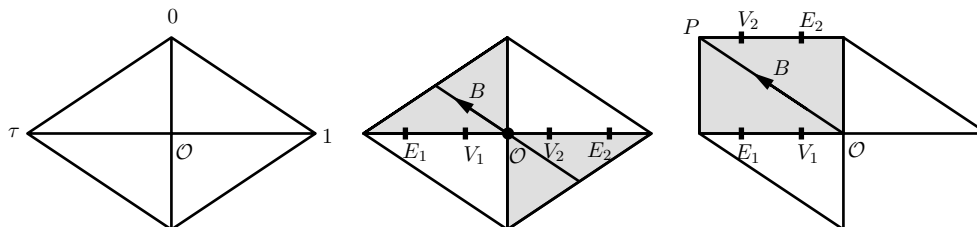


Figure 21: The rectangle. As in Section 3.4.1, we have the same situation for the formation of a rectangular domain that is half of the Riemann surface $\mathcal{T}_k(d)$ and on which B is the path of integration. The only difference is that the underlying rhombic torus is not, in general, equal to \mathcal{T}_1 .

this motion identifies points on \mathcal{H}_k whose normal vectors differ by a rotation. Therefore, the Gauss map is not well-defined on the quotient torus \mathcal{H}_k/σ_k . However, as is customary for such functions, there are well-defined branches of the Gauss map defined on appropriate subdomains of \mathcal{H}_k/σ_k , and we will be careful to indicate which branch we are using when relevant: certainly divisor data is independent of the branch chosen.)

Because we want the family \mathcal{H}_k to be continuous in k , we require—as is the case on \mathcal{H}_1 —that $g(V_1) = \infty$ and $g(V_2) = 0$. This determines the divisors of gdh , $1/gdh$ and $\frac{dg}{g}$. See Figure 20.

4.1. *The rhombic $|dz|$ model*. In Section 3, we chose to represent \mathcal{T}_1 , the Riemann surface of \mathcal{H}_1 modulo translations, as a rhombus in the following manner: a diagonal is a horizontal line segment of length two, whose center point is the origin of \mathbf{C} . In dealing with family \mathcal{H}_k , we do not know in advance the underlying rhombic structure. Also, we will choose a different normalization for rhombi underlying \mathcal{H}_k/σ_k . Here is our convention.

For each \mathcal{H}_k/σ_k , the associated rhombus in the complex plane will be chosen to have the following properties: the top vertex of the rhombus sits at $0 \in \mathbf{C}$; the point $1 \in \mathbf{C}$ is the right-most vertex; the left-most vertex is at some unitary value τ ; the points V_1 and V_2 lie symmetrically placed on the diagonal from 1 to τ . The last statement is a consequence of Abel’s theorem applied

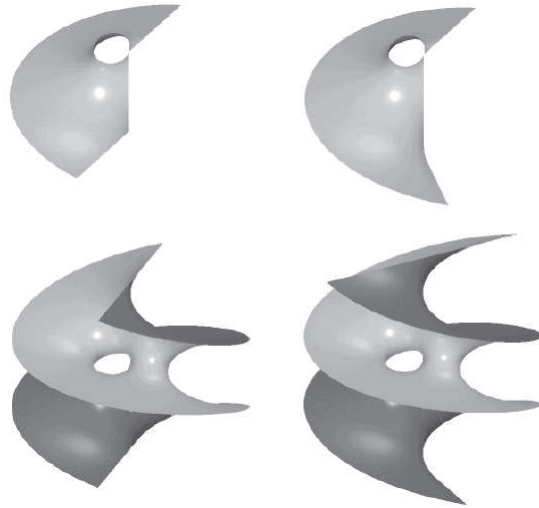


Figure 22: A fundamental domain of \mathcal{H}_k can be imagined qualitatively as a region of the helicoid bounded by two horizontal lines, between which the helicoid turns by an angle of $\theta = 2\pi k$ and in the middle of which there is a handle. The boundary lines are identified in the quotient as a single line. The only other line, besides the vertical axis, that survives the surgery necessary to insert the handle is a horizontal line in the middle, at the level of the handle. The surface on the bottom, left, is a fundamental domain of \mathcal{H}_1 . The surface on the bottom, right, is a fundamental domain of \mathcal{H}_k for $k \sim 1.25$. The two images on top are each one quarter of the surfaces below them. They are bounded by a segment of the vertical axis, two horizontal half lines and a closed loop that is not contractible in \mathcal{H}_k/σ_k . See also [23].

to dh (or a consequence of the symmetry of the surface imposed by Lemma 1). In this setup, the center point of the rhombus lies at $\mathcal{O} = \frac{1+\tau}{2}$, and a point on the horizontal diagonal must be of the form $\mathcal{O} \pm t(\frac{1-\tau}{2})$, $-1 \leq t \leq 1$. In particular, the points $V_i, E_i, i = 1, 2$ are of the form

$$(24) \quad \begin{aligned} E_1 &= \mathcal{O} - b \frac{1-\tau}{2} \\ E_2 &= \mathcal{O} + b \frac{1-\tau}{2} \\ V_1 &= \mathcal{O} - a \frac{1-\tau}{2} \\ V_2 &= \mathcal{O} + a \frac{1-\tau}{2} \end{aligned}$$

for some $0 < a < b < 1$.

Because we want the family \mathcal{H}_k to include \mathcal{H}_1 , we may assume that $a < b$, as we know this to be the case for that surface. We will refer to this model of \mathcal{T} as the rhombic or the rhombic $|dz|$ model, the latter when we wish to

emphasize that we are understanding the rhombus as coming equipped with a (nonsingular) cone metric. In subsequent sections, we will develop two other models of \mathcal{T} using the forms gdh and dh .

The positions of the ends E_i and the vertical points V_i are not independent. For $k = 1$, we observed in Section 3 that $a + b = 1$, a consequence of Abel’s theorem. In general, we have the following result.

PROPOSITION 10. *Suppose given Weierstrass data that satisfy the geometric conditions (4) for \mathcal{H}_k/σ_k ; in particular, g possesses the divisor specified in Figure 20. If k is an integer, then $a + kb$ is also an integer and*

$$1 \leq a + kb \leq k.$$

In particular if $k = 1$, $a + b = 1$.

If such Weierstrass data exist for a continuously varying family of \mathcal{H}_k/σ_k that contains \mathcal{H}_1/σ_1 , then

$$(25) \quad a + kb = k$$

Proof. If k is an integer, then the function g is single-valued. We will apply Abel’s Theorem to g , whose divisor is given in Figure 20. From (24), we have

$$-kE_1 - V_1 + V_2 + kE_2 = (a + kb)(\tau - 1).$$

Therefore, by Abel’s theorem, $(a + kb)(\tau - 1)$ is in the lattice, which implies that $a + kb$ is an integer. Since $0 < a < b < 1$, we see that $a + kb$ is an integer between 1 and k . In particular, when $k = 1$, we have $a + b = 1$.

For any (possibly nonintegral) $k > 0$, consider the meromorphic one-form $\frac{dg}{g}$, whose divisor and residues are given in Figure 20. Let γ_1 and γ_2 be the cycles on $\mathcal{T} = \mathbf{C}/\{1, \tau\}$ given by the vectors 1 and τ , respectively. For any closed one-form μ with simple poles at P_1, \dots, P_r , and residues a_1, \dots, a_r , the bilinear relation [12] gives

$$(26) \quad 2\pi i \sum_{j=1}^r P_j a_j = \omega_2 \alpha_1 - \omega_1 \alpha_2,$$

where $\alpha_i = \int_{\gamma_i} \mu$ and $\omega_i = \int_{\gamma_i} dz$, $i = 1, 2$. Applying (26) to $\mu = \frac{dg}{g}$ we have

$$2\pi i(-kE_1 - V_1 + V_2 + kE_2) = \alpha_1 \tau - \alpha_2,$$

and using (24), we obtain

$$(27) \quad 2\pi i(a + kb)(1 - \tau) = \alpha_1 \tau - \alpha_2.$$

It is left to evaluate α_1 and α_2 .

In Figure 23, we have drawn curves $\tilde{\gamma}_1$ and $\tilde{\gamma}_2$ that are homotopic to γ_1 and γ_2 , respectively. On the semi-circular arcs near the E_i , the integral of $\frac{dg}{g}$ will

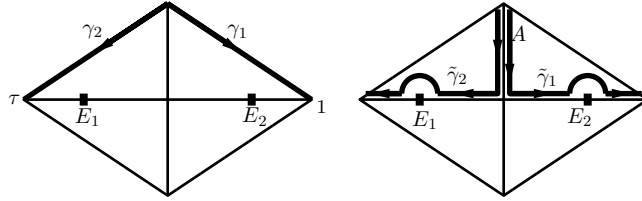


Figure 23: On the left, a rhombic torus is represented as a planar rhombus with sides 1 and τ . The paths γ_1 and γ_2 correspond to the vectors $\overline{0, 1}$ and $\overline{0, \tau}$. The ends E_1 and E_2 are labelled. On the right, the paths $\tilde{\gamma}_1$ and $\tilde{\gamma}_2$ are drawn. Each begins by descending A , the top half of the vertical diagonal, then follows their respective halves of the horizontal diagonal, avoiding the ends, E_i , by traversing semicircular paths. Each $\tilde{\gamma}_i$ is homotopic to γ_i .

give one-half of $2\pi i$ times the residue, with a sign change due to the orientation of the semicircles associated to $\tilde{\gamma}_1$. From the residues given in Figure 20, we know that the contributions to the integral of $\frac{dg}{g}$ along the semicircles is the same on $\tilde{\gamma}_1$ as on $\tilde{\gamma}_2$ and is equal to $-\pi i(k + 1)$.

The horizontal line segments of each $\tilde{\gamma}_i$ are mapped by the immersion into horizontal lines, which implies that on each of the segments, the Gauss map g takes values on radial lines in \mathbf{C} . Since $\frac{dg}{g} = d \log g$, the integral of $\frac{dg}{g}$ along these lines depends only on the change in $|g|$ along these segments. We can assume without loss of generality that each of the semicircular arcs begins and ends at points where $|g|$ has the same value. Since $|g| = 1$ at the center and at the vertex of the rhombus—both points on the vertical diagonal which is mapped into a vertical line—we can conclude that the total contribution to α_i from integrating $\frac{dg}{g}$ along these segments is zero.

It remains to compute $\int_A \frac{dg}{g}$, where A is the top half of the vertical diagonal. See Figure 23. Before doing this, we observe that since this segment is common to $\tilde{\gamma}_1$ and $\tilde{\gamma}_2$ we now know that

$$(28) \quad \alpha_1 = \alpha_2 = -\pi i(k + 1) + \int_A \frac{dg}{g};$$

and we denote this common value as α . From (27) we have

$$2\pi i(a + kb)(1 - \tau) = -\alpha(1 - \tau)$$

or

$$(29) \quad a + kb = \frac{-\alpha}{2\pi i}.$$

As noted above, the vertical diagonal is mapped by the immersion into the vertical axis of \mathcal{H}_k along which g is unitary. By our assumption that \mathcal{H}_k has the geometric properties outlined in (4) and in Lemma 1, the tangent planes at

the endpoints of A are vertical planes making an angle of πk with one another. Hence

$$(30) \quad \int_A \frac{dg}{g} = -\pi i(k + N(k))$$

for some integer $N(k)$. Therefore from (28)

$$(31) \quad \alpha = -\pi i(k + 1) - \pi i(k + N(k)) = -\pi i(2k + N(k) + 1)$$

and from (29)

$$(32) \quad a + kb = -\frac{\alpha}{2\pi i} = k + \frac{(N(k) + 1)}{2}.$$

Equation (32) is valid for any value of $k > 0$. If we assume that we have Weierstrass data for a continuous family of \mathcal{H}_k/σ_k , then the integer-valued function $N(k)$ is a constant. If that family includes \mathcal{H}_1 then it follows from (32) and the first part of the proposition that $N(k) = -1$. Thus (32) states that $a + kb = k$, which is (25). \square

Since $0 < a < b < 1$ we have

COROLLARY 2. *Under the assumptions of Proposition 10,*

$$a < \frac{k}{k + 1} < b, \quad \text{and} \quad \lim_{k \rightarrow \infty} b = 1.$$

Remark 9. The integral $\int_A \frac{dg}{g}$ in Proposition 10 measures the turning of the normal along the vertical axis of \mathcal{H}_k : the full turning in one period of \mathcal{H}_k will be $2\pi(k - 1)$ according to the equation (30) in the proof of Proposition 10 and the fact that $N(k)$ is identically equal to -1 . On the helicoid, \mathcal{H} , the normal turns by $2\pi k$ on each \mathcal{H}/σ_k . We interpret this as saying that the presence of a handle in each fundamental domain of \mathcal{H}_k has the effect of costing one full turn of the normal. In particular, the normals on \mathcal{H}_1 do not wind around the vertical axis at all, a surprising geometric consequence of Abel’s theorem.

4.1.1. *The period conditions.* The Weierstrass data we produce must satisfy the horizontal and vertical period conditions (12) and (13):

$$(33) \quad \int_B g dh = \overline{\int_B \frac{1}{g} dh};$$

$$(34) \quad \operatorname{Re} \int_B dh = 0.$$

The curve B is defined in Figures 15 and 21.

4.2. *The $|gdh|$ model and the solution of the horizontal period problem.* We will produce candidate Weierstrass data that depend on the conformal type and

placement of the distinguished points. They will satisfy the divisor conditions of Figure 20, all the symmetry conditions of Lemma 1, the distinguished-point-placement requirements of (25) and the horizontal period condition (33), but not necessarily the vertical period condition (34). We will do this by constructing a second model, to which we will sometimes refer as the “ $|gdh|$ model”, but more often—for reasons that will become evident—as the *slit model* or the $|d\zeta|$ -model.

The construction of \mathcal{T}_1 in Section 3.3 involved slicing the ζ -plane along $[-1, 1]$ and making identifications. Into this model of \mathcal{T}_1 we are going to sew in a copy of the cone S_{k-1} . This cone-metric construction procedure is described in Section 2.3, Example 2. For each $d > 0$ and $k > 0$, we slice the ζ -plane from di to ∞ along the imaginary axis, and sew in S_{k-1} , placing the cone point of S_{k-1} with positive cone angle at the point of \mathcal{T}_1 corresponding to $\zeta = di$, and the cone point with negative cone angle at ∞ . We will refer to the torus underlying this metric space as $\mathcal{T}_k(d)$ and the metric torus as the slit model of $\mathcal{T}_k(d)$. It has three cone points, $\zeta = 0$, $\zeta = di$, and $\zeta = \infty$, with cone angles 6π , $2\pi k$ and $-2\pi(k + 1)$, respectively. We label these points v_2 , e_2 and e_1 respectively. See Figure 24.

The multivalued one-form $d\zeta$ on the ζ plane with an S_{k-1} sewn in descends to a multivalued one-form on $\mathcal{T}_k(d)$ with a zero of order $k - 1$ at e_2 , a pole of order $k + 1$ at e_1 and a double zero at v_2 . (Our choice of notation for these points comes from the desire to have the e_i and the v_i correspond to the E_i and V_i , respectively, in the rhombic model.) We will also refer to this one-form on $\mathcal{T}_k(d)$ as $d\zeta$.

All these special points lie on a fixed point set of an involution of $\mathcal{T}_k(d)$, namely the imaginary axis (fixed under $\zeta \rightarrow -\bar{\zeta}$). The rhombic torus $\mathcal{T}_k(d)$ is conformally diffeomorphic to one of the tori constructed in Section 3, which underlie the $|dz|$ model. It is clear that we may choose a conformal diffeomorphism — from the rhombus model to the slit model of the torus we have just constructed — that has the following properties:

- i. The imaginary axis of the ζ -plane is the image of the horizontal diagonal of a (rhombic) fundamental domain;
- ii. The preimages E_1 and E_2 of $e_1 = \infty$ and $e_2 = di$ (respectively) are symmetric with respect to the vertical diagonal of the rhombus;
- iii. The point E_1 , the preimage of the point $e_1 = \infty$ in the slit model, lies to the left of the center point \mathcal{O} in the rhombus.

As pointed out in Section 4.1, Abel’s theorem applied to dh forces us to define V_1 as the point symmetric to V_2 on the horizontal diagonal of the rhombus and therefore to identify v_1 as a uniquely specified point on the imaginary axis of the ζ -plane. Because of the order of points on the horizontal diagonal of the rhombus, we know that v_1 lies on the negative imaginary axis of the ζ -plane.

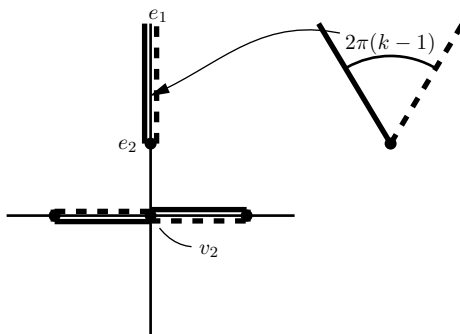


Figure 24: The torus $\mathcal{T}_k(d)$ is constructed by sewing into the torus \mathcal{T}_1 the cone S_{k-1} described in Section 2. The sewing is done along the ray in the imaginary axis beginning at di and terminating at ∞ . The point di is labeled e_2 , the point at ∞ is labeled e_1 , and the origin is labeled v_2 . Note that when $k = 1$ we sew nothing in: $\mathcal{T}_1(d) = \mathcal{T}_1$ with a distinguished point at $\zeta = di$. We may also remove an S_k from \mathcal{T}_1 , for $0 < k < \frac{1}{2}$, allowing us to define $\mathcal{T}_k(d)$ for $k > \frac{1}{2}$.

Note that for each choice of k and d , our geometric normalization determines $a = a(k, d)$ and $b = b(k, d)$ uniquely. Also, the lattice generated by $\{1, \tau\}$ that is associated to $\mathcal{T}_k(d)$ changes as k and d vary. That is $\tau = \tau(k, d)$.

Definition 9. The *one-form gdh* on the torus $\mathcal{T}_k(d)$ is given by $d\zeta$ in the slit model. On the rhombic model of $\mathcal{T}_k(d)$ it is given by the *pullback of $d\zeta$* under the conformal diffeomorphism between the two models, and the *conformal diffeomorphism* is determined by conditions (i)–(iii) in this section.

Remark 10. Our construction in this section is ambiguous when $k = 1$ and we make it precise here in a manner that is consistent with the discussion of \mathcal{H}_1 in Section 3. When $k = 1$ we are not sewing in a cone at all, which means that $\tau(1, d)$ is constant: the rhombus we get is the rhombus of \mathcal{T}_1 constructed in Section 3. For any choice of conformal diffeomorphism that places the inverse image of the point at infinity at E_1 (a point on the horizontal diagonal to the left of \mathcal{O}), let E_2 be the symmetric point on the horizontal diagonal to the right of \mathcal{O} . Then the image of E_2 under this conformal diffeomorphism is some point, $\zeta = di$, on the positive imaginary axis.

The one-form *gdh* is multivalued when k is not an integer. The periods of *gdh* (and its companion one-form $\frac{1}{g}dh$ to be defined below) will be defined according to the following convention.

Convention. If α is a curve in the slit model of $\mathcal{T}_k(d)$ or in the rhombic model, we specify a base point p on α and a choice of branch for *gdh* at p .

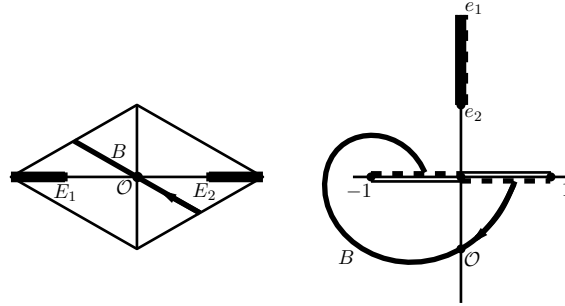


Figure 25: The path B of integration for the vertical period problem illustrated on the left in the rhombic model and on the right in the slit model. The cut referred to in the convention runs in the rhombic model from E_1 to E_2 , passing through the vertex of the rhombus. It is indicated by a bold line in the illustration on the left. Its counterpart runs from e_1 to e_2 in the slit model on the right, and is also indicated by a bold line.

We use this branch to evaluate $\int_{\alpha} gdh$. In practice we will choose a preferred branch of gdh . In the slit model of $\mathcal{T}_k(d)$, we choose a branch of $d\zeta$ that is real on the part of the real axis where $|\zeta| > 1$; this branch extends in a unique manner to $\mathcal{T}_k(d)$ after removing a cut from e_2 to e_1 . The cut we will choose is in the cone and is the image of the segment of the horizontal diagonal in the rhombus model that runs from E_2 to E_1 , passing through the vertex of the rhombus. It follows that, on the rhombus, we are choosing the branch of gdh that is well-defined in the complement of this same slit, and that is also imaginary along the remaining segment of the horizontal diagonal.

When dealing with specific curves that do not cross the branch cuts, we will always choose this branch to evaluate and we will not need to specify a point on the curve in question.

With this convention in mind we evaluate $\int_B gdh$, where B is the cycle in the rhombic model in Figure 25. It is illustrated there with its diffeomorphic image, also labelled B , in the slit model. Since these curves do not cross the cut used to define the principal branch of gdh , we have

$$(35) \quad \int_B gdh = \int_B d\zeta = \pm 1 \in \mathbf{R}.$$

We note that this choice of branch is consistent with the case $k = 1$, as described in the proof of Lemma 2. The one-form gdh has the divisor specified in Figure 20. Also, as was the case for the gdh constructed for \mathcal{H}_1 in Section 3, it follows immediately from the definition of gdh and the convention above that all of the periods of gdh are real.

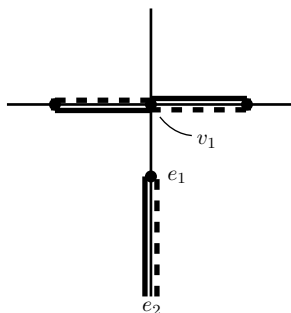


Figure 26: The one-form $\frac{1}{g}dh$ can be considered as the form descended from $d\zeta$ to the slit model of the torus that is constructed in the diagram above. The point e_1 is placed at $-di$ and the point e_2 is placed at ∞ .

4.2.1. *The $|\frac{1}{g}dh|$ model and the horizontal period condition .* We will now specify the multivalued one-form $\frac{1}{g}dh$. Recall from Section 2.7 the involution r of the rhombus which is a 180° -rotation about the center point \mathcal{O} . Note that $r(E_1) = E_2$ and $r(V_1) = V_2$. We expect geometrically that $g \circ r = \frac{1}{g}$ and $r^*dh = -dh$. This motivates the formal definition of $\frac{1}{g}dh$ on the rhombic model:

$$(36) \quad \frac{1}{g}dh := -r^*(gdh).$$

The one-form $\frac{1}{g}dh$ has the divisor specified in Figure 20. Furthermore, the pair $\{\frac{1}{g}dh, gdh\}$ satisfies the horizontal period condition (33). To see this, note that the cycle B in Figure 25 satisfies $r \circ B = -B$ and therefore

$$\int_B \frac{1}{g}dh = - \int_B r^*(gdh) = - \int_{r \circ B} gdh = \int_B gdh.$$

Since we know from (35) that gdh has real periods, we see that

$$(37) \quad \int_B \frac{1}{g}dh = \overline{\int_B gdh}$$

is satisfied. This is the horizontal period condition (33). For future reference, we state this result as a proposition.

PROPOSITION 11. *For every $k > 1/2$ and every $d > 0$, the one-forms gdh and $\frac{1}{g}dh$, defined in Definition 9 and (36), respectively, satisfy the horizontal period condition (33) in the sense of the Convention of the previous section.*

Remark 11. Let ϕ be the diffeomorphism from the rhombus to the slit model of $\mathcal{T}_k(d)$ which is used to define gdh in Definition 9:

$$gdh = \phi^*(d\zeta).$$

Using (36), we have $-\frac{1}{g}dh = (\phi \circ r)^*(d\zeta)$, where r is the 180° -rotation about the center of the rhombus. Let \tilde{r} be the conformal involution of the slit model of $\mathcal{T}_k(d)$ induced by r : that is, $\tilde{r} = \phi \circ r \circ \phi^{-1}$. Then

$$-\frac{1}{g}dh = (\tilde{r} \circ \phi)^*(d\zeta).$$

Clearly \tilde{r} interchanges the e_i , interchanges the v_i , fixes \mathcal{O} and leaves the imaginary axis invariant. If f is the involution of the slit model of $\mathcal{T}_k(d)$ induced by $\zeta \rightarrow -\zeta$, then

$$\frac{1}{g}dh = (f \circ \tilde{r} \circ \phi)^*(d\zeta) = \phi^*(f \circ \tilde{r})^*(d\zeta).$$

This equation above tells us that $\frac{1}{g}dh$ is the one-form on the rhombus produced by pulling back the one-form $d\zeta$ on the modified slit model in Figure 26.

4.2.2. *Symmetries inherent in the $|gdh|$ and $|\frac{1}{g}dh|$ models.* We show in this section that the Weierstrass data we have just defined satisfies the geometric conditions required of \mathcal{H}_k/σ_k in (4) and in Lemma 1.

The metric induced by the Weierstrass immersion (5) is given by (6):

$$(38) \quad ds = \frac{1}{2} \left(|gdh| + \left| \frac{1}{g}dh \right| \right).$$

Two different branches of gdh (or $\frac{1}{g}dh$) differ by a unitary constant. Thus the metric expression in (38) does not depend on our choice of branch.

We may define g and dh to be square roots of the ratio and the product, respectively, of gdh and $\frac{1}{g}dh$, and we choose the sign of the square root as we did in Section 3 for \mathcal{H}_1 . The function g is then likely to be multi-valued, and our convention extends to choosing the branch determined by our choice of branch of gdh and $\frac{1}{g}dh$. Let r be the involution of the rhombic $|dz|$ model defined by 180° -rotation about the center point \mathcal{O} , and let μ_h and μ_v be reflection in the horizontal and vertical diagonals, respectively.

LEMMA 3. i) *The involutions r , μ_v and μ_h are isometries of the metric ds in (38). The involution μ_h is an isometry of the rhombus equipped with the $|gdh|$ metric. The involutions r and μ_v are isometries between the rhombus equipped with the metric $|gdh|$ and the rhombus equipped with the metric $|\frac{1}{g}dh|$.*

ii) *The forms gdh and $\frac{1}{g}dh = -r^*(gdh)$ are fixed by $-\bar{\mu}_h^*$ and interchanged by $-r^*$ and $\bar{\mu}_v^*$.*

iii) *The one-form dh is imaginary on the horizontal diagonal and real on the vertical diagonal of the rhombus. There is a definition of g , consistent with our convention so that the product of g and dh agrees with the form gdh , and the quotient of dh by g agrees with the form $\frac{1}{g}dh$. Moreover, g is unitary on the vertical diagonal, and g^2 is real on the horizontal diagonal and satisfies*

$g^2 \circ r = \frac{1}{g^2}$. In particular, any branch of the multivalued function g takes segments of the horizontal diagonal disjoint from E_1 and E_2 to a straight line.

We note that the principal branch of gdh and $\frac{1}{g}dh$ are mapped into one another by these automorphisms (see our ‘‘Convention’’ in the previous section.)

COROLLARY 3. *The Weierstrass immersion (5) defined by the forms gdh and $\frac{1}{g}dh$ maps the vertical diagonal into a vertical line and the horizontal diagonal into horizontal lines that project onto lines in the (x_1, x_2) -plane making an angle of $\pm\pi k$ with one another.*

Proof of Lemma 3. Statement i) follows immediately from statement ii) and the form of the metric (38).

Statement ii) for $-r^*$ follows immediately from the definition of $\frac{1}{g}dh$ and the fact that $r^2 = \text{id}$. The meromorphic one-form $\bar{\mu}_h^*(gdh)$ has the same divisor as gdh . Along the portion of the horizontal diagonal where (our chosen branch of) gdh is imaginary, we therefore have $\mu_h^*(gdh) = gdh$. Hence

$$(39) \quad \bar{\mu}_h^*(gdh) = -gdh,$$

(and, analogously $\bar{\mu}_h^*(\frac{1}{g}dh) = -\frac{1}{g}dh$). Similarly, $\bar{\mu}_v^*(gdh)$ has the same divisor as $\frac{1}{g}dh = -r^*(gdh)$. Hence

$$\bar{\mu}_v^*(gdh) = c\frac{1}{g}dh = -cr^*(gdh)$$

for some nonzero constant c . Since $r \circ \mu_v = \mu_h$, applying r^* to the equation above and using (39) give $c = 1$. Hence,

$$(40) \quad \bar{\mu}_v^*(gdh) = \frac{1}{g}dh.$$

Since $\mu_h \circ r = r \circ \mu_h$ and $\mu_v^2 = \text{id}$, the equalities (39) and (40) imply statement (ii) for μ_h .

For statement iii), observe that since

$$(41) \quad dh^2 = gdh \cdot \frac{1}{g}dh,$$

the identities (39) and (40) imply that $\mu_v^*(dh^2) = \overline{dh^2} = \mu_h^*(dh^2)$. Therefore when applied to tangent vectors along both diagonals, we have

$$(42) \quad dh^2 = \overline{dh^2},$$

implying that dh is either real or imaginary on the diagonals. Along the horizontal diagonal, the form gdh is by definition imaginary when applied to tangent vectors, and the same is true for $\frac{1}{g}dh$, either by our convention, by ii),

or by construction of $\frac{1}{g}dh$. Hence, dh^2 is real and negative along the segment of horizontal diagonal from E_1 to E_2 through \mathcal{O} , which implies that dh is imaginary. We also know that dh has no zeros on the vertical diagonal, as neither gdh nor $\frac{1}{g}dh$ vanish there. Since the form dh must be real for vertical directions at \mathcal{O} (because dh is imaginary on tangent vectors to the horizontal diagonal), the form dh is real on the entire vertical diagonal.

Our next goal is to provide a definition of g that is consistent with our conventions and in accord with statement (iii).

To begin, define a multi-valued function G by

$$(43) \quad G = gdh / \frac{1}{g}dh.$$

Since both gdh and $\frac{1}{g}dh$ are imaginary when applied to tangent vectors to the horizontal diagonal, the function G is real there. Since we are expecting a multivalued g —defined only up to integer powers of $e^{2\pi ik}$ —we have shown what is required in statement iii) for the horizontal diagonal. Applying (40) and the fact that $\bar{\mu}_v$ is an involution to (43), we have

$$\bar{\mu}_v^*(G) = \frac{1}{G}.$$

This implies that when applied to tangent vectors to the vertical diagonal we have $\bar{G} = \frac{1}{G}$, i.e. $|G| = 1$ as required. Also, $G \circ r = \frac{r^*gdh}{r^*(\frac{1}{g}dh)} = \frac{-\frac{1}{g}dh}{-gdh} = 1/G$. We define g to be the square root of G . (This is permissible since we can do it on a branch and then extend.) The statements in iii) for g follow directly from those for G . This completes the proof of the lemma. \square

Proof of Corollary 3. The involutions μ_h and μ_v are isometries of the metric ds by statement i) of Lemma 3. Therefore, their fixed-point sets are geodesics. On a minimal surface, a geodesic is a straight line if and only if it is an asymptotic curve. Moreover, a curve on a minimal surface is asymptotic if and only if $\frac{dg}{g}dh$ is imaginary along it [16]. Along the vertical diagonal, the form dh is real on tangent vectors and the function g is unitary according to statement iii) of Lemma 3. Thus the form $\frac{dg}{g}dh$ is imaginary on tangent vectors to the vertical diagonal, which means that the vertical diagonal corresponds to an asymptotic curve, hence a straight line on the minimal surface. Since g is unitary along the vertical diagonal, the corresponding straight line on the minimal surface is vertical.

By statement iii) of Lemma 3, the form dh is imaginary on the horizontal diagonal — and on any interval there not containing E_1 or E_2 . Hence $x_3 = \operatorname{Re} \int dh = 0$ on any interval of the horizontal diagonal. It follows that the image of segments of this diagonal bounded by E_1 and E_2 are mapped to curves in horizontal planes in \mathbf{R}^3 . Also by statement iii) of Lemma 3, the function g takes values on a line through the origin. This implies that $dh dg/g$

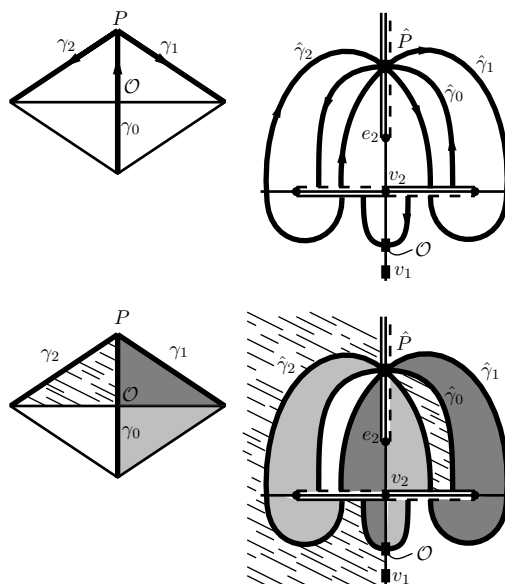


Figure 27: Upper left: The rhombus with the paths γ_1 and γ_2 indicated. The vertical diagonal is labeled γ_0 . Upper right: The paths $\hat{\gamma}_i$ —the images of the paths γ_i under the conformal diffeomorphism—are drawn in the slit model. Note that $\hat{\gamma}_1$ and $\hat{\gamma}_2$ pass through the image of the vertex point in the slit model and no other point on the imaginary axis. The path $\hat{\gamma}_3$, the image of vertical diagonal of the rhombus, passes through both \hat{P} and \mathcal{O} . Lower left: The rhombus divided into four domains by the γ_i and the horizontal diagonal. Lower right: The slit domain divided into four domains corresponding to those in the rhombus model under the conformal diffeomorphism.

is imaginary along those segments, so their images are horizontal straight lines. The values of g along these lines increase or decrease by integer multiples of πk because $\int_{\alpha} g dh = 2\pi k i$ for any simple closed curve α surrounding E_1 or E_2 . Hence projection of successive lines make angles of $\pm\pi k$ with one another. \square

For future reference, we gather together the key results of Sections 4.2.1 and 4.2.2 (Proposition 11 and Corollary 3).

PROPOSITION 12. *For any values of $k > 1/2$ and $d > 0$, the Weierstrass data defined on $\mathcal{T}_k(d)$ produce an \mathcal{H}_k satisfying the horizontal period condition (33). If the data on $\mathcal{T}_k(d)$ also satisfy the vertical period condition (34), then the minimal surface defined by this data satisfies the conditions (4).*

To prove Theorem 3, we must show (among other things) that we cannot only choose for each $k > 1$ a value of $d > 0$ for which the vertical period condition (34) is solved, but also that we can choose a continuous path $(k(t), d(t))$

along which $k(t)$ takes on all values between 1 and ∞ . We will formulate our approach to this problem in Sections 4.3 and 4.4, then carry it out in Sections 5 and 6. Before doing so, we verify that our candidates for Weierstrass data satisfy a necessary condition.

4.2.3. *The placement of the ends and vertical points.* Proposition 10 establishes a necessary condition on the Weierstrass data, specifically restrictions on the relative positions of the E_i and V_i , in order for the continuous choice of d to be possible. We prove in this section (see also the alternative proof in Appendix A) that the Weierstrass data we have defined satisfies this condition for all admissible pairs (k, d) .

PROPOSITION 13. *For all finite $k > 1/2$ and all finite $d > 0$, the points E_i and V_i defined by the construction of gdh satisfy (25):*

$$a + kb = k$$

when written in the form (24): $E_1 = \mathcal{O} - b(\frac{1-\tau}{2})$, $E_2 = \mathcal{O} + b(\frac{1-\tau}{2})$, $V_2 = \mathcal{O} + a(\frac{1-\tau}{2})$.

Remark 12. In Proposition 10, we showed that if an \mathcal{H}_k family exists, then the placement of the ends and vertical points satisfies the condition $a + kb = k$. In Proposition 13, we verify that the data we are constructing in the gdh model do indeed satisfy this condition. We do not assume here that the surfaces \mathcal{H}_k exist and we use only the properties of the gdh and $\frac{1}{g}dh$ models to prove the proposition. On the other hand, the function G in the proof of Lemma 3 will turn out to be the function g^2 (the square of the stereographic projection of the Gauss map on the desired surfaces).

We restate here the immediate consequence of Proposition 10, namely Corollary 2, now valid for our constructed models:

$$(44) \quad a < \frac{k}{k+1} < b, \quad \text{and} \quad \lim_{k \rightarrow \infty} b = 1.$$

Proof. (An alternate proof using theta functions may be found in the appendix.) We begin by recalling from the proof of Lemma 3 the definition of the function

$$G = \frac{gdh}{\frac{1}{g}dh},$$

a multivalued function with poles at E_1 and V_1 , and zeros at E_2 and V_2 , of orders given in the following table:

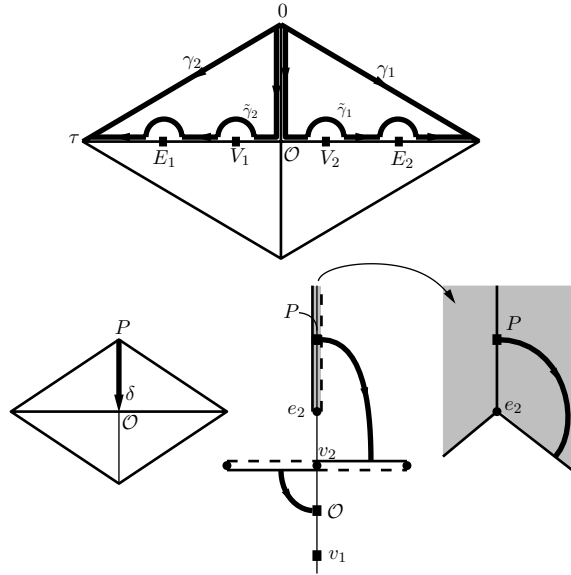


Figure 28: The paths of integration in the proof of Proposition 13. Top: The rhombic model with paths of integration realized on the models of $\mathcal{T}_k(d)$. The paths $\tilde{\gamma}_i$ are homotopic to the paths γ_i . Each of the paths $\tilde{\gamma}_i$ consists of the top half of the vertical diagonal, two semicircular arcs centered at the E_i and three line segments on the horizontal diagonal. Bottom left: The part of the arcs $\tilde{\gamma}_i$ consisting of the top half of the vertical diagonal is labeled δ . Bottom right: The image of δ in the slit model is illustrated here. It begins at a point, labeled P , in the sewn-in cone (this point corresponds to the vertex point in the rhombic model), then descends to the slit, passing through it to end at the point \mathcal{O} corresponding to the identically labeled center point in the rhombus.

$\phi(\delta(t))$ is precisely $gdh(\dot{\delta}(t))$. It follows from Lemma 3, part ii) and the fact that δ is fixed by μ_h that

$$(49) \quad G \circ \delta = \frac{gdh(\dot{\delta})}{\frac{1}{g}dh(\dot{\delta})} = \frac{gdh(\dot{\delta})}{gdh(\dot{\delta})}$$

and therefore $G \circ \delta(t) = e^{2i\theta(t)}$, where $\theta(t)$ is the angle determined by the tangent to the image of δ under the conformal map ϕ . Therefore the integral of dG/G along δ is $2\pi i$ times the total turning of the normal of the image (under ϕ) of δ . A curve homotopic to the image of δ is drawn in Figure 28 and is also labeled δ . It is clear that its normal turns through an angle of $-\pi(k-1)$ as it leaves P and passes through half of the sewn-in cone. It is also clear that the normal does not turn at all from the time the curve leaves the cone until it reaches \mathcal{O} . This proves the first assertion.

Proof of Assertion 2. Since gdh is the pullback of $d\zeta$ under ϕ from the rhombic to the slit model, it follows from Lemma 3 and our convention that any branch of gdh on the rhombus takes values of the form $i\lambda(t)e^{(2\pi ik)n}$ on an interval of the horizontal diagonal bounded by E_1 and E_2 ; here, $\lambda(t)$ is some nonzero real valued function, k is determined by our choice of $\mathcal{T}_k(d)$, and n is an integer determined by the branch of gdh we chose.

The same is true for $\frac{1}{g}dh$ with the same value of k , but with a possibly different integer n and also a possibly different real-valued function $\lambda(t)$. Therefore, the function G on the interval in question takes values on an open ray in \mathbf{C} , from which it follows that the integral of $\frac{dG}{G}$ on this interval is equal to the difference of the values of $\log |G|$ at its endpoints. Since we are free to choose the two “semi-circular” arcs of $\tilde{\gamma}$, so that $|G|$ is constant along them, it follows that the sum of the integrals of $\frac{dG}{G}$ along the three horizontal line segments of $\tilde{\gamma}_1$ is equal to $\log(|G(P)|) - \log(|G(\mathcal{O})|)$. But both P and \mathcal{O} are on the vertical diagonal, where G is unitary, which establishes Assertion 2. \square

4.3. *The $|dh|$ model and the global formulation of the vertical period problem.* We now address the vertical period problem on $\mathcal{T}_k(d)$. To do this, we will describe what amounts to a fourth model for the torus $\mathcal{T}_k(d)$, in terms of which the dh -period problem becomes a question in flat (singular) geometry.

We begin with the rhombic model described in Section 4.1. Consider half of the rhombic torus, produced by identifying the top-left and bottom-right rectangles as in Figure 21. The vertical period problem (34) is still

$$(50) \quad \operatorname{Re} \int_B dh = 0,$$

but now we consider, as in Section 3, the curve B to be a path in the rectangle \mathcal{R} . It follows from Lemma 3(iii) that dh is imaginary on the horizontal sides of the rectangle (as that side corresponds to the imaginary axis in the $|gdh|$ model) while it is real on the vertical edges, corresponding to the vertical axis of \mathcal{H}_k/σ_k . The divisor of dh is given in Figure 29.

	E_1	V_1	V_2	E_2
dh	∞	0	0	∞

Figure 29: The divisor of dh .

We define the map W from the rectangle to the complex plane by

$$(51) \quad W(p) = \int_{\mathcal{O}}^p dh,$$

where \mathcal{O} is the point on the rectangle \mathcal{R} corresponding to the center of the rhombus.

The vertical period problem (51) is solved when

$$(52) \quad \operatorname{Re} \int_B dh = \operatorname{Re} W(P) = 0$$

where P is the left vertex of the rectangle.

4.4. *The (k, d) rectangle \mathcal{P} .* Our goal in Section 5 will be to prove the existence statement of Theorem 3. This we will do by proving that for every $k > \frac{1}{2}$ there is a finite positive value d so that (52) is satisfied, and that there is a continuous family of solutions $(k(t), d(t))$ for which $k(t)$ assumes all values of k in the open interval $(\frac{1}{2}, \infty)$. This we accomplish by an intermediate-value-theorem argument with boundary estimates coming from $d = 0$ and $d = \infty$ for fixed $k \in (\frac{1}{2}, \infty]$.

Formally, this requires first adjoining, to the parameter space of tori $\mathcal{T}_k(d)$ (with $(k, d) \in (\frac{1}{2}, \infty) \times (0, \infty)$, as defined in Section 4.2), a set of punctured tori parametrized by $(k, d) \in [(\frac{1}{2}, \infty) \times \{0, \infty\}] \cup [\{\infty\} \times [0, \infty]]$ and then showing that the height function $h = \int_B dh$ is continuous on the union \mathcal{P} of the parameter space with these boundary points. The added points will be “degenerate” in the following sense. For $1/2 < k < \infty$ and $0 < d < \infty$, the surface $\mathcal{T}_k(d) \setminus \{e_1, e_2, v_1, v_2\}$ is conformally a four-punctured torus. When we set $k = \infty$, $d = 0$, or $d = \infty$, we describe a torus with fewer than four punctures. These punctured tori are degenerate four-punctured tori because, informally, some of the punctures have coalesced; formally, these tori are noded surfaces.

We begin by carefully defining the total parameter space \mathcal{P} . In Section 5 we will study the height function, h on \mathcal{P} and prove that it is continuous. In Section 6, we will estimate the height function in order to apply an intermediate-value argument to prove the existence part of Theorem 3.

4.4.1. *The definition of \mathcal{P} .* To each $(k, d) \in (\frac{1}{2}, \infty) \times [0, \infty]$, we associate a punctured Riemann surface. The formal setting for this is the augmented Teichmüller space $\overline{\mathcal{T}}_{1,4}$ of four-times-punctured tori. This space is the bordification of the Teichmüller space $\mathcal{T}_{1,4}$ of four-times-punctured tori obtained by attaching, to $\mathcal{T}_{1,4}$, strata representing surfaces with nodes; the nodes are obtained by pinching simple closed curves on a (topological) four-times punctured torus. (We will stick to our suggestive, but somewhat sloppy terminology of discussing the “coalescing” of distinguished points $\{p_1, \dots, p_k\}$ on the torus — here we of course are referring to the pinching off of a curve surrounding the points $\{p_1, \dots, p_k\}$. See Remark 2.) In this sense, our definition of the rectangle \mathcal{P} is simultaneously a map of the rectangle $(\frac{1}{2}, \infty) \times [0, \infty]$ into $\overline{\mathcal{T}}_{1,4}$.

We begin the definition of \mathcal{P} on its interior $(\frac{1}{2}, \infty) \times (0, \infty)$. We have in fact done this in Sections 4.1 and 4.2 using the slit model. We remind the reader that in the slit model, the parameter d determines the placement of e_2 , while v_2 is always located at the origin of the ζ -plane. The pair (k, d) determine

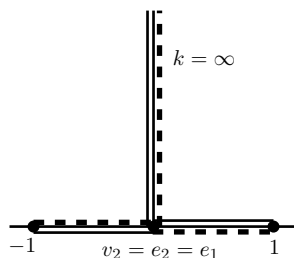


Figure 30: The degenerate structure $T_\infty(0)$.

the conformal structure of $\mathcal{T}_k(d)$, and a specifically defined diffeomorphism with a rhombus representation of $\mathcal{T}_k(d)$ determines the location of the four distinguished points E_1, E_2, V_1 and V_2 . Their positions (see (24)) determine the functions $a = a(k, d)$ and $b = b(k, d)$ satisfying $a + kb = k$ according to (25) and Proposition 13.

For $d = 0$, and $\frac{1}{2} < k < \infty$, we are sewing in a cone point at v_2 with $v_2 = e_2$. In particular, if we want the structures $\mathcal{T}_k(d)$ to be continuous at $d = 0$, we are required to have $a(k, 0) = b(k, 0)$, and by (25), we have $a = b = k/(k+1)$. In particular, this will force $e_1 = v_1$. Hence $\mathcal{T}_k(0)$ must be a rhombic torus with two distinguished points. As $k \rightarrow \infty$, we have $a = b \rightarrow 1$, which means that these two distinguished points should converge at the vertex in the rhombic model of $\mathcal{T}_\infty(0)$. We define $\mathcal{T}_\infty(0)$ to be the torus produced by sewing in a cone of simple exponential type at v_2 as in Figure 30. All the points V_1, V_2, E_1 and E_2 then coincide with $a = b = 1$.

We now define $\mathcal{T}_k(\infty)$ for $\frac{1}{2} < k \leq \infty$. Here, we are sewing in a $2\pi k$ cone at infinity. The underlying torus will be defined to be \mathcal{T}_1 (see Section 3) and the points e_1 and e_2 coincide. This can only happen when $b = b(k, \infty) = 1$ in (24). Hence by (25), we have $a = 0$. We require $E = E_1 = E_2$ to be at the vertex and $V = V_1 = V_2$ to be at the center of the rhombus \mathcal{T}_1 .

Finally, we define $\mathcal{T}_\infty(d)$. For $d = 0$ or $d = \infty$, we have already done so. For $0 < d < \infty$, we are sewing in a cone of simple exponential type at the point di in the slit model. This means that the points labelled e_1 and e_2 coincide *but it does not necessarily mean that the v_i have to coincide. In fact, as we will prove in Proposition 14 below, the points v_1 and v_2 are distinct.* Thus, in this case, we will have *three* distinct points: $E = E_1 = E_2, V_1$ and V_2 . Here $b = b(\infty, d) = 1$ but $a = a(\infty, d) \neq 0, 1$.

PROPOSITION 14. *For $k = \infty$ and any value of $d \in (0, \infty)$, the points V_1 and V_2 defined by the construction of $\mathcal{T}_\infty(d)$ do not coincide. In particular, in the form (24) we have the expression*

$$V_1 = \mathcal{O} - a \left(\frac{1 - \tau}{2} \right) \quad V_2 = \mathcal{O} + a \left(\frac{1 + \tau}{2} \right),$$

with $a \neq 0, 1$.

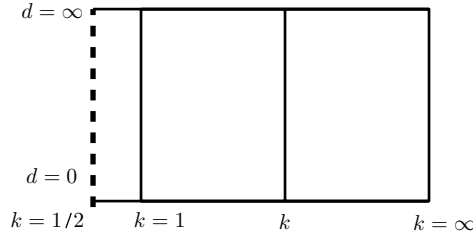


Figure 31: The (k, d) rectangle. Each point corresponds to a $\mathcal{T}_k(d)$, on which we have defined gdh , $\frac{1}{g}dh$, g and dh .

Proof. We begin in the slit model of $\mathcal{T}_\infty(d)$. Since we are sewing in a cone of simple exponential type, we know that $e_2 = di$ and $e_1 = \infty$ coincide on the torus $\mathcal{T}_\infty(d)$. We will label that point e . When $d > 0$, we have $v_2 = 0 \neq e$. Let us now look at what this says in the rhombic model of $\mathcal{T}_\infty(d)$. First, the ends E_i must coincide at a point we label E and that point must be the vertex of the rhombus. In particular, $b = 1$. Consider the points V_1 and V_2 corresponding to v_1 and v_2 . Because $v_2 \neq e$ we know that $V_2 \neq E$. In particular, $a \neq 1$. We will now show, by contradiction, that $a \neq 0$. This is equivalent to showing that $V_1 \neq V_2$, which is in turn equivalent to showing that $v_1 \neq v_2 = 0$.

Suppose $V_1 = V_2 = \mathcal{O}$ in the rhombic model. Then the one-forms $\frac{1}{g}dh = -r^*(gdh)$ and gdh have the same divisors. This means that the cone metrics $|gdh|$ and $|\frac{1}{g}dh|$ have the same cone points: a cone point at \mathcal{O} with cone angle 6π , and an exponential cone point of simple type at E , the vertex of the rhombic model. The vertex of the rhombus is a fixed point of r^* , and therefore $r^*_{|\mathcal{O}} = -id$. Therefore

$$\frac{1}{g}dh|_E = -r^*(gdh)|_E = gdh|_E,$$

which implies that the exponential cone points of the $|gdh|$ and $|\frac{1}{g}dh|$ metrics are asymptotically isometric. It then follows from Proposition 4 of Section 2.3 that $|\frac{1}{g}dh|$ and $|gdh|$ define the same cone metric up to a constant scale factor. Since the metrics agree at the fixed points of r , they are in fact equal: $|\frac{1}{g}dh| = |gdh|$.

We now use statement ii) of Lemma 3. It says, among other things, that $|gdh|$ and $|\frac{1}{g}dh|$ are interchanged by $\bar{\mu}_v^*$, where μ_v^* is reflection in the vertical diagonal of the rhombus. (Lemma 3 is presented in a context where it is natural to assume that $k < \infty$, but its proof does not use this, allowing us to use its statement ii) here.) Therefore, the involution μ_v^* is an isometry of the metric $|gdh|$. The fixed-point set of μ_v^* is the vertical diagonal, which meets the horizontal diagonal at precisely the points \mathcal{O} and E .

We now look at what this implies in the slit model. Here, gdh is the one form induced by $d\zeta$. This means that the fixed point set of μ_v^* , considered now as acting in the slit model, must consist of straight line segments and rays. Moreover, reflection in these lines and rays must induce μ_v^* in the slit model. Since μ_v^* in the rhombic model leaves the horizontal axis invariant, it follows that μ_v^* in the slit model leaves the imaginary ζ -axis invariant. This is possible only if the fixed point set is either the imaginary ζ -axis or the real ζ -axis. However, μ_v^* cannot be reflection in the imaginary axis because reflection in the imaginary axis is μ_h^* and $\mu_h^* \neq \mu_v^*$. Similarly, μ_v^* cannot be reflection in the real axis of the slit domain because it takes $e = di$ to $-di$, and $-di$ is not a cone point. Therefore, the assumption that $V_1 = V_2 = \mathcal{O}$ leads to a contradiction. \square

Remark 13. The definition of the Weierstrass data for $\mathcal{T}_\infty(d)$, $d \neq 0, \infty$, was forced by the desire to have the data $\mathcal{T}_k(d)$ depend continuously on (k, d) as $k \rightarrow \infty$, something we will prove to be the case in the next section. In addition to the properties proved in Proposition 14, these data have other critical properties. First, they automatically solve the horizontal period problem. Second, they define a (possibly multivalued) conformal minimal immersion at which there is no period at any end. Third, they have the properties of statement (iii) of Lemma 3. These assertions are proved in the first four paragraphs of the proof of Lemma 8 in Section 6.

5. Continuity and boundary estimates for the height function

In the previous section we defined for each pair $(k, d) \in \mathcal{P} = (\frac{1}{2}, \infty] \times [0, \infty]$, a point $\mathcal{T}_k(d)$ in the closure of the Teichmüller space, $\mathcal{T}_{1,4}$ of four-times punctured tori. This torus $\mathcal{T}_{k,d}$ carried a pair of one-forms gdh and $\frac{1}{g}dh$.

PROPOSITION 15. *The mapping $(k, d) \rightarrow \mathcal{T}_k(d)$ is continuous on \mathcal{P} .*

We will prove Proposition 15 in Section 5.1 and its subsections. As the proof is long, the reader may wish to skip to Section 5.2 on a first reading.

Remark 14. Because the one-forms gdh and $\frac{1}{g}dh$ both vary continuously (on, say, a family of continuously varying models), it follows from Proposition 15 that the development map W in (51) is also continuous as a function of $(k, d) \in \mathcal{P}$.

Definition 10. The real-valued function $h : \mathcal{P} \rightarrow \mathbf{R}$ is defined by the left-hand side of (52) (i.e. $h(k, d) = \text{Re} \int_B dh = \text{Re} W(P)$), where for $(k, d) \in \mathcal{P}$ the path B and the one-form dh are taken in $\mathcal{T}_k(d)$.

It follows from Proposition 15 that

PROPOSITION 16. *The function $h : \mathcal{P} \rightarrow \mathbf{R}$ is continuous.*

Proof of Proposition 16. The one-form dh on $\mathcal{T}_k(d)$ is determined up to a factor by the conformal structure of $\mathcal{T}_k(d)$ and the divisor of dh on $T_{k,d}$. Of course, Proposition 15 asserts that the conformal structures and divisors of $\mathcal{T}_k(d)$ vary continuously in \mathcal{P} . We know from Lemma 3(iii) that for $(k, d) \in \mathcal{P}^\circ$, the one-form dh on $T_{k,d}$ is always imaginary on the horizontal diagonal and real on the vertical diagonal. Thus if we insist that the forms dh defined on $(k, d) \in \partial\mathcal{P}$ also satisfy Lemma 3(iii), then we need only establish the continuity in (k, d) of the cone metric $|dh|$ to verify continuity of the forms dh ; the phase is already continuous. On the other hand, the line element $|dh|$ can be expressed as $|dh| = \{|gdh| \cdot |\frac{1}{g}dh|\}^{1/2}$, and thus any scale of $|dh|$ is determined by the scales of $|gdh|$ and $|\frac{1}{g}dh|$. We know that these scales are determined and are clearly continuous by the restriction that the slit $[-1, 1]$ on the slit model always has $|gdh| = |d\zeta|$ -length and $|\frac{1}{g}dh|$ -length equal to two. This then corresponds to the continuity of the $|dh|$ -length of a curve on $\mathcal{T}_k(d)$ for $(k, d) \in \mathcal{P}^\circ$. The proposition then follows once we note that as the underlying conformal structures of (unpunctured) tori vary continuously over \mathcal{P} , then so do representatives of the cycle B , and hence so does $h = \text{Re} \int_B dh$. \square

5.1. *The proof of Proposition 15.* We prove the continuity in successive steps, each step focusing on continuity on a particular region on \mathcal{P} . We begin with a preliminary observation, separating out the important issues of convergence of punctured tori from the minor issue of convergence of underlying (unpunctured) tori.

LEMMA 4. *For every closed subrectangle $[\frac{1}{2} + \varepsilon, \infty] \times [0, \infty] \subset \mathcal{P}$, with $\varepsilon > 0$, the corresponding punctured tori form a compact set.*

Proof. For $(k, d) \in \mathcal{P}$, we will work with the slit model of the $\mathcal{T}_k(d)$. Consider two cycles γ_1 and γ_2 in this model which connect the lower edge of the slit with its corresponding upper edge via a path that avoids the positive imaginary axis. They may be chosen to be symmetric with respect to the imaginary axis. (See Figure 32.) The space of tori is compact if, and only if, those curve classes have extremal lengths which are uniformly bounded above and uniformly bounded away from zero.

Recall from Section 2.5 that there are two equivalent definitions of extremal length, one (the geometric) which lends itself to upper bounds, and one (the analytic) which lends itself to lower bounds. Note that in each of the homotopy classes of γ_1 and γ_2 , because the cone angle of e_2 is bounded away from π , there is a fixed annulus of positive modulus which embeds in the torus and is disjoint from the imaginary axis. This is independent of (k, d) . By Def-

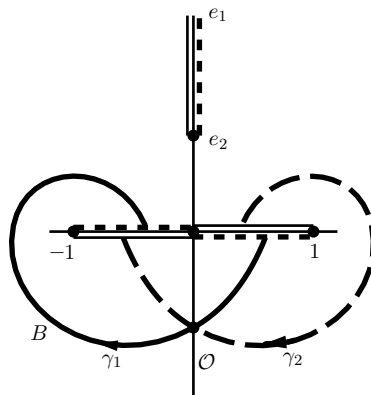


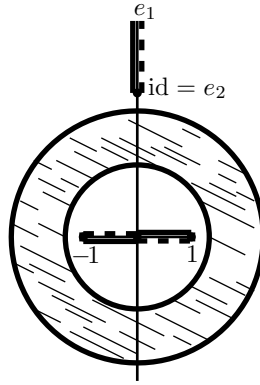
Figure 32: The paths γ_1 and γ_2 used in the proof of Lemma 4.

inition 6 of Section 2.5, this provides a uniform upper bound for the extremal lengths of those curves. Next, to prove a lower bound for the extremal lengths of $[\gamma_1]$ and $[\gamma_2]$, it is enough by Definition 4 to exhibit a conformal metric ρ for which $\ell_\rho(\gamma_i)^2 / \text{Area}(\rho)$ is bounded below. But such a metric is evident: on the box $[-2, 2] \times [-1, 1] \subseteq \mathbf{E}^2$, set $\rho \equiv 1$ and, on the complement, set $\rho \equiv 0$ (here, we implicitly set $\rho \equiv 0$ on the conical region sewn in along the imaginary axis above $(0, di)$). It is clear that in this metric $\ell_\rho(\gamma_i) \geq 1$ while $\text{Area}(\rho) = 8$, proving the positive lower bound. \square

5.1.1. *Continuity in the interior of \mathcal{P} .* Continuity on the interior of \mathcal{P} is almost self evident. Here we take $\frac{1}{2} < k < \infty$ and $0 < d < \infty$, and note, roughly, that small changes in either k or d in those ranges only change the $|gdh|$ structure slightly, and so the conformal structure of the torus with the four distinguished points $\{V_1, V_2, E_1, E_2\}$ changes only slightly.

However, in preparation for the next two subsections, we will discuss continuity in the interior carefully and in the context of the methods used later.

In the rhombic or $|dz|$ -model, there is a flat cone metric that is isometric to the pullback to the rhombus of the $|d\zeta|$ metric on in the slit model. Recall that this is the $|gdh|$ metric on the rhombus, and we note that it is determined up to a scaling factor by its divisor (by Proposition 3); this factor, say C , is a normalizing constant. In particular, the location and type of the cone points (the ends and vertical points) are uniquely determined by the metric $|gdh|$ or even enough of its geometric invariants such as $d_{|gdh|}(V_2, E_2)$ or the lengths, $\ell_{|gdh|}(\gamma_i)$, of the shortest representative of the free homotopy class of γ_i . Since under a perturbation of (k, d) , all the geometric invariants on the slit model change but slightly, it follows that the positions of the ends and vertical points vary only slightly in the rhombic model. Because V_1 and V_2 are symmetrically placed with respect to \mathcal{O} , it follows that V_1 also depends continuously on (k, d) . By Lemma 4, the underlying unpunctured torus varies continuously. Therefore, $T_k(d) : \mathcal{P} \rightarrow \bar{\mathcal{T}}$ is continuous on the interior of \mathcal{P} .

Figure 33: The annulus $A(1, d)$.

5.1.2. *Continuity on the top edge away from the right-hand corner.* By Lemma 4, we know that the underlying rhombic tori subconverge, so that our attention is focused on the positions of the points E_1 , E_2 , V_1 , and V_2 in the rhombic model.

Recall that the points in the rhombic model labeled by E_i (resp. V_i) correspond to the points in the slit model labeled by e_i (resp. v_i).

Assuming that $k \leq k_0 < \infty$ we want to prove that E_1 and E_2 coalesce as $d \rightarrow \infty$. Since $E_2 - E_1 = 2b = 2b(k, d)$ according to (24), the coalescence of the E_i is equivalent to the requirement that $b(k, d) \rightarrow 1$ as $d \rightarrow \infty$ with $k \leq k_0$. Again we have, by (24), that $V_2 - V_1 = 2a = 2a(k, d)$, and also that $a + kb = k$, a consequence of Proposition 10. It follows from the boundedness of k that $b(k, d) \rightarrow 1$ as $d \rightarrow \infty$ if and only if $a(k, d) \rightarrow 1$ as $d \rightarrow \infty$. Hence the coalescence of the E_i is equivalent to coalescence of the V_i .

The coalescing of E_1 and E_2 as $d \rightarrow \infty$ for $k \leq k_0 < \infty$ follows from a simple extremal length argument. Consider, for small fixed $\delta > 0$, an annulus $A(1 + \delta, d - \delta)$ in the slit model with center at the origin (v_2), inner radius $1 + \delta$ and outer radius equal to $d - \delta$ (with $d > 1$). This annulus has a large modulus and a core curve encircling e_1 and e_2 . It is clear that the core curve of $A(1 + \delta, d - \delta)$ separates the slit from the topological disk in the complement of $A(1 + \delta, d - \delta)$ that contains e_1 and e_2 . For d large, the modulus of $A(1 + \delta, d - \delta)$ is nearly $\frac{1}{2\pi} \log d$, and therefore the extremal length of a curve encircling e_1 and e_2 (which we know to be bounded above by $\frac{3\pi}{\log d}$ by Definition 5) becomes arbitrarily small as $d \rightarrow \infty$. Therefore e_1 and e_2 coalesce on the compact set of rhombi under discussion and it follows immediately that the same is true for E_1 and E_2 in the rhombic model.

5.1.3. *Uniform estimates near the right-hand edge away from the bottom vertex.* In order to prove continuity along the right-hand edge, we need to have good estimates for the positions of the E_i , as functions of k and d , as k and/or

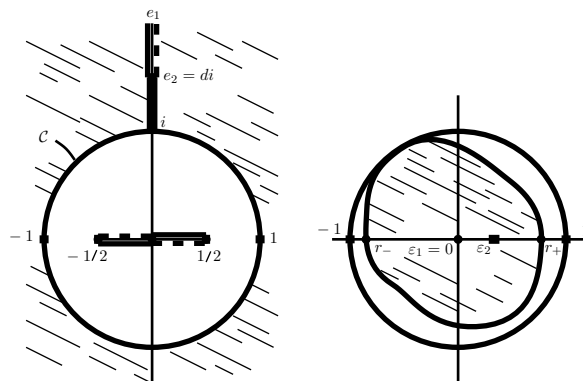


Figure 34: The Δ model. On the left: The (scaled) rhombic model with the circle \mathcal{C} , exterior to which is the simply connected domain D . On the right: the disk Δ , isomorphic to D (with the metric induced by $|d\zeta|$ in the slit model). The disk Δ has been normalized so that the point corresponding to e_1 is at the origin, the point corresponding to e_2 is on the positive real axis, and Δ lies inside the unit disk but not inside any smaller disk.

d go to ∞ . To do this we concentrate on a simply connected neighborhood of these points. We begin in the slit model. It is convenient for the exposition to do a single homothety of the slit model, scaling it so that the slit on the real axis is now along the segment $[-1/2, 1/2]$. Consider a circle \mathcal{C} of, say, radius 1 about the origin. This circle \mathcal{C} separates the model into two components: one, say T , contains the slit and is topologically a punctured torus, and the other, say D , contains e_2 and e_1 and is topologically a disk. This disk with the metric $|d\zeta| = |gdh|$ is isometric to a domain, say Δ , which we expect to be nearly a disk with the metric

$$ds_\Delta := C \left| \frac{(\xi - \epsilon_2)^{k-1}}{(\xi - \epsilon_1)^{k+1}} \right| |d\xi|.$$

(See Appendix B, Lemma 10.) Here, ϵ_i represents the position in the domain Δ of the point e_i in the slit model, and C is a constant depending upon the geometries of Δ and of the slit model with the metric $|gdh| = |d\zeta|$. We translate the domain Δ so that $\epsilon_1 = 0$; then the metric ds_Δ takes the form

$$(53) \quad ds_\Delta = C \left| \frac{(\xi - \epsilon_2)^{k-1}}{\xi^{k+1}} \right| |d\xi|$$

$$(54) \quad = C \left| 1 - \frac{\epsilon_2}{\xi} \right|^{k-1} \frac{|d\xi|}{|\xi|^2}.$$

When $|\epsilon_2|$ is small, we can expect $\partial\Delta$ to be a nearly round circle of radius nearly $1/C$; we will later show that $|\epsilon_2|$ must be small along any path in \mathcal{P} along which $(k, d) \rightarrow (\infty, \infty)$.

We are interested in determining the asymptotics of C and ε_2 as k or d tends to infinity; this involves matching the geometric invariants of (Δ, ds_Δ) with those of $(D, |gdh|)$. To do this we insist that (Δ, ds_Δ) should be bounded by a ds_Δ -round circle of ds_Δ -circumference 2π and that the ds_Δ -distance from this circle to ε_2 should equal the $|gdh|$ -distance from \mathcal{C} to E_2 , which of course is $d - 1$. These are conditions that hold true for the isometric domain $(D, |gdh|)$.

We now introduce two additional normalizations. First, we rotate Δ so that ε_2 lies on the positive real axis. Second, we dilate Δ —and consequently alter the constant C —so that $\partial\Delta \subset D_1(0)$ with $\partial D \cap \partial D_1(0) \neq \emptyset$; i.e., we do a homothety to Δ so that it just fits within the unit ball $B_1(0)$, touching $\partial B_1(0)$ at one point at least. (See Figure 34.)

LEMMA 5. $C = 1 + o(1)$, $\varepsilon_2 = \frac{1}{kd} + o(\frac{1}{d})o(\frac{1}{k})$ as $k \rightarrow \infty$.

Proof. We first prove that C is bounded and that $\varepsilon_2 \rightarrow 0$ as $k \rightarrow \infty$. Continuing with our description of the domain Δ , we next make use of the symmetry of our situation. In the slit model, the disk D is symmetric with respect to reflection in the imaginary-axis, and the portion of the imaginary axis between e_2 and \mathcal{C} is the unique geodesic connecting e_2 to ∂D . In particular, $\partial\Delta$ meets the positive real axis in one point, say r_+ , and meets the negative real axis in one point, say r_- . As the metric ds_Δ is invariant under reflection in the real axis, we conclude that the portion of the real axis joining ε_2 to $r_+ \in \partial\Delta$ is a geodesic. As there is but one geodesic joining e_2 to $\partial D = \mathcal{C}$, we conclude that the isometry taking D to Δ must take the imaginary axis between \mathcal{C} and e_2 to the positive real axis between r_+ and ε_2 .

We can now get a crude bound on C . Consider the intersection of $\partial\Delta$ with $D_{\frac{|r_-|}{4}}(r_-)$, the disk around r_- of radius $\frac{|r_-|}{4}$. The arc $\partial\Delta \cap D_{\frac{|r_-|}{4}}(r_-)$ must be properly embedded in the ball $D_{\frac{|r_-|}{4}}(r_-)$. Also, in that ball, we have that $|\xi - \varepsilon_2| > |\xi|$ as $\varepsilon_2 \in \mathbf{R}_+$. This gives the estimate

$$\frac{|\xi - \varepsilon_2|^{k-1}}{|\xi|^{k+1}} > \frac{1}{|\xi|^2} > \frac{1}{|\frac{5}{4}r_-|^2} = \frac{16}{25} \cdot \frac{1}{r_-^2},$$

valid for $\xi \in D_{\frac{|r_-|}{4}}(r_-)$. Because the arc $\partial\Delta \cap D_{\frac{|r_-|}{4}}(r_-)$ passes through the center point r_- of that disk, its $|d\zeta|$ -length is at least $\frac{|r_-|}{2}$. But this implies that it has ds_Δ -length of at least $\frac{|r_-|}{2} \cdot \frac{4C}{5|r_-|}$. Since the whole ds_Δ -length of $\partial\Delta$ is 2π , we see that $C < \frac{5}{2} \cdot 2\pi = 5\pi$.

We have established that C is uniformly bounded, and we now turn our attention to estimating ε_2 . Consider the arc on the positive real axis connecting ε_2 and r_+ . The ds_Δ -length of this arc must be $d - 1$, the distance from e_2 to \mathcal{C} in the $|d\zeta|$ -metric in the slit model. Since this also must be the distance in

the ds_Δ -metric we may compute that

$$\begin{aligned}
 (55) \quad d - 1 &= d(\partial\Delta, \varepsilon_2) = \int_{\varepsilon_2}^{r_+} ds_\Delta = \int_{\varepsilon_2}^{r_+} C \left| 1 - \frac{\varepsilon_2}{\xi} \right|^{k-1} \frac{|d\xi|}{|\xi|^2} \\
 &= C \int_{\varepsilon_2}^{r_+} \left(1 - \frac{\varepsilon_2}{\xi} \right)^{k-1} \frac{d\xi}{\xi^2} = \frac{C}{\varepsilon_2 k} \left(1 - \frac{\varepsilon_2}{r_+} \right)^k.
 \end{aligned}$$

Now, since $\partial\Delta \subset \overline{B_1(0)}$, we know that $0 < \varepsilon_2 < r_+ < 1$. Hence

$$d - 1 < \frac{C}{\varepsilon_2 k} (1 - \varepsilon_2)^k < \frac{C}{\varepsilon_2 k},$$

which implies that

$$\varepsilon_2 < \frac{C}{k(d - 1)} < \frac{C'}{kd},$$

where $C' = \frac{Cd_0}{d_0 - 1}$ is a constant depending on the lower bound, d_0 of d , which we assume to be larger than 1. Hence, $\varepsilon_2 \rightarrow 0$ as either $d \rightarrow \infty$ or $k \rightarrow \infty$.

With the boundedness of C and the decay of ε_2 established, we easily prove the finer estimates of the lemma. We have normalized Δ so that $\partial\Delta$ meets the unit circle (in the $|\delta\xi|$ metric) at least at one point. Consider such a point, say ξ_0 . Then since $\varepsilon_2 \rightarrow 0$, and C is uniformly bounded, the metrics ds_Δ in (53) subconverge on a sequence (k, d) and in a fixed neighborhood of ξ_0 to

$$C_\infty \left| \frac{d\xi}{\xi} \right|^2,$$

where C_∞ is the limit of the constants C in the chosen subsequence.

Now, we would like to claim that $C_\infty = 1$, but whatever it is, in the metric $C_\infty \frac{|d\xi|^2}{|\xi|^2}$, the arc $\partial\Delta$ passing through ξ_0 will have constant geodesic curvature only if $\partial\Delta$ is the unit circle. But if $\partial\Delta$ is the unit circle, its geodesic curvature will be equal to one (and its length will be 2π) only if $C_\infty = 1$. This gives the estimate

$$C = 1 + o(1),$$

which is the first estimate of the lemma. (Here by $o(1)$, we are indicating a quantity which tends to zero as either $k \rightarrow \infty$ or $d \rightarrow \infty$.) In addition this argument implies that

$$(56) \quad r_+ = 1 + o(1).$$

To get the finer estimates on ε_2 , we return to (55). For d or k large we must have $C = 1 + o(1)$, and the estimate (56). Thus, we can rewrite (55) as

$$\begin{aligned}
 d - 1 &= \frac{1 + o(1)}{\varepsilon_2 k} \left(1 - \frac{\varepsilon_2 k}{k(1 + o(1))} \right)^k \\
 &= \frac{1 + o(1)}{\mu} \left(1 - \frac{\mu(1 + o(1))}{k} \right)^k,
 \end{aligned}$$

where we have written $\mu = \varepsilon_2 k$ in the last term in order to show the factor $(1 - \frac{\mu}{k})^k$ to be uniformly bounded for large k . Expanding the right-hand side of the above yields

$$d - 1 = \frac{1}{\mu} (1 + o(1) - \mu(1 + o(1)) + O(\mu^2)),$$

from which we conclude that

$$d = \frac{1}{\varepsilon_2 k} + \frac{o(1)}{\varepsilon_2 k} + o(1) + O(\varepsilon_2 k),$$

or that

$$\varepsilon_2 = \frac{1}{kd} + o\left(\frac{1}{d}\right) o\left(\frac{1}{k}\right)$$

as desired. (The error term indicates a quantity that tends to zero when multiplied by either k or d as either k or d tends to infinity.) This concludes the proof of the lemma. \square

5.1.4. Continuity along the right-hand edge away from the bottom vertex.

We now use the estimates of Lemma 5 in the previous subsection to prove continuity along the right-hand edge when $d > 2$. In fact it will be evident that the proof can be modified to hold for any point on that edge of the form (∞, d) , $d > 0$. In particular, it holds at the top right-hand vertex of \mathcal{P} , the point (∞, ∞) .

We know from Lemma 4 that the underlying compact rhombic tori associated to the slit model determined by (k, d) also converge to a nontrivial, nondegenerate rhombus as $kd \rightarrow \infty$. (We will assume throughout that $d > 2$.)

We will prove first that, as $k \rightarrow \infty$, the points E_1 and E_2 coalesce. This is required because the (k, d) structures we have defined in Section 4 on the right-hand edge, where $k = \infty$, have this property. Note that we will allow $(k, d) \rightarrow \infty$ along any path where $k \rightarrow \infty$ and $d > 2$. In particular, we allow d to tend to ∞ with k .

We have constructed in Section 5.1.3 an isometric model Δ of a domain D on the slit model containing points ε_1 and ε_2 corresponding to the points E_1 and E_2 (respectively). It is evident from Lemma 5 that $\varepsilon_2 \rightarrow \varepsilon_1 = 0$ in this model, as $kd \rightarrow \infty$. However, we need to prove that in the corresponding rhombic model, the corresponding points E_1 and E_2 are coalescing to a point as $k \rightarrow \infty$. To do this, we must relate the disk Δ with metric ds_Δ (which we will refer to as the Δ -model) to a domain inside the rhombic model.

We do this by constructing yet another model of the surface, a hybrid of the slit model and the Δ -model in Section 5.1.3. More precisely, we make a two-step construction of a metric torus that we will denote by N . First, we apply a quasi-conformal map (with quasiconformal constant close to one) of the topological disk Δ so that it becomes a round disk of radius one. Then, recalling that the Δ -model is a model for the exterior of the disk of radius one

in the slit model, we sew the interior of the disk of radius one in the slit model to the disk Δ (with metric ds_Δ) along the common round-circle boundary; here we require the point r_+ in Δ to glue to the imaginary axis of the slit model. As the circle is round, this determines the gluing completely. It is clear that if we were to equip Δ with the $|d\zeta|$ metric and perturb it only slightly quasi-isometrically, then the diameter of the resulting torus N is bounded.

In this construction, we alter the metric and conformal structure of the surface by the initial quasi-conformal map, and so it is crucial that this deformation be quite small. However, we have already seen that the normalizing constant C is $1 + o(1)$ as $k \rightarrow \infty$ and, by (56), $r_+ = 1 + o(1)$. Thus the boundary $\partial\Delta$ lies at radius $1 + o(1)$, with geodesic curvature $\kappa = 1 + o(1)$. Now, as $\varepsilon_2 = \frac{1}{kd} + o(\frac{1}{kd})$, we see that if we define our quasi-conformal map to be the identity on a disk of radius $\frac{3}{kd}$ and a radial stretch (the stretching dependent on the polar angle) on the exterior of that disk, then the map is $(1 + o(\frac{1}{\log kd}))$ -quasiconformal.

The metric torus N allows us to estimate the distance separating the points representing E_1 and E_2 . More precisely, consider the extremal length of the curve class Γ^* consisting of all curves freely homotopic to the circle \mathcal{C} in the slit model, a curve that encircles e_1 and e_2 . Now the extremal length $\text{Ext}_\Gamma(\Omega)$ of a curve system Γ in a domain Ω will be dilated or contracted by a factor of K under a K -quasi-conformal map $F : \Omega \rightarrow \Omega'$; i.e.,

$$(57) \quad \frac{1}{K} \text{Ext}_\Gamma(\Omega') \leq \text{Ext}_{\Gamma'}(\Omega') \leq K \text{Ext}_\Gamma(\Omega),$$

where $\Gamma' = F(\Gamma)$. Thus the extremal length of the particular class Γ^* will be within a factor of $1 + o(\frac{1}{\log kd})$ of the extremal length $\text{Ext}_{\Gamma^*}(N)$ on the hybrid model N . But the extremal length $\text{Ext}_{\Gamma^*}(N)$ is easy to compute. From Lemma 5, we have $\varepsilon_2 = \frac{1}{kd} + o(\frac{1}{dk})$. Using this estimate together with the fact that N has finite diameter in the sense described above we find that

$$\text{Ext}_{\Gamma^*}(N) = \frac{2\pi}{\log kd \cdot c_N} + o\left(\frac{1}{dk}\right)$$

as $k \rightarrow \infty$, with c_N a constant that depends on the diameter of N , which is bounded above and below. (See Ohtsuka [32, Thms. 2.55, 2.80].) Taking into account the distortion of extremal length caused by the quasi-conformal map of the slit model (which we denote here by $M_{|d\zeta|}$) to N , we see from the above equation that

$$(58) \quad \begin{aligned} \text{Ext}_{\Gamma^*}(M_{|d\zeta|}) &= \left[1 + o\left(\frac{1}{\log kd}\right)\right] \left[\frac{2\pi}{\log(kd \cdot c_N)} + o\left(\frac{1}{\log kd}\right)\right] \\ &= \frac{2\pi}{\log(kd \cdot c_N)} + o\left(\frac{1}{\log kd}\right) \end{aligned}$$

as $k \rightarrow \infty$. Of course, as the slit model $M_{|d\zeta|}$ is conformal to the rhombic model, say $M_{|dz|}$, we see that

$$(59) \quad \text{Ext}_{\Gamma^*}(M_{|dz|}) = \frac{2\pi}{\log kd \cdot c_N} + o\left(\frac{1}{\log kd}\right)$$

as $k \rightarrow \infty$; here, Γ^* refers to the system of curves encircling E_1 and E_2 in the rhombic model. In particular, this extremal length goes to zero as $k \rightarrow \infty$. Thus, E_1 and E_2 coalesce in the limit rhombic model.

We now consider the limiting behavior of the points V_1 and V_2 in the rhombic model. To do so, we will establish a quantitative version of the coalescence of E_1 and E_2 in order to use the relation (59) to estimate the separation of V_1 and V_2 . This is now straightforward, for we know that (again see [32, Thms. 2.55, 2.80]) that from (59) and (58))

$$\text{Ext}_{\Gamma^*}(M_{|dz|}) = \frac{2\pi}{\log \frac{c_M}{|E_1 - E_2|}} + o\left(\frac{1}{\log |E_1 - E_2|}\right),$$

as $k \rightarrow \infty$. Thus, combining the last two estimates for $\text{Ext}_{\Gamma^*}(M_{|dz|})$, we find

$$(60) \quad \begin{aligned} |E_1 - E_2| &= \frac{1}{kd} \cdot \frac{c_M}{c_N} (1 + o(1)) \\ &= \frac{C}{kd} + o\left(\frac{1}{d}\right) o\left(\frac{1}{k}\right) \end{aligned}$$

as $k \rightarrow \infty$.

Now in the notation of (24), $|E_1 - E_2| = 2(1 - b)$ and $|V_1 - V_2| = 2a$, and using (25) or Proposition 13 (namely $a + kb = k$) and the above estimate for $|E_1 - E_2|$ we find

$$(61) \quad \begin{aligned} |V_1 - V_2| &= 2a = 2k(1 - b) = k|E_1 - E_2| \\ &= k \cdot \left(\frac{C}{kd} + o\left(\frac{1}{d}\right) o\left(\frac{1}{k}\right) \right) = \frac{C}{d} + o\left(\frac{1}{d}\right) o(1) \end{aligned}$$

as $k \rightarrow \infty$. (Here the term $o(1)$ indicates a quantity that tends to zero as $k \rightarrow \infty$.)

Thus, not only do E_1 and E_2 coalesce as $(k \rightarrow \infty)$, but so do V_1 and V_2 , provided $d \rightarrow \infty$. This corresponds to the definition of the twice-punctured torus at $(k, d) = (\infty, \infty)$. If d is finite, it is clear from (61) that the V_i do not coalesce as $k \rightarrow \infty$. This is consistent with Proposition 14, which proves that V_1 and V_2 must be distinct on the right-hand edge when $0 < d < \infty$. That same proposition shows, when we assume that $E_1 = E_2$ and the underlying conformal structure of the compact rhombic torus is determined—exactly our situation—that the positions of the V_i are determined. Therefore the limiting data are precisely the data we specified on the interior of the right-hand edge.

5.1.5. *Continuity on the bottom edge.* Finally, we concern ourselves with continuity of the map $\mathcal{P} \rightarrow \overline{T_{1,4}}$ on the set where $k \in (\frac{1}{2}, \infty]$ and $d \geq 0$

is bounded above. The architecture of the argument is identical to that of Section 5.1.4, with only the details (and level of complication) changing. In particular, we will again find a homotopically trivial curve \mathcal{C} in the slit model and describe an isometric model for the simply connected component Δ of its complement. Most of our work will involve a careful study of the asymptotics of the representatives of V_1, V_2, E_1 and E_2 inside a suitably modified model Δ . We end the argument by showing that the asymptotic relationships found in Δ have corresponding statements within the rhombic model.

As before, we begin by showing that the convergence is easily guaranteed when we bound k from above. In particular, consider a sequence $\{(k_n, d_n)\}$ with $k_n \leq k_0 < \infty$ and $d_n \rightarrow 0$; with no loss in generality, as we can always pass to a subsequence, we assume that $(k_n, d_n) \rightarrow (k_\infty, 0)$. We then need to show that V_2 and E_2 coalesce, as it will then be clear by symmetry that V_1 and E_1 coalesce. Thus, it is enough to show that the curve system consisting of the curves surrounding the segment $i[0, d_n]$ has small extremal length, or equivalently, that we can embed, into the slit model, annuli of large modulus whose core curve surrounds $i[0, d_n]$. Note that since $id_n = e_2$ and $0 = v_2$, this will show that e_2 and v_2 coalesce. This core curve is slightly awkward to describe: it consists of circles centered at $0, \frac{1}{2}$ and $-\frac{1}{2}$ of radius $2d_n$, with the standard identifications. See Figure 35.

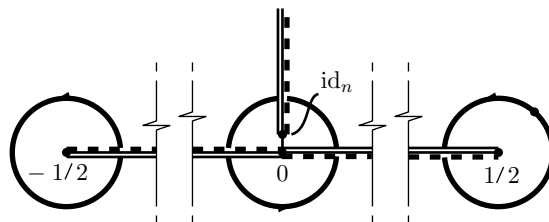


Figure 35: The core curve of radius $2d_n$, bounding a small disk around $v_2 = 0$.

With this core curve defined, it is easy to find fat annuli with that core: consider the annuli of outer radius $\frac{1}{5}$ and inner radius $2d_n$ about $0, \frac{1}{2}$ and $-\frac{1}{2}$. For $\{k_n\}$ bounded, the moduli of these annuli go to infinity as $d_n \rightarrow 0$. Therefore V_2 and E_2 (hence also v_1 and e_1) coalesce.

Our goal then is to show the coalescence of v_1, v_2, e_1 and e_2 as $(k_n, d_n) \rightarrow (\infty, 0)$.

We begin by describing the curve \mathcal{C} in the slit model. It is crucial that we can draw a single curve \mathcal{C} in the ζ -plane of the slit model, namely $\mathbf{C} \setminus [-1/2, 1/2]$, which surrounds v_1, v_2, e_1 and e_2 , under the assumption that $(k, d) \in [1, \infty] \times [0, d_0]$. Such a curve is drawn in Figure 36. (Formally, it is the union of four curves in the plane: circles of radius $1/10$ centered at $-1/2$ and $1/2$, a semi-circle of radius $1/10$ in the lower half plane centered at 0 , and a curve that begins at $1/10$, enters the upper half plane before entering the lower half plane

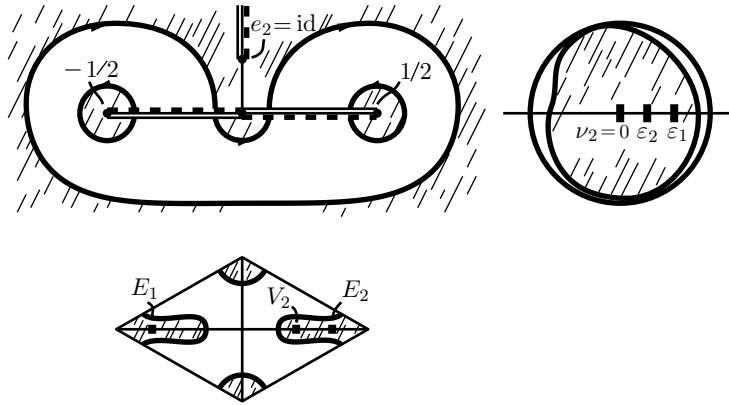


Figure 36: Top: The curve \mathcal{C} in the slit model is drawn on the left as is described in the text. It separates the torus into a simply connected domain D (shaded) containing v_2 , e_1 and e_2 , and the complement of D , a domain of genus one. The curve \mathcal{C} is symmetric with respect to the imaginary axis. It consists of two circular arcs of radius $\frac{1}{10}$, a semi-circular arc of radius $\frac{1}{10}$ and a curve, symmetric with respect to the imaginary axis, that crosses the imaginary axis once in the bottom halfplane. On the right is a representation of the Δ -model normalized as in the discussion preceding Lemma 6. The point $\nu_2 = 0$ corresponds to the point v_2 , and the points $\varepsilon_2 < \varepsilon_1$ on the positive real axis correspond to the points $e_2 = \text{id}$ and $e_1 = \infty$, respectively, in the slit model. The ds_Δ metric on Δ is isometric to the $|d\zeta|$ -metric on D in the slit model. Bottom: Illustrated here is the shaded region in the rhombic model that corresponds to the region D bounded by \mathcal{C} in the slit model.

at 1, then leaves the lower half plane at -1 and finally meets the $[-1/2, 1/2]$ slit again at $-1/10$.) The reader can easily check that one component, say D , of the complement contains v_1 , v_2 , e_1 and e_2 , while the other component, say T , is a punctured torus.

Let Δ be a model disk for D ; we construct a model metric ds_Δ on D with singular points ν_2 , ε_1 , and ε_2 corresponding to the points v_2 , e_1 and e_2 , respectively, on D . This metric is isometric to the $|gdh|$ -metric (the metric induced by $|d\zeta|$ restricted to D). We define ds_Δ by

$$(62) \quad ds_\Delta = \left| \frac{C(\xi - \nu_2)^2(\xi - \varepsilon_2)^{k-1}}{(\xi - \varepsilon_1)^{k+1}} d\xi \right|.$$

We are permitted to normalize the domain Δ and, concomitantly, the metric ds_Δ , by composing our developing map with a Euclidean isometry; furthermore, as we have already included an unknown scaling constant C in the form of the metric ds_Δ , we see that we are also permitted a composition by a homothety. (See Lemma 10 in Appendix B for details.)

With these allowances in mind, we see that we may assume that $\nu_2 = 0$, that ε_1 lies on the positive real axis and that, after a homothety, the disk Δ is contained in the unit disk $B_1(0)$ while $\partial\Delta$ meets the unit circle at at least one point.

There is one further normalization that follows not from general facts about isometries, but from the specific form of the metric $|gdh|$ on the slit model: the $|gdh|$ -metric when considered on the slit model (i.e the $|d\zeta|$ -metric) admits a reflection that fixes pointwise the imaginary axis and ν_2 . (See Lemma 3(i) and its proof.) Thus, we may assume that (Δ, ds_Δ) admits an isometry that fixes $\nu_2 = 0$, $\varepsilon_2, \varepsilon_1$, the shortest geodesic from ν_2 to ε_2 , and a geodesic from ε_2 to ε_1 .

Now, since the metric (62) is written in terms of the $|d\xi|$ -distances $|\xi - \nu_2|, |\xi - \varepsilon_1|$ and $|\xi - \varepsilon_2|$, we see that this isometry must preserve not just ds_Δ distances from ν_2, ε_2 and ε_1 , but also $|d\xi|$ -distances (in the space $(\Delta, |d\xi|)$) from ν_2, ε_2 and ε_1 ; this is only possible if ε_2 is real. Next we claim that we may assume that $0 < \varepsilon_2 < \varepsilon_1$. To see this, note first we must have $\varepsilon_2 > 0$, or else there would not exist a path Γ (like the one on the imaginary axis in the slit model) which is a geodesic from ε_2 to ε_1 and whose distance from ν_2 increases along the path. Then next, we see that we must have $\varepsilon_1 < \varepsilon_2$, so that there exists a geodesic from ν_2 to ε_1 whose distance from ν_2 is an increasing function *and* which passes through ε_2 .

This effect of symmetry simplifies the derivations, contained in the next lemma, of the asymptotics of C, ε_1 and ε_2 . However, the proof of this lemma is rather long and a bit intricate. (Happily, though, the conclusion of the proof of Proposition 15 is then nearly immediate.)

LEMMA 6. *Consider the metric on the model disk Δ given by*

$$(63) \quad ds_\Delta = \left| \frac{C\xi^2(\xi - \varepsilon_2)^{k-1}}{(\xi - \varepsilon_1)^{k+1}} d\xi \right|,$$

which is normalized as above (in particular, with $\nu_2 = 0$). Then

- (i) $C \asymp 1$;
- (ii) *As $d \rightarrow 0$, we have that $\varepsilon_2 \rightarrow 0 = \nu_2$; in fact $\varepsilon_2 = O\left(\frac{1}{\log \frac{1}{d}}\right)$.*
- (iii) *As $k \rightarrow \infty$, we have that $|\varepsilon_1 - \varepsilon_2| = O\left(\frac{1}{k}\right)$.*

Here the expression $C \asymp 1$ means that there are constants $A > 0$ and $B < \infty$ so that $A < C < B$.

Proof. We begin by proving that C is bounded away from zero. Recall that the distance in the ds_Δ -metric between ν_2 and $\partial\Delta$ is equal to the distance in the $|gdh|$ metric between ν_2 and \mathcal{C} in the slit model, which is equal to

$d + \frac{1}{10}$ by construction. Since we are assuming that $d < d_0$, it follows that this distance between ν_2 and $\partial\Delta$ is bounded above and below. Consider the restriction of ds_Δ to the negative real axis. Along that axis, for any (k, d) , we always have $|\xi| < |\xi - \varepsilon_1|$, and $|\xi - \varepsilon_2| < |\xi - \varepsilon_1|$. Thus, we always have that $ds_\Delta|_{\{x < 0\}} \leq C|d\xi|$. If $C \rightarrow 0$, then the distance in the ds_Δ -metric between ν_2 and $\partial\Delta$ would also go to 0. However, the distance in the ds_Δ -metric between ν_2 and $\partial\Delta$ is equal to the distance in the $|gdh|$ metric between ν_2 and \mathcal{C} in the slit model, and this distance is bounded away from 0. Hence C must be bounded below.

We next claim that there is an upper bound on C . This argument is actually a bit involved, and so we separate it off as a claim.

Claim: C is bounded above. To see that there is an upper bound on C , we proceed in several steps, always using that the curve \mathcal{C} is of fixed length in the slit model, hence also in Δ . Recall that we have normalized Δ so that there is one point, say $\theta_0 \in \partial\Delta$, which meets the unit circle.

To begin, suppose that $\operatorname{Re} \theta_0 \geq \varepsilon_1$, and note that this implies that $|\theta_0| > |\varepsilon_2 - \theta_0| > |\varepsilon_1 - \theta_0|$. Then, at θ_0

$$\left| \frac{\xi^2(\xi - \varepsilon_2)^{k-1}}{(\xi - \varepsilon_1)^{k+1}} \right| > 1.$$

If the portion of \mathcal{C} with $\operatorname{Re} \xi \geq \varepsilon_1$ has $|d\xi|$ -length bounded from below, then we see that the normalizing constant C is bounded above, as

$$\begin{aligned} C_1 &> \int_{\mathcal{C} \cap \{\operatorname{Re} \xi \geq \varepsilon_1\}} ds_\Delta = \int_{\mathcal{C} \cap \{\operatorname{Re} \xi \geq \varepsilon_1\}} \left| \frac{\xi^2(\xi - \varepsilon_2)^{k-1}}{(\xi - \varepsilon_1)^{k+1}} \right| |d\xi| \\ &> C \int_{\mathcal{C} \cap \{\operatorname{Re} \xi \geq \varepsilon_1\}} |d\xi| \geq C \cdot C_2 \end{aligned}$$

for C_1 a length that is bounded above, and C_2 a length that is bounded below.

In general then, we may assume that $\operatorname{Re} \theta_0 - \varepsilon_1$ has no positive lower bound, for if it did, we would find a portion of \mathcal{C} with $\operatorname{Re} \xi > \varepsilon_1$ and with length bounded below, and end with the same contradiction as in the last paragraph. To further refine the conditions that concern us, suppose for the moment that there is a lower bound on $\varepsilon_1 - \varepsilon_2$, say $\varepsilon_1 - \varepsilon_2 \geq \varepsilon_0 > 0$. Then in that case the quantity $|(\xi - \varepsilon_2)|/|\xi - \varepsilon_1| > 1 + \varepsilon'_0$ for all ξ within a distance of $(\varepsilon_1 - \varepsilon_2)/4$ of θ_0 . Thus, in this case

$$\begin{aligned} C_1 &> \int_{\mathcal{C} \cap \{|\xi - \theta_0|_{ds_\Delta} < \frac{1}{4}(\varepsilon_1 - \varepsilon_2)\}} ds_\Delta \\ &> C \cdot \left(2 \cdot \frac{1}{4}(\varepsilon_1 - \varepsilon_2)\right) \cdot (1 + \varepsilon'_0)^{k-1} \cdot \int \left| \frac{\xi}{\xi - \varepsilon_1} \right|^2 d\xi \rightarrow \infty \end{aligned}$$

as $k \rightarrow \infty$. Thus, we see that it is only possible for $C \rightarrow \infty$ if the $\theta_0 - \varepsilon_1$ does not have a positive lower bound and $\varepsilon_1 - \varepsilon_2 \rightarrow 0$.

We next dispose of a minor case by noting that it is not possible for $\theta_0 \rightarrow 1$ while $C \rightarrow \infty$. This is because these hypotheses guarantee that there is an arc, say C' , of $|d\xi|$ -length of at least $(\theta_0 - \varepsilon_1)/4$ along which $|\xi - \varepsilon_1| < |\xi - \varepsilon_2|$. Thus, since on this arc, the modulus $|\xi|$ is bounded below, by, say C_3 , we see that this arc C' has ds_Δ -length of at least

$$C \cdot C_3^2 \cdot 1^{k-1} \cdot \frac{(\theta_0 - \varepsilon_1)}{4} \int_{C'} \frac{|d\xi|}{|\xi - \varepsilon_1|^2}.$$

Since $|\xi - \varepsilon_1| < 5/4|\theta_0 - \varepsilon_1|$, the claim follows.

So we may now suppose that $C \rightarrow \infty$, $\varepsilon_1 - \varepsilon_2 \rightarrow 0$, $\operatorname{Re} \theta_0 - \varepsilon_1$ has no positive lower bound and θ_0 is bounded away from 1 (so that θ_0 is bounded away from ε_1). In that case, the method of two paragraphs back provides a lower bound on the decay of $\varepsilon_1 - \varepsilon_2$: in particular, we claim that $k(\varepsilon_1 - \varepsilon_2) \rightarrow \infty$. To see this, consider a portion C' of \mathcal{C} within $|d\xi|$ -distance of $1/2$ from θ_0 , which lies in $\{\operatorname{Re} \xi < \varepsilon_1\}$ and has $|d\xi|$ -length of $C_3 > 0$. (It is sufficient to assume that if $C \rightarrow \infty$, such an arc must exist by the arguments in the previous paragraphs after minor modifications.) Then if the total length of \mathcal{C} is L , we have

$$\begin{aligned} L &> \int_{C'} \left| \frac{\xi^2(\xi - \varepsilon_2)^{k-1}}{(\xi - \varepsilon_1)^{k+1}} \right| |d\xi| \\ &> C \cdot C_3 \cdot (1/2)^2 \inf_{C'} \left| \frac{\xi - \varepsilon_2}{\xi - \varepsilon_1} \right|^{k-1} \cdot \frac{1}{2^2}, \end{aligned}$$

here using the trivial bound $|\xi - \varepsilon_1| < 2$ which comes from both ξ and ε_1 lying in the unit ξ -disk. We might as well assume that $\inf_{C'} \left| \frac{\xi - \varepsilon_2}{\xi - \varepsilon_1} \right| < 1$, or else the assumption that $C \rightarrow \infty$ immediately provides a contradiction. Thus we may continue with

$$\begin{aligned} L &> \frac{C_3}{16} C \inf_{C'} \left| 1 + \frac{\varepsilon_1 - \varepsilon_2}{\xi - \varepsilon_1} \right|^{k-1} \\ &= \frac{C_3}{16} C \inf_{C'} \left| 1 + \frac{k(\varepsilon_1 - \varepsilon_2)}{k(\xi - \varepsilon_1)} \right|^{k-1} \end{aligned}$$

Now, if $k(\varepsilon_1 - \varepsilon_2) < K_0$ for some fixed K_0 , then since on C' , we have $\operatorname{Re}(\xi - \varepsilon_1) < 0$ and $|\xi - \varepsilon_1| > C_4$ by hypothesis, we find that

$$L > C e^{-\frac{K_0}{C_5}}$$

where C_5 depends on C_4 , C_3 and $|\theta_0 - \varepsilon_1|$: since θ_0 may be assumed bounded away from 1, we see that $|\theta_0 - \varepsilon_1|$ is bounded away from zero.

From this last expression and our assumption that $C \rightarrow \infty$, we see that it is impossible that $k(\varepsilon_1 - \varepsilon_2) < K_0$ for some fixed K_0 , and so $\limsup_k k(\varepsilon_1 - \varepsilon_2) = \infty$.

Finally, consider the point r_+ where $\partial\Delta$ meets the positive real axis, and consider the curve $\mathcal{C}^* = \mathcal{C} \cap B(r_+, (r_+ - \varepsilon_1)/4)$ which is the intersection of the

curve \mathcal{C} with the ball around r_+ of radius $(r_+ - \varepsilon_1)/4$. Certainly \mathcal{C}^* has $|d\xi|$ -length of at least $2(1/4(r_+ - \varepsilon_1))$ and we have both that $|\xi - \varepsilon_1| < \frac{5}{4}|r_+ - \varepsilon_1| < \frac{5}{4}$ and $|\xi|^2 > (\varepsilon_1 + \frac{3}{4}(r_+ - \varepsilon_1))^2 > \frac{3}{4}(r_+ - \varepsilon_1)^2$, on \mathcal{C}^* and so

$$\begin{aligned} L &> \int_{\mathcal{C}^*} C \left| \frac{\xi^2(\xi - \varepsilon_2)^{k-1}}{(\xi - \varepsilon_1)^{k+1}} \right| |d\xi| \\ &> C \cdot 1/2(r_+ - \varepsilon_1)(4/5)^2(\varepsilon_1 + 3/4(r_+ - \varepsilon_1))^2 \inf_{\mathcal{C}^*} \left| \frac{\xi - \varepsilon_2}{\xi - \varepsilon_1} \right|^{k-1} \\ &> C \cdot 9/50(r_+ - \varepsilon_1)^3 \inf_{\mathcal{C}^*} \left| \frac{\xi - \varepsilon_2}{\xi - \varepsilon_1} \right|^{k-1}. \end{aligned}$$

Thus

$$\begin{aligned} L &> \frac{9}{50}C(r_+ - \varepsilon_1)^3 \inf_{\mathcal{C}^*} \left| 1 + \frac{\varepsilon_1 - \varepsilon_2}{\xi - \varepsilon_1} \right|^{k-1} \\ &> \frac{9}{50}C(r_+ - \varepsilon_1)^3 \inf_{\mathcal{C}^*} \left| 1 + \frac{k(\varepsilon_1 - \varepsilon_2)}{k(\xi - \varepsilon_1)} \right|^{k-1}. \end{aligned}$$

Now, choose a subsequence of values of k along our path so that $k(\varepsilon_1 - \varepsilon_2)$ is monotone and tends to infinity. Now, by construction, $\operatorname{Re}(\xi - \varepsilon_1) \in (\frac{3}{4}(r_+ - \varepsilon_1), \frac{5}{4}(r_+ - \varepsilon_1))$ (so that in particular, $\operatorname{Re}(\xi - \varepsilon_1) > 0$). Since we can restrict to a portion of our path so that $k(\varepsilon_1 - \varepsilon_2) \geq 1$, we find

$$\left| 1 + \frac{k(\varepsilon_1 - \varepsilon_2)}{k(\xi - \varepsilon_1)} \right|^{k-1} \geq C_6 e^{C_7 \operatorname{Re} \frac{1}{\xi - \varepsilon_1}} \geq C_6 e^{C_7 \frac{1}{5/4(r_+ - \varepsilon_1)}}.$$

Thus

$$L > \frac{9}{50}CC_6(r_+ - \varepsilon_1)^3 e^{\frac{4C_7}{5(r_+ - \varepsilon_1)}}.$$

Next, choosing a further subsequence so that $r_+ - \varepsilon_1$ converges, we see that – independently of the (bounded) limit of $r_+ - \varepsilon_1$ – the right-hand side of the inequality above must tend to infinity, a contradiction. This proves the claim. \square

We have established the statement (i) of the lemma. For statements (ii) and (iii) to hold, it is necessary that along any path in \mathcal{P} for which $(k, d) \rightarrow (\infty, 0)$, we have that $\varepsilon_1, \varepsilon_2$ and ν_2 all coalesce at $\xi = 0$.

We next assert that ε_1 is bounded away from $\partial\Delta$. This is because, once we know that C is uniformly bounded on sequences in our domain, we see that if $d_{|d\xi|}(\varepsilon_1, \partial\Delta) \rightarrow 0$, then $\ell_{ds_\Delta}(\partial\Delta) \rightarrow \infty$ as the line element on the limit point of ε_1 would necessarily blow up uniformly: here note that since $\varepsilon_2 < \varepsilon_1$ and the pole of $|\xi - \varepsilon_1|^{(k+1)}$ has order two greater than that of the zero of $|\xi - \varepsilon_2|^{(k-1)}$, this blow-up is independent of the asymptotics of ε_2 .

We prove statement (iii) of the lemma, before later turning our attention to statement (ii). Consider the arc from V_2 to \mathcal{C} in the $|gdh|$ -model $M_{|gdh|}$

represented by the segment $i[-1/10, 0]$ in the $|g_{dh}|$ model. This arc makes an angle of 3π at V_2 with the arc $i[0, d]$ connecting V_2 and E_2 in that model $M_{|g_{dh}|}$. As the arc $i[0, d]$ in $M_{|g_{dh}|}$ is represented by $[0, \varepsilon_2]$ in Δ , we see that the arc $i[-1/10, 0]$ in $M_{|g_{dh}|}$ is represented by a path Γ on the negative real axis from 0 to $\partial\Delta$ in the model Δ : this is true either by symmetry or because we check that this path Γ is geodesic and makes an angle of 3π with the positive real ray emanating from $0 \in \Delta$. Suppose that Γ meets \mathcal{C} at a point $-\delta$. Then, computing in the coordinates $\xi = x + iy$, because of our isometry between ds_Δ and $|g_{dh}|$, we know that

$$\begin{aligned} \frac{1}{10} &= d_{|g_{dh}|}(V_2, \mathcal{C}) = \int_{-\delta}^0 ds_\Delta \\ &= \int_{-\delta}^0 C \left| \frac{\xi}{\xi - \varepsilon_1} \right|^2 \left| \frac{\xi - \varepsilon_2}{\xi - \varepsilon_1} \right|^{k-1} d\xi = C \int_{-\delta}^0 \left(\frac{x}{x - \varepsilon_1} \right)^2 \left(\frac{x - \varepsilon_2}{x - \varepsilon_1} \right)^{k-1} dx \\ &< \delta^2 C \int_{-\delta}^0 \frac{1}{(x - \varepsilon_1)^2} \left(\frac{x - \varepsilon_2}{x - \varepsilon_1} \right)^{k-1} dx \\ &= \delta^2 C \int_{-\delta}^0 \frac{1}{(x - \varepsilon_1)^2} \left(1 + \frac{\varepsilon_1 - \varepsilon_2}{x - \varepsilon_1} \right)^{k-1} dx, \end{aligned}$$

with the inequality coming from $x^2 < \delta^2$ on the domain of integration. Now, we can integrate this last integral explicitly to get

$$\begin{aligned} \frac{1}{10} &< \delta^2 C \left(\frac{-1}{\varepsilon_1 - \varepsilon_2} \right) \frac{1}{k} \left(1 + \frac{\varepsilon_1 - \varepsilon_2}{x - \varepsilon_1} \right)^k \Big|_{-\delta}^0 \\ &= \frac{\delta^2 C}{(\varepsilon_1 - \varepsilon_2)k} \left[\left(1 - \frac{\varepsilon_1 - \varepsilon_2}{\varepsilon_1 + \delta} \right)^k - \left(1 - \frac{\varepsilon_1 - \varepsilon_2}{\varepsilon_1} \right)^k \right] < \frac{\delta^2 C}{(\varepsilon_1 - \varepsilon_2)k}. \end{aligned}$$

The final inequality follows from the observation that both terms in the difference are positive (using $\varepsilon_1 > \varepsilon_2 > 0$), both are less than one and the first is clearly more than the second. But recall that we normalized Δ to be included in the unit disk, so that $\delta < 1$. We conclude that

$$(64) \quad \frac{1}{10} < \frac{C}{(\varepsilon_1 - \varepsilon_2)k} \text{ or that } (\varepsilon_1 - \varepsilon_2) < \frac{C_1}{k}.$$

This establishes statement(iii); note also that the estimate (64) is independent of the behavior of d . We use this estimate (64) on $\varepsilon_1 - \varepsilon_2$ to establish statement (ii). Here we proceed similarly, but focus our attention on the path $\overline{V_2 E_2}$ in $M_{|g_{dh}|}$, and correspondingly on the arc $[0, \varepsilon_2]$ in Δ . From the isometry we

constructed, since $\overline{V_2 E_2}$ has length d in $M_{|g_{dh}|}$, we have

$$\begin{aligned} d &= d_{|g_{dh}|}(V_2, E_2) = \int_0^{\varepsilon_2} ds_\Delta \\ &= \int_0^{\varepsilon_2} C \left(\frac{x}{x - \varepsilon_1} \right)^2 \left(\frac{x - \varepsilon_2}{x - \varepsilon_1} \right)^{k-1} dx \\ &> C \int_{\varepsilon_2/2}^{\varepsilon_2} \left(\frac{x}{x - \varepsilon_1} \right)^2 \left(\frac{x - \varepsilon_2}{x - \varepsilon_1} \right)^{k-1} dx, \end{aligned}$$

where here we restrict the integral of a positive quantity to a subinterval $[\varepsilon_2/2, \varepsilon_2]$. Of course, on that subinterval, we have that $x > \varepsilon_2/2$ and so our estimate becomes

$$d > \left(\frac{\varepsilon_2}{2} \right)^2 C \int_{\varepsilon_2/2}^{\varepsilon_2} \frac{1}{(x - \varepsilon_1)^2} \left(1 + \frac{\varepsilon_1 - \varepsilon_2}{x - \varepsilon_1} \right)^k dx.$$

We integrate explicitly as before to find

$$\begin{aligned} d &> \frac{-\varepsilon_2^2 C}{4k(\varepsilon_1 - \varepsilon_2)} \left(1 + \frac{\varepsilon_1 - \varepsilon_2}{x - \varepsilon_1} \right)^k \Big|_{\varepsilon_2/2}^{\varepsilon_2} = \frac{\varepsilon_2^2 C}{4k(\varepsilon_1 - \varepsilon_2)} \left(1 + \frac{2(\varepsilon_1 - \varepsilon_2)}{\varepsilon_2 - 2\varepsilon_1} \right)^k \\ &= \frac{\varepsilon_2^2 C}{4k(\varepsilon_1 - \varepsilon_2)} \left(1 - \frac{2(\varepsilon_1 - \varepsilon_2)}{\varepsilon_1 + (\varepsilon_1 - \varepsilon_2)} \right)^k. \end{aligned}$$

Now we invoke the previous estimate (64) that $k(\varepsilon_1 - \varepsilon_2) < C_1$ to obtain

$$d > \frac{\varepsilon_2^2 C}{4C_1} \left(1 - \frac{2 \cdot C_1}{k(\varepsilon_1 + (\varepsilon_1 - \varepsilon_2))} \right)^k > \frac{\varepsilon_2^2}{C_2} \left(1 - \frac{2C_1}{k\varepsilon_2} \right)^k$$

since the relevant denominator $k(\varepsilon_1 + (\varepsilon_1 - \varepsilon_2)) > k(\varepsilon_2 + 0)$ in our construction. Now, as $k \rightarrow \infty$, the term $(1 - 2C_1/k\varepsilon_2)^k \rightarrow e^{-2C_1/\varepsilon_2}$ which dominates ε_2^2 . Thus, we conclude that for k large we have

$$d > e^{-C_3/\varepsilon_2}$$

and so

$$\varepsilon_2 < \frac{C_3}{\log 1/d}$$

for k large, proving statement (ii) of the lemma. This then concludes the proof of the lemma. \square

We now proceed with the proof of continuity of the mapping $(k, d) \rightarrow \mathcal{T}_k(d)$ at $(\infty, 0)$. The argument is analogous to the argument in Section 5.1.4. It is evident that as $(k_n, d_n) \rightarrow (\infty, 0)$, the boundary $\partial\Delta$ converges to a curve in the ξ -disk which avoids a uniform neighborhood of zero. This is because the metric ds_Δ subconverges to the metric $|d\xi|/|\zeta|^2$, into which the curve \mathcal{C} must develop as a curve of uniformly bounded length. Moreover, by Lemma 6, for (k, d) near $(\infty, 0)$, we know that ε_1 is within a distance of $O\left(\frac{1}{\log \frac{1}{d}}\right) + O\left(\frac{1}{k}\right)$

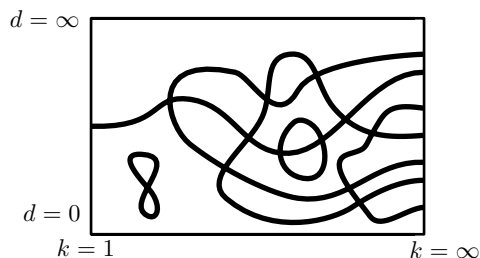


Figure 37: On the (k, d) rectangle, we have defined a function $h(k, d)$ whose value is the real part of the integral of dh on the path B of the underlying $\mathcal{T}_k(d)$. Illustrated here is a possible locus of the zeros of $h(k, d)$. See Figure 25. We know that the locus is an analytic set and that it has a unique point on the vertical line $k = 1$ (See Proposition 8 in Section 3.3.) corresponding to \mathcal{H}_1 . We show that there is at least one path connecting this point to a point on the right-hand side of the rectangle, where $k = \infty$. Note: the illustration in this figure is of the closed rectangle $[1, \infty] \times [0, \infty]$ which is properly contained in \mathcal{P} .

of the origin. We then create a new surface N by gluing the complement of D to a $1 + o\left(O\left(\frac{1}{\log \frac{1}{d}}\right) + O\left(\frac{1}{k}\right)\right)$ quasi-conformal image of Δ : here \mathcal{C} gets joined to $\partial\Delta$ at corresponding points. As in Subsection 5.1.4, we then conclude that $|E_1 - E_2| = O\left(\frac{1}{k}\right)$ and $|E_1 - V_2| = O\left(\frac{1}{\log \frac{1}{d}}\right)$ in the rhombic model. This concludes the argument for continuity result along the edge where $d = 0$ and $k \in [\frac{1}{2}, \infty]$.

This concludes the proof of Proposition 15.

5.2. *Estimates for the height function on the top and bottom of the rectangle \mathcal{P} and the solution of the period problem for \mathcal{H}_k .* We begin this section with estimates for the height function h near the boundary lines $(1/2, \infty] \times \{0\}$ and $(1/2, \infty] \times \{\infty\}$. In particular, we prove

PROPOSITION 17. *The function h is positive on $(\frac{1}{2}, \infty] \times \{0\}$ and negative on $(\frac{1}{2}, \infty] \times \{\infty\}$, i.e. $h|_{(\frac{1}{2}, \infty] \times \{0\}} > 0$ and $h|_{(\frac{1}{2}, \infty] \times \{\infty\}} < 0$.*

We postpone the proof of this proposition briefly, preferring to present the following proposition, actually a corollary to Proposition 17, which will be important in the proof of the main result (Theorem 3).

PROPOSITION 18. *There exists a continuous path $\Gamma \subset (\frac{1}{2}, \infty] \times (0, \infty)$ with the following properties: for every $k \in (\frac{1}{2}, \infty]$, the path Γ crosses the vertical segment $\{k\} \times (0, \infty)$; it passes through the point $(1, d_1)$ that corresponds to the Weierstrass data for \mathcal{H}_1 , the singly periodic genus-one helicoid; every*

point $(k, d) \in \Gamma$ corresponds to Weierstrass data for \mathcal{H}_k/σ_k for which both the horizontal and vertical period problems are solved.

Proof of Proposition 18. It is immediate from Proposition 17 and Proposition 16 that there is a neighborhood in \mathcal{P} of $(\frac{1}{2}, \infty] \times \{0\}$ on which the function h is positive, and a neighborhood of $(\frac{1}{2}, \infty] \times \{\infty\}$ on which it is negative. Therefore, there exists a boundary component of the region $\{h \leq 0\}$ which separates $(\frac{1}{2}, \infty] \times \{0\}$ from $(\frac{1}{2}, \infty] \times \{\infty\}$ in $(\frac{1}{2}, \infty] \times [0, \infty]$. This in turn implies that there is a connected curve, say Γ , on which h vanishes and where Γ has the following two properties: Γ cuts every vertical line segment (k, ∞) , $k > \frac{1}{2}$, at least once, and Γ terminates at a point on the right-hand edge of the form (∞, d_∞) , with $d_\infty \neq 0$. Since h is analytic in k and d , we may assert that Γ is piecewise smooth. Each point $(k, d) \in \Gamma$ corresponds to a solution of the vertical period problem for the Weierstrass data defined at (k, d) , data for which the horizontal period problem is solved by construction. Therefore, for every $k > \frac{1}{2}$, there exists a solution \mathcal{H}_k corresponding to a point on Γ , and we can assert the existence of a continuously varying (although not necessarily monotonic in k) family of such solutions. From our discussion in Section 3 (in particular, Proposition 8) of the uniqueness of the singly periodic genus one helicoid, \mathcal{H}_1 , we may assert that there is precisely one value of d , say d_1 , for which the vertical period problem for the data at $(1, d)$ has a solution. Thus, whatever choice of path Γ we make, it passes through this distinguished point on the vertical segment where $k = 1$. \square

Proof of Proposition 17. Our argument parallels that of Section 3.4. We begin with a discussion of the “top stratum” $(\frac{1}{2}, \infty] \times \{\infty\}$. By definition (see Section 4.4) the underlying compact torus on this stratum is \mathcal{T}_1 , the ends coincide and the vertical points coincide: that is, $E_1 = E_2 = E$ and $V_1 = V_2 = V$. In the notation of (24), we have that $a = 0$ and $b = 1$. Note that this is independent of choice of k , and hence h is constant on the top stratum. However, in the proof of Proposition 8, in particular the proof of claim (23), we showed that h is negative when $k = 1$ and $a = 0$. The situation described there is precisely the one we have here; the underlying torus is \mathcal{T}_1 , the ends coincide and the vertical points coincide. This is equivalent to $k = 1$ and $d = \infty$. This establishes the second statement of the proposition.

We next consider the “bottom” stratum $(\frac{1}{2}, \infty) \times \{0\}$. Here, of course, we have $a = b = k/(k+1)$ and $E_i = V_i$. Notice that for the moment we have excluded the point $(\infty, 0)$. Consider then a neighborhood of $v_2 = e_2$ in the slit model for values of (k, d) converging to $(k_0, 0)$. For each fixed (k, d) , the conformal map w from the slit model to itself that takes the $|gdh|$ structure to the $|\frac{1}{g}dh|$ structure takes this neighborhood into a neighborhood containing $v_1 = e_1$. From Figure 24 we see that, in that neighborhood, the total curvature of the cone metric $\{|gdh||w^*\frac{1}{g}dh|\}^{1/2}$ vanishes. Thus, using Proposition 15, we

can conclude that the limiting structure $|dh|$ is flat and nonsingular, and a (bounded, nondegenerate) homothety of the rhombic model (because the $|gdh|$ and $|\frac{1}{g}dh|$ structures converge as $d \rightarrow 0$).

The argument then follows exactly as in the proof of Proposition 8, especially the part that precedes the claim (23). In particular, the value of h is given by half the length of the vertical axis in the rhombic model. Because the collection of underlying closed tori associated to \mathcal{P} form a compact set by Lemma 4, the lengths of the vertical axes are uniformly bounded away from zero. Thus, the values of h along $[k_0, \infty) \times \{0\}$, for any $k_0 > \frac{1}{2}$, are also uniformly bounded away from zero. By continuity of h (Proposition 16), they are positive and bounded away from zero on an open neighborhood of the closed set $[k_0, \infty) \times \{0\}$ in \mathcal{P} . \square

6. The proof of Theorem 3

We will now prove the main theorem stated in Section 1, namely:

THEOREM 3. *For every $k > 1$, there exists a complete, σ_k -invariant, properly embedded minimal surface, \mathcal{H}_k , whose quotient by σ_k satisfies conditions (4). As $k \rightarrow \infty$, a limit surface exists and is an embedded $\mathcal{H}e_1$, i.e. a properly embedded minimal surface satisfying conditions (1).*

Proof. Proposition 18 at the end of Section 5.2 asserted the existence of a continuous curve, $\Gamma \in \mathcal{P}$, of Weierstrass data for which the vertical and horizontal period conditions are satisfied. The curve Γ crosses all verticals of the form $\{k\} \times (0, \infty)$, $\frac{1}{2} < k < \infty$. For any value of $k \in (\frac{1}{2}, \infty)$ the Weierstrass data at $(k, d) \in \mathcal{P}$ were constructed to guarantee that the conditions (4) hold provided the vertical period condition $h(k, d) = 0$ is satisfied. Therefore, Proposition 18 gives us a continuous family of properly immersed minimal surfaces \mathcal{H}_k satisfying (4). To complete the proof of the theorem we must show that each surface \mathcal{H}_k , $\frac{1}{2} < k < \infty$ in the family defined by Γ is embedded and that the limit surface—the surface corresponding to the Weierstrass data say (∞, d_∞) —is an embedded $\mathcal{H}e_1$ satisfying the conditions of (1).

LEMMA 7. *Let $\Gamma \subset \mathcal{P}$ be the path described above and in Proposition 18. Suppose $(k, d) \in \Gamma$ with $k \neq \infty$. Then the surface \mathcal{H}_k corresponding to (k, d) is embedded.*

Lemma 7 completes the proof of embeddedness of the continuous family of \mathcal{H}_k .

LEMMA 8. *At a point (∞, d_*) , $0 < d_* < \infty$, where $h(\infty, d_*) = 0$, the Weierstrass data define an $\mathcal{H}e_1$, a surface satisfying the conditions (1) of Section 1.2:*

- (i) $\mathcal{H}e_1$ is a properly immersed minimal surface;
- (ii) $\mathcal{H}e_1$ has genus one and one end, that end being asymptotic to the helicoid;
- (iii) $\mathcal{H}e_1$ contains a single vertical line (the axis) and a single horizontal line.

We will prove both lemmas after completing the proof of the theorem.

Given Lemma 8, all we need to show at this point is that the limit $\mathcal{H}e_1$ is embedded. To this end, consider the limit point of Γ , a point of the form (∞, d_∞) , $d_\infty \neq 0, \infty$, satisfying the requirement of Lemma 8, namely $h(\infty, d) = 0$. According to Lemma 8, its Weierstrass data produce an $\mathcal{H}e_1$, and according to Lemma 7, that $\mathcal{H}e_1$ is the limit of embedded minimal surfaces. By statement (ii) of Lemma 8, $\mathcal{H}e_1$ is embedded outside of a compact set. Because we may approximate the part of this $\mathcal{H}e_1$ inside the compact set by embedded minimal surfaces, the limit surface has no transverse intersections in this compact set. Invoking the maximum principle for minimal surfaces, we conclude that the only other possibility is that the Weierstrass immersion defining this $\mathcal{H}e_1$ is a multiple covering of its image. But as pointed out above, this $\mathcal{H}e_1$ is embedded outside of the compact set, so it must be embedded. (See the proof of Lemma 7 for a similar argument in more detail.) This completes the proof of Theorem 3. \square

Proof of Lemma 7. From Proposition 18 we know that the path Γ must pass through the point $(1, d_1)$ whose data define the unique singly periodic genus-one helicoid \mathcal{H}_1 . From Theorem 2 we know that \mathcal{H}_1 is embedded. Since each \mathcal{H}_k is asymptotic to a helicoid and therefore embedded outside of a suitably large cylinder about its vertical axis—and the radius of that cylinder can be chosen to be a continuous function on Γ —it follows along the lines of arguments that are now becoming standard in the subject that all the \mathcal{H}_k defined by data on Γ must be embedded. (There does not seem to be a generally stated argument in the literature that applies directly to our case, so we will give a proof here that all the \mathcal{H}_k are embedded.)

Let \mathcal{E} denote the points of $(k, d) \in \Gamma^\circ$ that correspond to an embedded \mathcal{H}_k . (The interior $\Gamma^\circ \subset \Gamma$ consists of Γ minus the right-hand endpoint where $k = \infty$.) Because Γ° contains the point, $(1, d_1)$, representing \mathcal{H}_1 , and \mathcal{H}_1 is embedded, the set \mathcal{E} is nonempty. Since Γ° is connected, showing that \mathcal{E} is both open and closed will prove the lemma.

Consider a point $(k, d) \in \Gamma^\circ$. It corresponds to an \mathcal{H}_k , a minimal surface that is invariant under the action of σ_k and whose quotient, modulo σ_k , has two ends asymptotic to the ends of the helicoid. All such surfaces have a vertical axis and we have normalized the family so that the vertical axis of any \mathcal{H}_k is the x_3 -axis. In particular we may assert that:

- (i) Any \mathcal{H}_k is embedded outside of some cylinder of sufficiently large radius about the x_3 -axis.

By Proposition 15 and the continuity of Γ we may also assert that:

(ii) *Given any connected subset $\mathcal{U} \subset \Gamma^\circ$ on which k is bounded away from $\frac{1}{2}$ and ∞ , there exists an $R > 0$ such that every minimal surface \mathcal{H}_k corresponding to $(k, d) \in \mathcal{U}$ is embedded outside of the vertical cylinder of radius R around the x_3 -axis. In fact, they are uniformly (in k) asymptotic to the ends of the same helicoid.*

To see this, note that such a subset \mathcal{U} is precompact in Γ° , and if we have a bound R that holds at $p \in \Gamma^\circ$, then the bound $R/2$ holds in a small neighborhood of Γ° near p .

\mathcal{E} is open in Γ° . Let $(k_0, d_0) \in \mathcal{E}$. Choose a neighborhood $\mathcal{U} \subset \Gamma^\circ$ of (k_0, d_0) on which k is bounded away from $\frac{1}{2}$ and ∞ and select $R > 0$ according to statement (ii) above. The \mathcal{H}_k with $k = k_0$ corresponding to (k_0, d_0) is embedded, and so there must be a (possibly smaller) neighborhood \mathcal{U}' of (k_0, d_0) in $\mathcal{U} \subset \Gamma^\circ$ for which every \mathcal{H}_k with $(k, d) \in \mathcal{U}'$ is embedded inside the vertical cylinder of radius R . By assertion (ii), they are all embedded outside the cylinder of radius R . Hence they are all embedded.

\mathcal{E} is closed in Γ° . The maximum principle forbids a sequence of embedded minimal surfaces from developing a self-intersection in the limit unless the limit surface is a (branched) cover of a minimal surface. Since the limit is an \mathcal{H}_k , the latter possibility cannot occur in our case because of assertion (i) above. \square

Proof of Lemma 8. We will not use the hypothesis $h(\infty, d_*) = 0$ until later in the argument. That is, we begin by discussing the properties of the interior of the right-hand edge of \mathcal{P} . At any point (∞, d) , with $d \neq 0, \infty$, the structure of $\mathcal{T}_\infty(d)$ is defined by the slit model for \mathcal{T}_1 with a cone, S_∞ , of simple exponential type sewn in along the positive imaginary axis with vertex at $v_2 = di$. (For the definition and properties of S_∞ see Sections 2.3 and 2.4.) By Proposition 15 and Lemma 4, we know that the underlying conformal structure is that of a nondegenerate rhombic torus. From Section 2.4, we know that the points $e_2 = di$ and $e_1 = \infty$ in the slit model actually correspond to the same point on the torus, a point that we will label e . From Proposition 14, we know that the vertical point v_2 corresponding to the origin in the slit model does not coincide with v_1 . This means that on the rhombic model of $\mathcal{T}_\infty(d)$, the point E corresponding to e must be at the vertex of the rhombus and points V_i corresponding to the v_i are distinct and—as usual—symmetrically placed with respect to the center of the rhombus. In the notation of Proposition 14 and of (24), we must have $0 < a < b = 1$.

The Weierstrass data at (∞, d) , with $d \neq 0, \infty$, are defined in order to solve the horizontal period problem. (Certainly we have made this clear in

Section 4 for points (k, d) on the interior of \mathcal{P} . The same argument works when $k = \infty$. Alternatively, one can use the continuity of structure in Proposition 15 to conclude that the horizontal period problem is also solved when $k = \infty$.) Therefore, the Weierstrass data at (∞, d) defines a multivalued minimal immersion of a rhombic torus into Euclidean space with periods (if any) that are all vertical.

In Lemma 8, (iii) we proved that at $(k, d) \in \mathcal{P}^\circ$, any branch of the minimal immersion defined by the Weierstrass data there has the property that it maps the horizontal diagonal through \mathcal{O} in the rhombic model to two horizontal lines in Euclidean space, and the vertical diagonal through \mathcal{O} in the rhombic model to a vertical line in Euclidean space. By Proposition 15, the same is true for the Weierstrass data at (∞, d) , with $d \neq 0, \infty$.

There are only two possible sources of multiple values for the minimal immersion defined by the Weierstrass data at (∞, d) , with $d \neq 0, \infty$. One, of course, is the possibility that the vertical period problem is not solved, i.e. that $h(\infty, d) \neq 0$. The second is the existence of a vertical period at the end. We will show in this paragraph that the latter does not happen. In the rhombic model, the periods at the ends, E_1, E_2 , for a (k, d) structure in the interior of \mathcal{P} are vertical and of length $+2\pi k$ at E_1 and $-2\pi k$ at E_2 . The vertical period around a small cycle that surrounds E_1 and E_2 is zero. It follows from the continuity of (k, d) structures given in Proposition 15 and the fact that the ends coalesce as $k \rightarrow \infty$, that the vertical period of a small cycle around the end E is zero.

The previous four paragraphs describe the geometric properties of the Weierstrass immersion associated to *any* (∞, d) , where $d \neq 0, \infty$. (See Remark 13.)

We now use for the first time the hypothesis that we are at a point where $h(\infty, d_*) = 0$. This implies immediately that the Weierstrass data associated to (∞, d_*) define a single-valued, proper, minimal immersion of a torus with one end into Euclidean space. The image must contain a vertical line and a horizontal line through the image, say p_0 , of \mathcal{O} (the center of the rhombus). In particular, the tangent plane to the surface at p_0 is a vertical plane, implying that it cannot contain any other horizontal line through p_0 . If the image surface contained any other horizontal or vertical line that did not pass through the image of \mathcal{O} then the surface would be singly periodic, an impossibility since the surface must have genus equal to one. This completes the proof of statements (i), (iii) and the first part of statement (ii) of the lemma.

We now turn our attention to the second part of statement (ii). We will give two different proofs that the end of this surface is asymptotic to a helicoid, the second proof assuming that the surface is a limit of minimal surfaces (which is the case of interest).

Proof using analysis of the special end structure. We consider the Weierstrass data at the end, E_1 , of the minimal surface associated with the point (∞, d_*) . These data give the limit of Weierstrass data at $(k, d) \in \mathcal{P}^\circ$ with $k \rightarrow \infty$ and $d \rightarrow d_*$. (Note that we are *not* assuming that $h(k, d) = 0$ for these data. Nor are we assuming that the limit is taken over specially chosen values of (k, d) .) From Figure 19 we can read off that dg/g has a simple pole at the ends E_1 and E_2 where its residues are k and $-k$, respectively. Using the fact, discussed in the first paragraph of the proof of the lemma, that E_1 and E_2 coalesce as $k \rightarrow \infty$, as well as Proposition 15, we see that the (well-defined) one form dg/g on the torus defined at (∞, d_*) has a double pole at the end E . Now, as $V_1 \neq V_2$, we see that dg/g has poles at both V_1 and V_2 with opposite residues. As g is regular elsewhere on the surface, we find that dg/g has no residue at the end E .

When we turn our attention to the one-form dh for values of $(k, d) \in \mathcal{P}^\circ$, a similar argument shows that the simple poles of dh at E_1 and E_2 coalesce, as $(k, d) \rightarrow (\infty, d_*)$, to a double pole at the end E . Moreover, since dh can have no poles on the surface, the residue theorem guarantees that the double pole at the unique end of the surface has no residue. Since we have already established (statement (iii)) that there are one horizontal and one vertical line diverging into the end at E , we may use Proposition 1 to conclude that the end at E is asymptotic to the end of a helicoid.

Proof using the asymptotic arguments of Section 5.1.4 to express dg/g and dh . We assume in this proof that there is a family $\Gamma \subset \mathcal{P}^\circ$ with endpoint at (∞, d_*) . This is slightly stronger than the hypotheses of the lemma, but sufficient for the application. By this method, we avoid the use of Proposition 1.

Let (∞, d_*) be a point of Γ on the line $\{k = \infty\} \subset \overline{\mathcal{P}}$, and let (k, d_k) converge to (∞, d_*) . Simplifying the notation somewhat, we let M_k denote the (embedded) minimal surface associated to the point (k, d_k) . Each of the surfaces M_k contains a unique vertical line, and a collection of horizontal lines; after translating, we can assume that for each M_k , the origin is located at the intersection of the vertical line with a horizontal line.

As the $|gdh|$ and $|\frac{1}{g}dh|$ flat structures converge, as $k \rightarrow \infty$, to the (nondegenerate) $|gdh|$ and $|\frac{1}{g}dh|$ flat structures associated to the point $(\infty, d_*) \in \mathcal{P}$, we see that surfaces M_k converge, uniformly on compacta, to a minimal surface, say M_∞ , whose $|gdh|$ and $|\frac{1}{g}dh|$ structures are associated to the point (∞, d_*) . In particular, M_∞ is topologically a torus: note here that it is crucial that the $|gdh|$ model of $\mathcal{T}_k(d)$ has a slit whose length is constant, hence bounded away from zero and infinity.

It is elementary at this point to see that the horizontal and vertical lines are unique; the surface is invariant with respect to the group of rotations about parallel lines and so could not be of finite but nontrivial topology if it were to include a pair of parallel lines.

Finally, we need to show that M_∞ has an end asymptotic to a helicoid. Naturally, it is enough to check that the Weierstrass data of the end E (the limit point of the ends E_1 and E_2 as $k \rightarrow \infty$) has leading terms which agree with those of a helicoid. For this, it is enough to recall the estimates of Lemma 5:

$$|E_1 - E_2| = \frac{C}{kd} + o\left(\frac{1}{kd}\right)$$

and

$$C = 1 + o(1),$$

where E_i referred to the ends in the rhombic model and the estimate was valid as $k \rightarrow \infty$ for points (k, d) with d bounded away from zero. As in the proof of Proposition 15, we take ζ to be the variable on the rhombus and we normalize the E_i to be real; then the form gdh may be represented on $M_{k,d}$ (near, say, E_1) in this notation as

$$\begin{aligned} gdh &= -iC \frac{(\zeta - E_2)^{k-1} (\zeta - V_2)^2}{(\zeta - E_1)^{k+1}} d\zeta \\ &= -iC \left(1 + \frac{(E_1 - E_2)}{(\zeta - E_1)}\right)^{k-1} \frac{(\zeta - V_2)^2}{(\zeta - E_1)^2} d\zeta \end{aligned}$$

with the factor of $-i$ coming from the rotation of the $|gdh|$ model to this model. Substituting in the estimates from Lemma 5 to this description and setting $E_1 = 0$, one finds

$$\begin{aligned} gdh &= -ic(1 + o(1)) \left(1 + \frac{\frac{1+o(1)}{d} + o(1)/d}{k\zeta}\right)^{k-1} \frac{d\zeta}{\zeta^2} \\ &\rightarrow -ice^{\frac{1}{d}\frac{1}{\zeta}} \frac{d\zeta}{\zeta^2} \end{aligned}$$

as $k \rightarrow \infty$ when ζ is centered at the limit point of the ends E_i (and c is some constant). The same estimates applied to $\frac{dg}{g}$ yield from Figure 20 that

$$\frac{dg}{g} = \left\{ \frac{k}{\zeta - E_1} - \frac{k}{\zeta - E_2} \right\} d\zeta = \frac{k(E_1 - E_2)d\zeta}{(\zeta - E_1)(\zeta - E_2)} \rightarrow \frac{1}{d} \frac{d\zeta}{\zeta^2}$$

for ζ as above. It is easy to check that these limits provide Weierstrass data for the helicoid as described in Section 2.6. \square

A. Appendix: The Weierstrass data for \mathcal{H}_k in terms of theta functions

Consider a rhombic torus $T_\tau = \mathbf{C}/\Lambda$, where $\Lambda = \{1, \tau\}$, on which we desire to write down Weierstrass data for the \mathcal{H}_k as presented in Figure 38. In the rhombic model described in Section 4.1, we specified in (24) the location of

E_1	V_1	V_2	E_2
g	∞^k	∞	0^k
dh	∞	0	∞ .

Figure 38: The divisors of g and dh .

the geometrically important points, i.e. the ends and the vertical points. The center of the torus is located at $\mathcal{O} = \frac{1+\tau}{2}$. In Section 4.2.3, we saw that the ends E_i and the vertical points V_i could be placed at

$$(65) \quad \begin{aligned} E_1 &= \mathcal{O} - b\frac{1-\tau}{2}, & E_2 &= \mathcal{O} + b\frac{1-\tau}{2}, \\ V_1 &= \mathcal{O} - a\frac{1-\tau}{2}, & V_2 &= \mathcal{O} + a\frac{1-\tau}{2}, \end{aligned}$$

where $a < b < 1$ by assumption. In particular $\frac{1}{2} < b < 1$.

We will use the theta function

$$\theta(z) = \theta(z, \tau) = \sum_{n=-\infty}^{\infty} e^{\pi(n+\frac{1}{2})^2\tau + 2\pi i(n+\frac{1}{2})(z+\frac{1}{2})}$$

to express g and dh . (This theta function is $\theta_{1,1}$ in Mumford [31, pp. 17–19]. It has the following properties:

$$(66) \quad \begin{aligned} \theta(0) &= 0, \text{ a simple zero;} \\ \theta(z+1) &= \theta(z); \\ \theta(z+\tau) &= e^{2\pi i(z+\frac{\tau+1}{2})}\theta(z); \\ \theta(z) &= \text{has no poles and no other zeros in a} \\ &\quad \text{fundamental domain of } T_\tau. \end{aligned}$$

We may use $\theta(z)$ to write down (perhaps multivalued) meromorphic functions on T_τ .

LEMMA 9. *Let $a_i, b_i \in \mathbf{C}$, and let $\alpha_i, \beta_i \in \mathbf{R}$, with $\sum \alpha_i = \sum \beta_i$. Then*

$$f(z) = \prod_{i=1}^n \frac{\theta(z - a_i)^{\alpha_i}}{\theta(z - b_i)^{\beta_i}}$$

has a zero of order α_i at a_i , a pole of order β_i at b_i , and, modulo $\Lambda = \{1, \tau\}$, no other poles or zeros. Furthermore, f satisfies

$$(67) \quad \begin{aligned} f(z+1) &= f(z); \\ f(z+\tau) &= e^{2\pi i(\sum \alpha_i a_i - \sum \beta_i b_i)} f(z). \end{aligned}$$

The lemma follows directly from the properties of θ listed in (66). Using Figure 38, we may express the data g and dh in terms of θ as follows.

$$dh = e^{it} \frac{\theta(z - V_1)}{\theta(z - E_1)} \frac{\theta(z - V_2)}{\theta(z - E_2)} dz,$$

$$g(z) = \rho \frac{\theta(z - V_2)}{\theta(z - V_1)} \frac{\theta(z - (E_2 + \tau))^k}{\theta(z - E_1)^k}.$$

The factor e^{it} in dh is determined not by the divisor, but rather by the requirement that dh be real on the vertical diagonal. Similarly, the real factor ρ in $g(z)$ is determined by the requirement that g be unitary on the vertical diagonal.

The presence of the shift by τ (i.e. $E_2 + \tau$ instead of E_2) in the term in the numerator of the expression for g is determined by our desire for g to have the correct transformation behavior, namely:

$$g(z + \tau) = e^{-2\pi ik} g(z).$$

A straightforward computation using the definition of g and (67) gives $g(z + \tau) = e^{2\pi iW} g(z)$, where $W = V_1 + k(E_1) - V_2 - k(E_2 + \tau)$. Using (65), we get

$$W = -2(a + kb) \frac{1 - \tau}{2} - k\tau = -(a + kb) + (a + kb - k)\tau.$$

Hence $W = -k$, as required geometrically on a surface invariant under the screw motion σ_k , if and only if $a + kb = k$. So in order to obtain the correct transformation behavior, we must assume that $a + kb = k$. This also gives another derivation both of the relationship $a + kb = k$ proved in Proposition 13 and of the turning of g along the vertical axis of \mathcal{H}_k discussed in Remark 9.

B. Appendix: Existence and uniqueness of flat cone metrics

We prove here Propositions 3 and 4 from Section 2.3, as well as a local representation lemma used in Section 5. Some of these results extend foundational results of Troyanov [38] in the case when the cone angles are finite and positive.

PROPOSITION 3. *Let M be a compact Riemann surface, and $\{p_1 \dots p_r \dots, p_{r+\ell}\} \subset M$ a collection of distinct points, with $r > 0$, $\ell \geq 0$. Suppose $\{a_1 \dots a_r\}$ is a collection of real numbers satisfying (11) and*

$$(68) \quad \sum_{j=1}^r a_j = -(2 - 2\text{genus}(M)) + r + 2\ell.$$

Then there exists a cone metric on M with finite cone points p_j with cone angles a_j ($j = 1, \dots, r$) and exponential cone points p_k , ($0 \leq k \leq \ell$) of simple type.

Remark 15. When $\ell = 0$, the proposition is a statement about cone metrics all of whose cone points are finite and (68) or (11) is the Gauss-Bonnet condition (10).

Proof. We recall a fundamental theorem on the existence of holomorphic one-forms with prescribed singularities, an eloquent statement of which can be found in Royden’s article [34]:

LEMMA. *Let M be a Riemann surface, E be a closed set in M , \mathcal{O} an open set containing E and G a bounded open set with smooth boundary Γ such that $E \subset G$ and $\overline{G} \subset \mathcal{O}$. Let Ω be an analytic differential in $\mathcal{O} \sim E$. Then there is an analytic differential ω in $M \sim E$ such that $\Omega - \omega$ has an analytic extension to all of \mathcal{O} if and only if (the flux condition) $\int_{\Gamma} \Omega = 0$.*

To apply this lemma, we begin by choosing a holomorphic one-form ω_0 on M . (If M has genus zero, a simple modification of the following construction will work, and we leave that to the reader.) Let $\{q_1, \dots, q_s\}$ be the zeros of ω_0 with the order of the zero at q_i equal to b_i . Let $E = \{q_1, \dots, q_s\} \cup \{p_1, \dots, p_{r+\ell}\}$. Let \mathcal{O} be the union of disjoint coordinate neighborhoods of the points of E , with each point corresponding to $z = 0$ in its respective neighborhood. In each coordinate neighborhood we specify the analytic differential Ω on $\mathcal{O} - E$ as follows:

- In the punctured neighborhood of q_i , $1 \leq i \leq s$, $\Omega = -b_i \frac{dz}{z}$;
- In the punctured neighborhood of p_j , $1 \leq j \leq r$, $\Omega = (a_j - 1) \frac{dz}{z}$;
- In the punctured neighborhood of p_k , $r+1 \leq k \leq r+\ell$, $\Omega = -(\frac{1}{z^2} + \frac{2}{z}) dz$.

Letting G be the open set consisting of the union of slightly smaller coordinate neighborhoods, we can use the lemma to assert the existence of meromorphic differential ω on M with principal parts specified near the singular set E provided the flux condition

$$-\sum_{i=1}^s b_i + \sum_{j=1}^r (a_j - 1) - 2\ell = 0$$

is satisfied. Since ω_0 is holomorphic, $-\sum_{i=1}^s b_i = 2(1 - \text{genus}(M))$, from which it follows that the flux condition is precisely our assumption (68). We may also choose ω to have purely imaginary periods on M . This can be done by adding to ω a holomorphic differential specified by having all its periods on M equal to the negative of the real part of the periods of ω . The resulting meromorphic one-form has the same poles and principal parts as ω and all of its periods imaginary on $M - E$.

Define $f = e^{\int \omega}$, a multivalued function on $M - E$. Because ω has imaginary periods, the function $|f|$ is well-defined on $M - E$, and of course, is never equal to zero. Let

$$\eta = f\omega_0.$$

Note that η is regular at the zeros of ω_0 , that $|\eta|$ is a well-defined metric away from $\{p_1 \dots p_r \dots, p_{r+\ell}\}$ and that $|\eta|$ has cone points with cone angles a_j at the points p_j , $1 \leq j \leq r$ and exponential cone points of simple type at the points p_k , $r + 1 \leq k \leq r + \ell$. □

Remark 16. If one or more of the zeros of the chosen holomorphic one-form ω_0 coincides with a desired cone point, it can be easily verified that the construction still produces a cone metric with the prescribed cone points and cone angles. Simply add the prescribed residues b_i and $a_j - 1$ at those points.

PROPOSITION 4. *A cone metric on a compact Riemann surface with cone points with finite cone angles is determined up to scaling by the location of these cone points and their cone angles. The same result is true if one or more of the cone points is an exponential cone point of simple type, provided that these cone points are asymptotically isometric.*

Proof. Let $|\mu_1|$ and $|\mu_2|$ be cone metrics on M with the same cone points and cone angles, and let M' be the Riemann surface M with the cone points removed. Because $K = \frac{-\Delta \log |\mu_i|}{|\mu_i|^2} = 0$ on M' , the function $\log(|\frac{\mu_2}{\mu_1}|)$ is harmonic on M' . In a neighborhood of a cone point p with finite cone angle α , we may write $|\mu_1| = |z^{\alpha-1} dz|$ and $|\mu_2| = |w^{\alpha-1} dw|$ with z and w local coordinates, the cone point p corresponding to 0 in both z and w coordinates. If $w = w(z)$ with $w'(0) = c \neq 0$, then

$$\lim_{q \rightarrow p} \frac{|\mu_2|}{|\mu_1|} = c^\alpha.$$

In particular, $\log(|\frac{\mu_2}{\mu_1}|)$ is bounded in a neighborhood of p . If all the cone points are finite, then $\log(|\frac{\mu_2}{\mu_1}|)$ is a harmonic function on M' that is bounded in a neighborhood of each puncture. Therefore $\log(|\frac{\mu_2}{\mu_1}|)$ extends to a bounded harmonic function on M and hence is the constant function: $\mu_2 = c\mu_1$ for some positive constant c .

We now do a similar analysis in the neighborhood of an exponential cone point of simple type. Suppose there are coordinates in a punctured neighborhood of $z = 0$ in which $|\mu_1| = |e^{\frac{1}{z}} \frac{dz}{z^2}|$ and coordinates in a punctured neighborhood of $w = 0$ for which $|\mu_2| = |e^{\frac{1}{w}} \frac{dw}{w^2}|$, the common cone point corresponding to the puncture in each disk. Let $w = w(z)$ be a conformal change of coordinates with $w(0) = 0$. We may write $|\mu_2| = |e^{\frac{1}{w}} \frac{w' dz}{w^2}|$.

Then, for $w = z + o(z^2)$, we have

$$(69) \quad \left| \frac{\mu_2}{\mu_1} \right| = \left| e^{\frac{1}{w} - \frac{1}{z}} \frac{z^2}{w^2} w' \right|$$

$$(70) \quad = e^{o(1)} (1 + o(z))(1 + o(z)).$$

The remainder of the proof goes through as in the case of finite cone points. □

Remark 17. If $w = cz + o(z^2)$ where $c \neq 1$, then the ratio above acquires a term of size $e^{\frac{1}{r}}$ as $r \rightarrow 0$, and the proof fails. A counterexample in the case where the hypothesis doesn't hold is given in Section 2.4.

We next prove a lemma that was useful in our estimates in Section 5. While the statement extends to more general settings, we restrict ourselves here to the situation our estimates require. This restriction then allows for a simpler proof.

LEMMA 10. *Let D be a topological disk equipped with a flat singular metric ds_D with up to two cone points (say, p_1 and p_2) with positive cone angles (say, $2\pi\alpha_1$ and $2\pi\alpha_2$) and up to a single cone point (say p_0) with negative cone angle (say, $2\pi\alpha_0$). Next suppose that the cone angle at p_1 exceeds the cone angle at p_2 , i.e. $\alpha_1 > \alpha_2$. Suppose also that a geodesic Γ between p_2 and p_0 passes through p_1 , and that this geodesic bisects the angle found by removing all possible extensions of Γ to a geodesic from p_2 to p_0 . Suppose finally that the sum of the cone angles vanish. Then D admits a conformal and isometric development onto a topological disk Δ equipped with a metric ds_Δ of the form*

$$ds_\Delta = C \prod_{i=0}^2 |z - q_i|^{\alpha_i - 1},$$

where q_i is the point in Δ corresponding to $p_i \in \Delta$. This representation is unique up to a rigid motion of the plane containing Δ ; a homothety of the plane containing Δ is an isometry of ds_Δ after a corresponding change in the normalizing constant C .

Proof. We place q_0 at the origin, q_1 at the point $1 \in \mathbf{C}$, and consider $q_2 > q_1$ as a variable point on \mathbf{R}_+ . The possible locations of q_2 are then on a segment. We consider the family of flat singular metrics on the family of domains $\Delta(q_2)$ with

$$ds_{\Delta(q_2)} = \prod_{i=0}^2 |z - q_i|^{\alpha_i - 1}$$

where the cone angle at p_i is $2\pi\alpha_i$, as described in the statement of the lemma. The metric is then determined by the location of q_2 , as all choices of q_1 and q_2 on \mathbf{R} determine a metric whose geodesic connecting q_2 with q_0 passes through q_1 ; we then seek a metric where $d_{\Delta(q_2)}(q_1, q_2) = \text{dist}_\Delta(p_1, p_2)$. In fact, in the present simplified situation of at most three singular points, this is fairly straightforward, as we merely consider the function $d(q_2) = d_{\Delta(q_2)}(q_1, q_2)$. Certainly $d(q_2) \rightarrow 0$ as $q_2 \rightarrow q_1$ and $d(q_2) \rightarrow \infty$ as $q_2 \rightarrow \infty$. So by the continuity of d on the variable q_2 and the intermediate value theorem, we conclude that it is possible to find $q_2 \in (1, \infty)$ with $d(q_2) = \text{dist}_\Delta(p_1, p_2)$ as required.

Note next that when we restrict $ds_{\Delta(q_2)}$ to the complement $\Delta'(q_2) = \Delta(q_2) - \{q_0, q_1, q_2\}$, we obtain a flat metric. We may then develop the flat metric ds_{Δ} on $\Delta' = \Delta - \{p_0, p_1, p_2\}$ onto $\Delta'(q_2)$ (with p_i being sent to q_i). This developing map then develops ∂D onto a Jordan curve in $\Delta'(q_2)$.

We next turn to uniqueness. Certainly after fixing the positions of q_0 and q_1 , the position of q_2 is determined by the singularity at q_2 and the development of the geodesics from q_1 to q_0 and q_2 respectively. So suppose we have two metrics, say ds_1 and ds_2 on D with the same singularities at q_0 , q_1 , and q_2 . Then the function $h = \log ds_1/ds_2$ is harmonic, as each ds_i is flat, and vanishes on ∂D , as the development of Δ' onto $\Delta'(q_2)$ was isometric. Thus h vanishes identically, proving the required uniqueness. \square

INDIANA UNIVERSITY, BLOOMINGTON, IN
E-mail address: matweber@indiana.edu

STANFORD UNIVERSITY, STANFORD, CA
E-mail address: hoffman@math.stanford.edu

RICE UNIVERSITY, HOUSTON, TX
E-mail address: mwolf@math.rice.edu

REFERENCES

- [1] L. AHLFORS, *Conformal Invariants: Topics in Geometric Function Theory*, McGraw-Hill Book Co., New York, 1973.
- [2] A. ALARCON, L. FERRER, and F. MARTÍN, A uniqueness theorem for the singly periodic genus-one helicoid, *Trans. Amer. Math. Soc.* **359** (2007), 2819–2829.
- [3] A. BOBENKO, oral communication.
- [4] A. I. BOBENKO, Helicoids with handles and Baker-Akhiezer spinors, *Math. Z.* **229** (1998), 9–29.
- [5] M. CALLAHAN, D. HOFFMAN, and J. HOFFMAN, Computer graphics tools for the study of minimal surfaces, *Comm. ACM* **31** (1988), 648–661.
- [6] T. H. COLDING and W. P. MINICOZZI II, The Calabi-Yau conjectures for embedded surfaces, *Ann. of Math.* **167** (2008), 211–243.
- [7] ———, The space of embedded minimal surfaces of fixed genus in a 3-manifold I; Estimates off the axis for disks, *Ann. of Math.* **160** (2004), 27–68.
- [8] ———, The space of embedded minimal surfaces of fixed genus in a 3-manifold II; Multi-valued graphs in disks, *Ann. of Math.* **160** (2004), 69–92.
- [9] ———, The space of embedded minimal surfaces of fixed genus in a 3-manifold III; Planar domains, *Ann. of Math.* **160** (2004), 523–572.
- [10] ———, The space of embedded minimal surfaces of fixed genus in a 3-manifold IV; Locally simply-connected, *Ann. of Math.* **160** (2004), 573–615.
- [11] P. COLLIN, Topologie et courbure des surfaces minimales proprement plongées de \mathbf{R}^3 , *Ann. of Math.* **145** (1997), 1–31.
- [12] H. FARKAS and I. KRA, *Riemann Surfaces*, Springer-Verlag, New York, 1992.
- [13] L. FERRER and F. MARTÍN, Minimal surfaces with helicoidal ends, *Math. Z.* **250** (2005), 807–839.

- [14] W. M. GOLDMAN, Projective structures with Fuchsian holonomy, *J. Differential Geom.* **25** (1987), 297–326.
- [15] L. HAUSWIRTH, J. PÉREZ, and P. ROMON, Embedded minimal ends of finite type, *Trans. Amer. Math. Soc.* **353** (2001), 1335–1370.
- [16] D. HOFFMAN and H. KARCHER, Complete embedded minimal surfaces of finite total curvature, in *Encyclopedia of Mathematics*, pages 5–93 (R. Osserman, ed.), Springer-Verlag, New York, 1997.
- [17] D. HOFFMAN, H. KARCHER, and F. WEI, Adding handles to the helicoid, *Bull. Amer. Math. Soc.* **29** (1993), 77–84.
- [18] ———, The genus one helicoid and the minimal surfaces that led to its discovery, in *Global Analysis and Modern Mathematics*, 119–170 (K. Uhlenbeck, ed.), Publish or Perish Press, Houston, TX, 1993.
- [19] ———, The singly periodic genus-one helicoid, *Comment. Math. Helv.* **74** (1999), 248–279.
- [20] D. HOFFMAN and J. MCCUAN, Embedded minimal ends asymptotic to the helicoid, *Comm. Anal. Geom.* **11** (2003), 721–735.
- [21] D. HOFFMAN and W. MEEKS, III, A complete embedded minimal surface in R^3 with genus one and three ends, *J. Differential Geom.* **21** (1985), 109–127.
- [22] ———, Embedded minimal surfaces of finite topology, *Ann. of Math.* **131** (1990), 1–34.
- [23] D. HOFFMAN and F. WEI, Deforming the singly periodic genus-one helicoid, *Experiment. Math.* **11** (2002), 207–218.
- [24] L. JORGE and W. H. MEEKS III, The topology of complete minimal surfaces of finite total Gaussian curvature, *Topology* **22** (1983), 203–221.
- [25] H. KARCHER, oral communication.
- [26] F. KLEIN, *Vorlesungen Über die Hypergeometrische Funktion*, Springer-Verlag, New York, 1933.
- [27] S. LANG, Elliptic Functions, Second Edition, *Graduate Texts in Mathematics* **112**, Springer-Verlag, New York, 1987.
- [28] W. H. MEEKS III and H. ROSENBERG, The geometry of periodic minimal surfaces, *Comment. Math. Helv.* **68** (1993), 538–578.
- [29] ———, The uniqueness of the helicoid and the asymptotic geometry of properly embedded minimal surfaces with finite topology, *Ann. of Math.* **161** (2005), 727–758.
- [30] J. B. MEUSNIER, Mémoire sur la courbure des surfaces, *Mém. Mathém. Phys. Acad. Sci. Paris, prés. par div. Savans* **10** (1785), 477–510.
- [31] D. MUMFORD, *Lectures on Theta. I*, Birkhäuser, Boston, 1983.
- [32] M. OHTSUKA, *Dirichlet Problem, Extremal Length and Prime Ends*, Van Nostrand Reinhold, New York, 1970.
- [33] R. OSSERMAN, *A Survey of Minimal Surfaces*, Dover Publications, New York, 2nd edition, 1986.
- [34] H. ROYDEN, Function theory on compact Riemann surfaces, *J. Analyse Math.* **18** (1967), 295–327.
- [35] K. STREBEL, *Quadratic Differentials*, Springer-Verlag, New York, 1984.
- [36] M. TRAISET, oral communication.
- [37] M. TRAISET and M. WEBER, Hermite polynomials and helicoidal minimal surfaces, *Invent. Math.* **161** (2005), 113–149.

- [38] M. TROYANOV, Les surfaces euclidienne à singularités coniques, *L'Enseignement Mathématique* **32** (1986), 79–94.
- [39] M. WEBER, On the embeddedness of the genus one helicoid, Habilitationsschrift, University of Bonn, 2000.
- [40] ———, The genus-one helicoid as a limit of screw-motion invariant helicoids with handles, *Clay Math. Proc.* **2**, in *Global Theory of Minimal Surfaces*, 243–258, Amer. Math. Soc., Providence, RI, 2005.
- [41] ———, Period quotient maps of meromorphic 1-forms and minimal surfaces on tori, *J. Geom. Anal.* **12** (2002), 325–354.

(Received June 8, 2004)

(Revised April 26, 2006)